UNIVERSITY OF JYVÄSKYLÄ
DEPARTMENT OF CHEMISTRY
RESEARCH REPORT No. 136

URANYL SALOPHENS: SYNTHESIS AND USE AS DITOPIC RECEPTORS

BY
LAURA ILANDER

Academic Dissertation
for the Degree of
Doctor of Philosophy

Jyväskylä, Finland
2010

DEPARTMENT OF CHEMISTRY, UNIVERSITY OF JYVÄSKYLÄ RESEARCH REPORT No. 136

URANYL SALOPHENS: SYNTHESIS AND USE AS DITOPIC RECEPTORS

BY

LAURA ILANDER

Academic Dissertation for the Degree of
Doctor of Philosophy

To be presented, by permission of the Faculty of Mathematics and Science of the University of Jyväskylä, for public examination in Auditorium KEM 4, on April 20th, 2010 at 12 noon.

UNIVERSITY OF JYVÄSKYLÄ

Jyväskylä, Finland
ISBN 978-951-39-3842-0
ISSN 0357-346X

URN:ISBN:978-952-86-0171-5
ISBN 978-952-86-0171-5 (PDF)
ISSN 0357-346X

Jyväskylän yliopisto, 2024

ABSTRACT

Uranyl salophens are ditopic receptors that can simultaneously bind both the anion and cation of the salt at the same time. The anion is bound to the seventh coordination site of the uranium atom in the uranyl moiety and the cation binds to the aromatic π-system of the salophen moiety through cation···π and C-H···π interactions. The uranyl salophens offer a great potential for further functionalization, which makes them ideal building blocks for the purposes of supramolecular chemistry and molecular recognition. As an introduction to the subject, the review of the literature gives both a brief account of the history and recent advances in the uranyl salophen chemistry as well as a description of their synthesis and use as receptors and catalysts.

In the experimental part, altogether 12 novel uranyl-salophen complexes and some of their starting compounds were prepared and characterized by ^{1}H and ^{13}C NMR, mass spectrometry and elemental analysis. The complexation behavior of the prepared uranyl salophens was studied both in the solution and in the solid state. In the solution the binding constants for phenyl methoxy uranyl salophens towards various quaternary ammonium chlorides were determined by NMR titrations. In the solid state, the structures of 12 new solvent complexes and 13 new complexes with other guest molecules (R_4NX, DABCO or Cs_2CO_3) and 3 novel dimer arrangements were determined by single crystal X-ray crystallography.

Author's address

Laura Ilander
Department of Chemistry
P.O. BOX 35
40014 University of Jyväskylä, Finland

Supervisor

Academy Professor Kari Rissanen
Department of Chemistry
University of Jyväskylä
Jyväskylä, Finland

Reviewers

Professor Matti Haukka
Department of Chemistry
University of Eastern Finland
Joensuu, Finland

Docent Ari Lehtonen
Department of Chemistry
University of Turku
Turku, Finland

Opponent

Professor Risto Laitinen
Department of Chemistry
University of Oulu
Oulu, Finland

PREFACE

This work was carried out at the Department of Chemistry, University of Jyväskylä during 2005-2010.

I express my gratitude to my supervisor Academy Professor Kari Rissanen for the opportunity to work in his research group. I want to also thank Dr. Arto Valkonen, Dr. Luca Russo and Academy Professor Kari Rissanen for the single crystal X-ray structure measurements. Dr. Massimo Cametti is thanked for his guidance in the NMR-titrations and for the synthesis of compounds **9**, **100**, **103** and **128**. FM Minna Kärnä is thanked for the synthesis of R_4NCl salts DMDEACl **98a** and DMDPACl **98b**. Laboratory technicians Reijo Kauppinen, Mirja Lahtiperä and Elina Hautakangas are kindly thanked for NMR, MS and elemental analysis measurements and Leena Koskela for her kind help during the laboratory work. Professor Matti Haukka and Docent Ari Lehtonen are gratefully thanked for reviewing this Ph.D. thesis and emeritus Professor Matti Nurmia for revising the language. I also wish to express my gratitude to my parents for their support. And finally, the warmest gratitude goes to my husband Aki, who has stood by me through these busy years.

Jyväskylä, March, 16th 2010

Laura Ilander

ABBREVIATIONS

NMR	nuclear magnetic resonance
IUPAC	Internationl Union of Pure and Applied Chemistry
DMSO	dimethylsulfoxide
DMF	dimethylformamide
CPK	(Corey, Pauling, Koltun) space-filling model
NMP	N-methyl pyridine
NMiQ	N-methyl isoquinoline
TMA	tetramethyl ammonium
TEA	tetraethyl ammonium
TPA	tetrapropyl ammonium
TBA	tetrabutyl ammonium
DMDEA	dimethyl diethyl ammonium
DMDPACl	dimethyl dipropyl ammonium
DMDBA	dimethyl dibutyl ammonium
ACh	acetyl choline
MS	mass spectrometry
EA	elemental analysis
NOESY	nuclear Overhouse effect spectroscopy
GS-COSY	gradient selection correlation spectroscopy
AIBN	azobisisobutyronitrile
NBS	N-bromosuccinimide
s	singlet
d	doublet
t	triplet
m	multiplet

TABLE OF CONTENTS

1. INTRODUCTION

Supramolecular chemistry is a rather new field in science. Its origins are in nature, in the chemistry found in living biological structures. Supramolecular complexes consist of at least two independent compounds held together by weak interactions. Besides the weak interactions, demands for the successful self-assembly are reflected both in the size and shape of the components and their preorganization. Later on these supramolecular complexes have been developed into functional nanostuctures with many applications in different fields of life[1-2].

Weak, noncovalent interactions are considerably weaker (by one or two orders of magnitude) than covalent interactions. However, a combination of several noncovalent bonds at the same time forms a strong but still flexible system. The term noncovalent encompasses an enormous range of attractive and repulsive forces such as hydrogen bonds, ion pairs, ion-dipole and, dipole-dipole interactions, cation-π interactions, π-π stacking, Van der Waals forces, and

hydrophobic effects[1, 3]. The cation-π interaction was of special interest in this study because of the large π-systems in the uranyl salophen receptors studied[4].

Supramolecular chemistry is host-guest chemistry and molecular recognition is a process where a host molecule chooses its guest molecule from a mixture of different molecules. Crystallography is the most precise method to obtain information about complex structures in the solid state. NMR-titration technique is used when complexation is studied in the solution. Development of a perfect host molecule for a certain guest molecule and studying it by crystallography is also called crystal engineering[5-6].

In this study, uranyl salophen complexes with different kinds of "side arms" were prepared and thoroughly analyzed. Numerous complexation experiments were done both in the solid state and in the solution. Most of the complexation work consisted of the use of tetraalkyl ammonium salts. Uranyl salophens are ditopic receptors and hence they bind both counter ions of the salt well. Many crystal structures of these complexes were determined and their equilibrium constants were studied by NMR. In addition to that, macrocyclic structures were obtained when the acidity of the phenolic hydrogen of the hydroxy uranyl salophen was noticed. Also dimerization of the uranyl salophens was studied by low temperature NMR-measurements and crystallography.

2. REVIEW OF THE LITERATURE

2.1 Uranyl salophens

N,*N*′-*o*-phenylenebis(salicylaldimine), the simplest of the salophen molecules, formed by the reaction of 1,2-diaminobenzene and salicyl aldehyde, is one of the most popular tetradentate Schiff base ligands known (Figure 1a). The salophens and its salen (*viz.* ethylenediamine) analogues have two sp^2 nitrogens and two deprotonated phenolic oxygens as donor atoms creating an efficient $N_2O_2^{2-}$ coordination site and they easily form neutral complexes with transition metal dications such as iron, copper, cobolt, nickel and manganese.[7-10] One of the most efficient is the uranyl dication UO_2^{2+} which forms stable neutral uranyl salophens (Figure 1b) and uranyl salens.[11-12] Because of the large ionic radius of the uranium atom, the salophen ligand cannot adopt a planar geometry and it is highly puckered or curved as shown in the computer calculated structure of the uranyl salophen in Figure 1c.[13] The uranyl salophens manifest

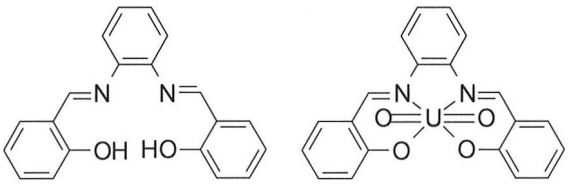

1a **1b**

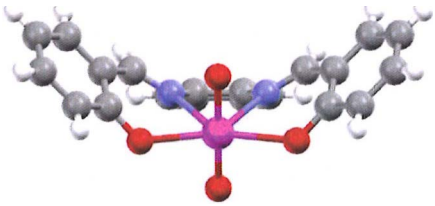

1c

Figure 1 A chemical structure of the salophen (1a), uranyl salophen (1b) and a computer calculated structure (1c) where the curved structure is easily seen.[13]

pentagonal bipyramidal coordination where the two uranyl dication oxygens occupy the apical positions and the salophen $N_2O_2^{2-}$ coordinating site forms the equatorial plane, while the seventh coordination site lies on the equatorial plane between the two phenolic oxygens.[14] The uranyl dication itself has a linear or very nearly linear triatomic O=U=O structure.[15] Excluding the UO_2^{2+} oxygen atoms, the uranyl dication has five coordination sites[16-19] and, being complexed by the tetradental salophen, the remaining equatorial binding site is highly electrophilic and it wants to bind to a suitable nucleophilic atoms, viz. either a neutral donor atom such as O or N of a solvent molecule or an anion. Hard anions such as fluoride and chloride are preferred over softer anions. In the uranyl salophen complexes, however, this seventh binding site is never empty. In the absence of anionic guest molecules or coordinative solvent molecules (e.g. DMSO, acetone, methanol, ethanol, water) in non-polar solvents, another salophen molecule fills the vacant coordination site.[20-21] The fifth equatorial

coordination site makes the uranyl salophens excellent receptors for the recognition or activation of a suitable guest. By attaching additional groups or "side arms" to the salophen moiety, for example aromatic rings, ditopic receptors can be created. The uranyl binds the anion and the aromatic sidearms bind the cation. The uranyl salophens have been successfully used as ditopic receptors both in solution and in solid state, as catalysts for other organic reactions and recently also as recognition sites attached to membranes.[11]

The uranyl salophens are intensively colored compounds, their colors ranging from orange to deep red. Their solubility depends on additional groups attached to the salophen core, simple salophens being soluble in polar non-protic solvents. In the ^{1}H NMR-spectrum, a singlet for the imine protons is shifted downfield (observed at ~ 9.5 ppm), more deshielded as imines usually as a consequence of the uranyl cation being bound to the iminic nitrogen atoms.[11]

The simplest uranyl salophen structure (Figure 1) was first published by Bandoli *et al.* in 1971.[16] It was synthesized in ethanol and the formed crystals were, as expected, characterized as ethanol complexes. Almost 20 years later, Reinhoudt *et al.* developed the research in this field by studying the ability of the uranyl salophens to bind neutral guests such as urea and pyridine.[11,14] Later on the ability of uranyl salophens to bind anions was discovered by the same group.[20] Because of biological interest of ionophores for anions, Reinhoudt continued by developing uranyl salophens that act as ionophores in membranes. That work is still continuing. Currently the uranyl salophens are being studied and used as ditopic receptors for organic and alkali metal salts.[11]

2.2 The synthesis and nomenclature of uranyl salophens

The simplest salophen molecule is synthesized by an acid catalyzed condensation reaction of two equivalents of **sal**icylaldehyde with **o**rtho**phen**ylendiamine (1,2-diaminobenzene) in good yields.[16] In the salen analogues, ethylenediamine or cyclohexyldiamine is used instead of an aromatic amine (Scheme 1). Salophen is a product of an imine formation reaction that proceeds via a nucleophilic attack

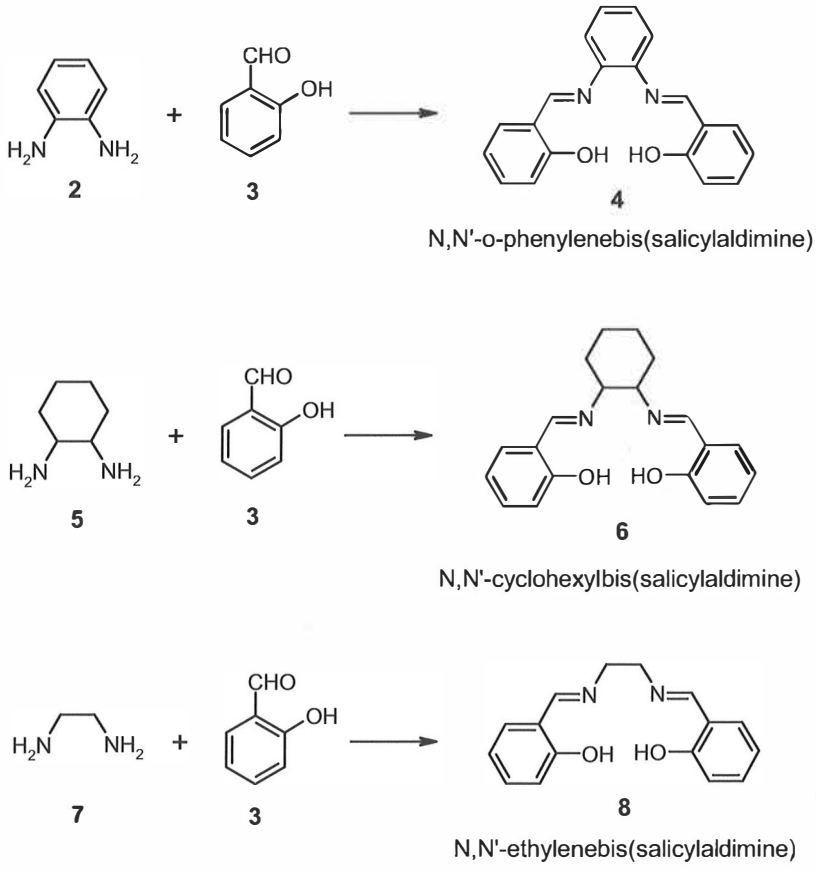

Scheme 1 The synthesis scheme for core salophen and salens.

by an amine group to a carbonyl carbon of an aldehyde or ketone. Methanol is the solvent most commonly used, because of its capability to dissolve charged intermediate products. When uranyl salophen is the target product, a uranyl salt, most commonly uranyl acetate or uranyl nitrate, is added to the reaction mixture. During the years, a large variety of uranyl salophens has been synthesized. Reaction conditions required depend heavily on the target uranyl salophen. Macrocyclic salophens require high dilution conditions whereas the unsubstituted uranyl salophens **1** can be synthetised via a simple, one-step synthesis procedure. Unsubstituted salophens can be synthesized at room temperature while the more complicated structures need refluxing conditions.[14]

The salophens are Schiff bases (*viz*. conjugated bis-imine compounds), a special and most stable family of imines. Imines are designated structurally as RR'C=NR''. In the case of Schiff bases, R is limited to the aryl group, R' is a hydrogen and R'' is either an alkyl or an aryl group.[22] Imines, including the Schiff bases (also called azomethines), were first discovered by Hugo Schiff (1834-1915) in 1862.[23-24] An IUPAC name for the core salophen **4**, without the uranyl dication, is *N,N'-o*-phenylenebis(acicylaldimine). For the salen structures, the *o*-phenylene moiety is replaced by cyclohexyl or ethylene corresponding to the structure of these two salen molecules (Scheme 1, comp. **6** and **8**). Despite the Schiff base moiety in the uranyl salophens, uranyl salophens are commonly named dioxouranium compounds instead of imines or azomethines. The dioxouranium name for compound **9** (Figure 2) is dioxo{[2,2'-[1,2-phenylene]bis(nitrilomethylidyne)bis-[6-(phenylmethoxy)-phenolato]](2-)-*N,N',O,O'*}uranium·H_2O.[14]

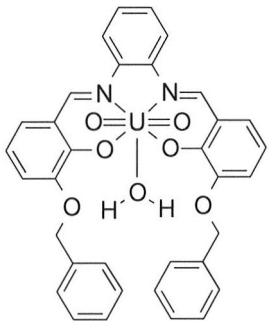

9

Figure 2 Dioxo{[2,2'-[1,2-phenylene]bis(nitrilomethylidyne)bis-[6-(phenylmethoxy)phenolato]](2-)-N,N',O,O'}uranium·H_2O.[14]

2.3 Dimer formation in non-coordinative solvents

As previously discussed, the fifth equatorial binding site in the uranium atom in the uranyl salophen structure is never empty. When the uranyl salophen is dissolved in a coordinative solvent such as DMSO, DMF, acetone, methanol, ethanol or acetonitrile, the fifth position is occupied by an oxygen atom of the solvent molecule.[21] Also water in the solvent can bind to the uranyl cation.[14] In the absence of other more suitable atoms in either guest or solvent molecule capable of binding to the uranyl cation, a vacant site is filled with an oxygen atom of another uranyl salophen leading to a uranyl salophen dimer.[21] Already in 1958, Comyns[25] noticed that the red color of uranyl acetylacetonate complexes became more intense on heating in non-coordinative solvents whereas in coordinative solvents such a phenomenon was not observed. Reinhoudt *et al.* were the first to publish a dimer structure composed of two uranyl salen molecules[20] (Figure 3).

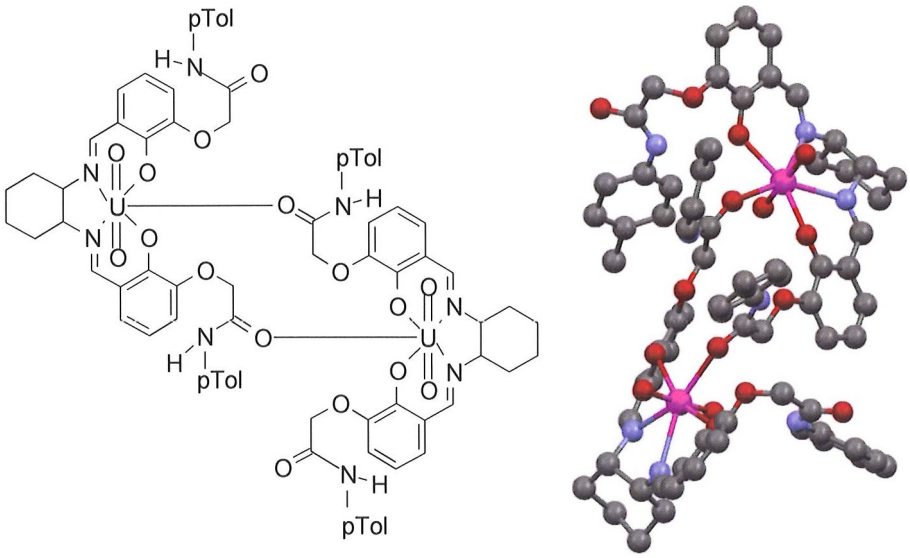

Figure 3 The chemical and crystal structure of uranyl salen dimer.[20]

In the dimer shown in the Figure 3 the fifth position of the uranyl cation is filled by an oxygen atom of the amido group of a second molecule and vice versa. In general the concept of self-complementarity is very important in nature.[26-31] According to Reinhoudt, the reason why the uranyl salophens give very broad spectra in $CDCl_3$ is this type of dimeric association.[20] An increase of solvent polarity prevents this association, and in DMSO-d_6, which is known to form complexes with uranyl salophens, the ^1H NMR spectrum is unambiguous. Even though this phenomenon was found already in 1994, it was not until 2007 that Takao and Ikeda published an extensive study of core uranyl salophens.[21] The core uranyl salophen **1** was studied in non-coordinative solvents and the crystal structure, shown in Figure 4, was achieved. In this structure each of the uranyl salophen moieties has pentagonal bipyramidal coordination geometry and these bipyramids share the edges of the equatorial pentagons with each other. The

salophen ligands are puckered /curved in a manner similar to those in monomeric uranyl salophen complexes.[21]

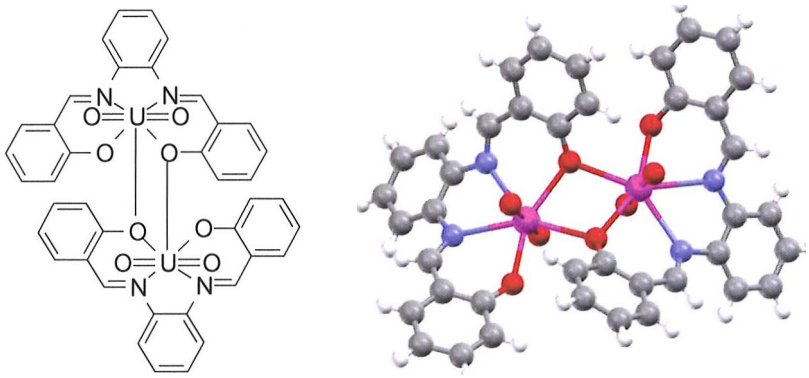

Figure 4 The chemical and crystal structure of the core uranyl salophen **1** dimer.[21]

Electrochemical measurements reveal that in non-aqueous solvents the oxidation state of the uranium atom changes from VI to V and vice versa.[32-37] That causes an exchange of the coordinated solvent molecules (DMSO and DMF were used in this study; both solvents are marked by L later in this text) with the free solvent molecules in the solution (Scheme 2).[38]

Scheme 2 summarizes the results obtained in chloroform and shows that the dissociation and association of L does happen in non-coordinative solvents and that the association reaction is fast.

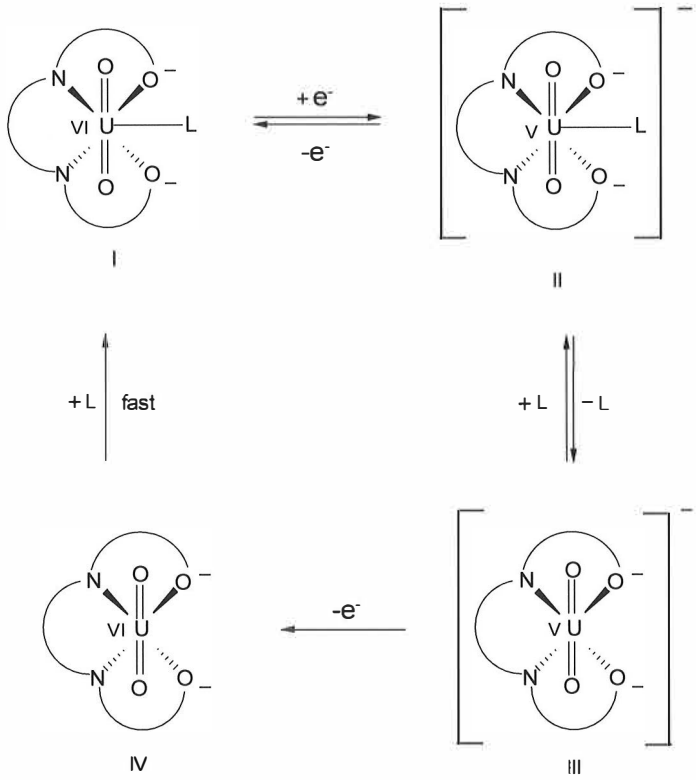

Scheme 2 Basic mechanism of electrochemical reactions of a uranyl salophen solvent complex in polar non-aqueous solvents.[38]

The equilibrium between the dimer and the uranyl salophen binding DMF or DMSO was also studied.[21] The ^{1}H NMR spectra of both DMSO and DMF complexes in $CDCl_3$ and CD_2Cl_2 were measured at various temperatures (213 K - 293K). Results show that there is an exchange of the L-molecules between uranyl salophen molecules and, independent of that, an equilibrium between L-complex and L-dissociated species, which is able to form the dimer shown in Figure 4. The overall reaction mechanism including the L exchange in uranyl salophen-L and the enantiomer exchange of the dimer is shown in Scheme 3.[21]

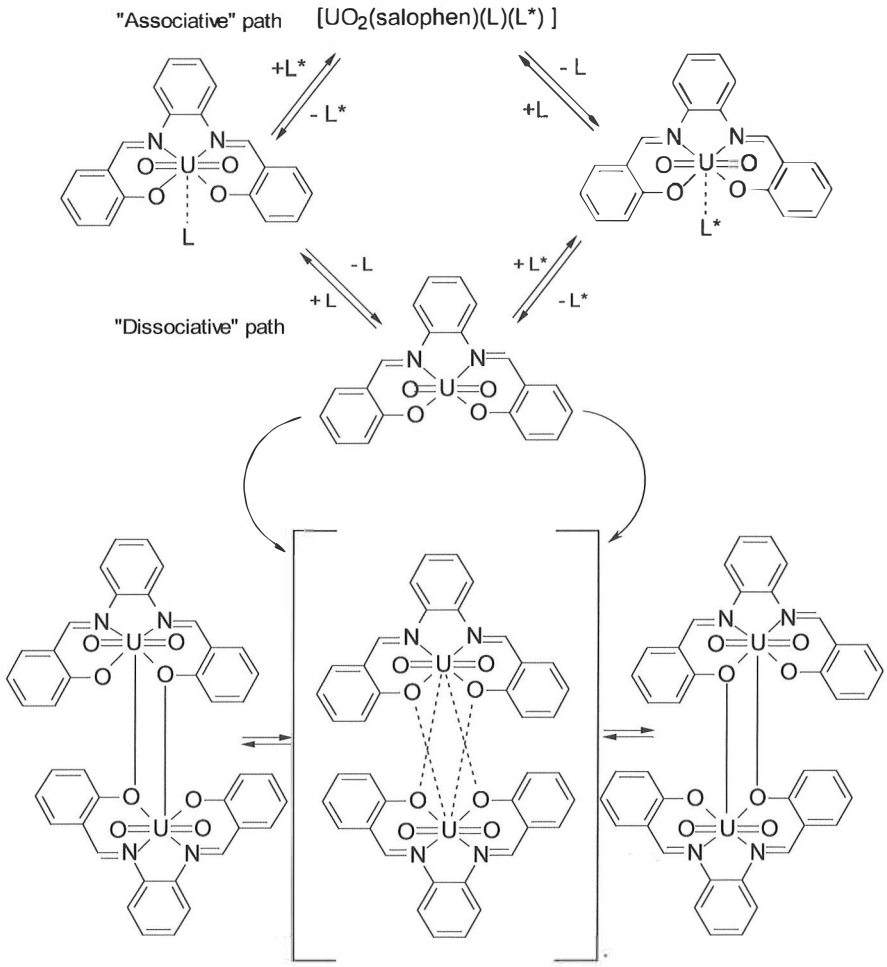

Scheme 3 An overall reaction mechanism including the L exchange in the uranyl salophen – L complex, the formation of a dimer, and an enantiomer exchange of the dimer.[21]

Scheme 3 summarizes that the change of the L-molecule on the uranyl salophen can happen along either an associative or a dissociative path. From the dissociative path the uranyl salophen with an empty fifth vacant site is able to dimerize. In the dimer structure there is an intramolecular exchange reaction

between the two enantiomers, where bridging and non-bridging phenolic groups exchange with each other by sliding. Of the two reactions happening in Scheme 3, L-exchange and the dimer formation, the first one is much faster than the second one, which causes the two independent reactions to happen. These two reactions cause two independent imine singlets in the ^{1}H NMR spectrum. The sliding causes also a splitting of the other peak because of two chemically different environments for the imine groups closest to and farther from the bridging phenolic oxygen atoms. When the results in CD_2Cl_2 and $CDCl_3$ solutions are compared, it seems that the dimer is produced more readily in $CDCl_3$ than in CD_2Cl_2.[21]

2.4 Uranyl salophens as receptors

2.4.1 Recognition of neutral molecules

The first uranyl salophen crystal structure published was the ethanol complex.[16] Later, more complexes with coordinative solvent molecules such as DMSO, DMF,[21] and water[39] with different kinds of uranyl salophen molecules have been published.

Urea has been found to bind weakly to a crown ether moiety,[40] but the binding can be strengthened by using an electrophilic center to bind urea in the cavity of the crown ether. Reinhoudt *et al.* joined the crown ether and the salophen moieties[39] (Figure 5., comp. **10)** and urea was the first neutral molecule complexed to the uranyl salophen by design.

Urease is a nickel containing metalloenzyme that catalyzes the degradation of urea to ammonia and carbamic acid.[41-43] The supposed mechanism suggests a

cooperative interaction between the two nickel ions within the enzyme. One of the nickel cations acts as a Lewis acid. The metal ion polarizes the carbonyl group of urea and activates it towards the nucleophilic attack. The remaining nickel ion binds a hydroxide ion from water. The hydroxide ion attacks the partially positive carbonyl carbon of the urea molecule. This type of

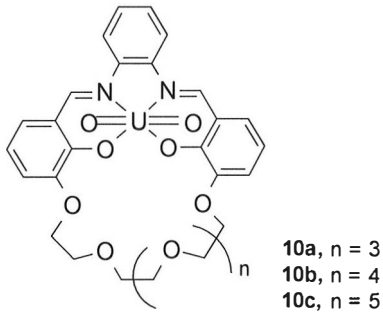

Figure 5 Chemical structures of the uranyl salophen receptors **10** for urea.[39]

complexation of a neutral guest by a host molecule by hydrogen bonding and coordination with a metal ion is frequently observed in metalloenzymes. To mimic this natural model, compound **11** shown in Figure 6 was synthesized and a complex with urea was crystallized by Reinhoudt *et al.*[44] An X-ray crystal structure however reveals that urea is only hydrogen bonded to the polyether moiety and to one of the phenolic oxygens. No bonding between urea O- or N-atoms and nickel was observed. When nickel is exchanged to the uranyl, coordination of urea is observed. As can be seen from the X-ray structure of the urea complex of **10c** (Figure 7), the urea molecule is coordinated to the uranium atom via the lone pair of electrons of the carbonyl oxygen and via hydrogen bonds of the amino groups to the phenolate oxygens and the five oxygens in the polyether chain.[44]

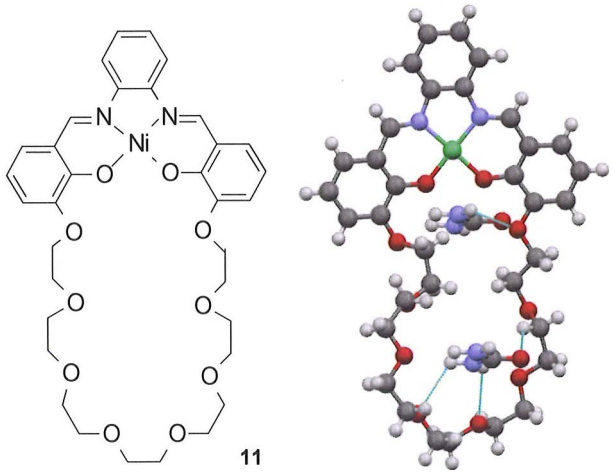

Figure 6 Chemical structure of compound **11** and the crystal structure of the complex of compound **11** and urea.[44]

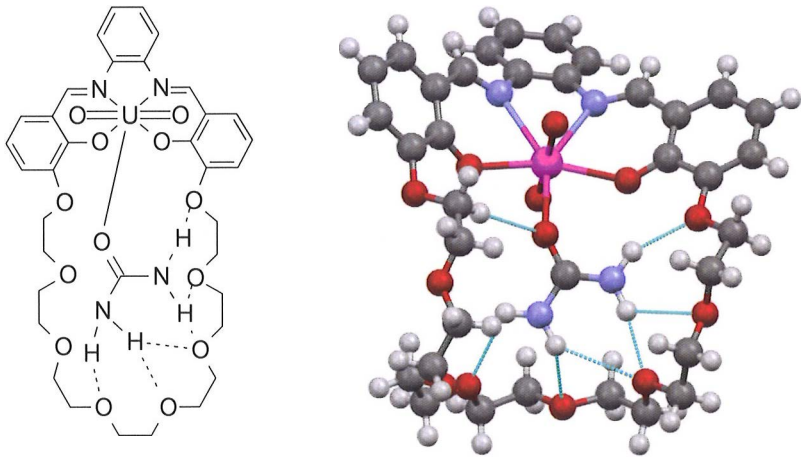

Figure 7 Crystal structure of the complex of uranyl salophen **10c** with urea.[44]

Later, the same group analyzed complexes of the same kind of uranyl salophen with unequal lengths of the polyether chain with formamide, acetamide, N-methylurea, (2-pyridylmethyl)urea, acetone and DMSO. Unfortunately no crystal

structures of these complexes are available. The effect of the polyether ring was proven by the fact that the smaller macrocycles do not bind the larger guest molecules like *N*-methylurea, (2-pyridylmethyl)urea, and DMSO, whereas the larger macrocycles did bind all the guests. The solubility of these receptors to organic solvents is too low to study the complexation systematically in solution.[44]

To improve the solubility towards lipophilic solvents, analoguous salen complexes were synthesized by the same group.[45] *Cis*-1,2-cyclohexyldiamine was used instead of an aromatic amine. Complexation properties of receptors **12** shown in Figure 8 towards acetamide, formamide, hydroxyurea, *N*-methylurea, urea and DMSO were studied.[45] As can be seen from the X-ray structures of **12a**-urea and **12c**-urea (Figure 9), the cyclohexyl moiety has a chair conformation and the guest molecule urea is bound in the macrocyclic cavity. In the **12a**-urea complex urea fits nearly perfectly in the cavity, whereas in the **12c**-urea complex the fit of urea in the cavity is not at all perfect due to the oversized cavity.[45]

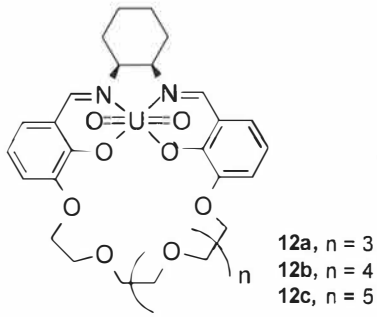

Figure 8 Chemical structures of uranyl-salen type urea receptors **12**.[45]

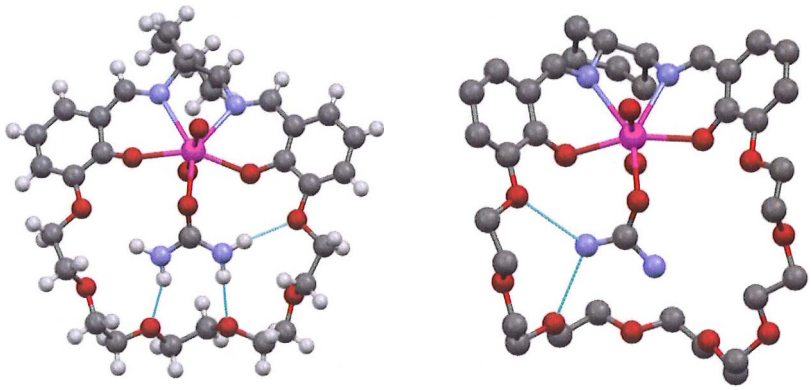

Figure 9 The crystal structures of complexes of **12a** and **12c** with urea.[45]

Also uranyl salophens **13** and **14** (Figure 10) are able to bind neutral molecules such as coordinative solvents (water, methanol, and DMSO) and urea.[46-47] These receptors have been used as macrocyclic carriers for urea through a supported liquid membrane (see page 67).

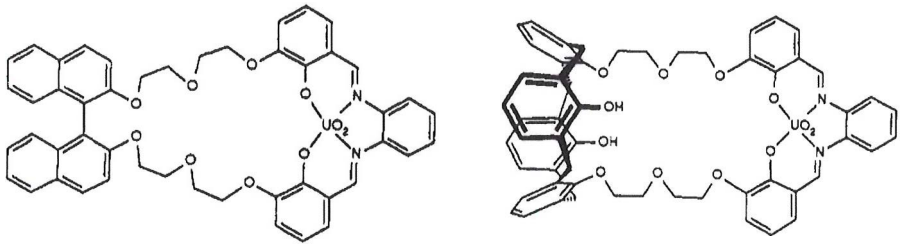

13 **14**

Figure 10 Macrocyclic uranyl salophen receptors and carriers for urea through a supported liquid membrane.[46]

In the early 1990's organic clefts were recognized as a new class of host molecules with very promising complexing properties. To promote complexation of aromatic neutral molecules, a cleft like uranyl salophens **9** (page 17, Figure 2) and **16** (Figure 11) was constructed by adding aromatic moieties into the core

salophen. When an aromatic bridge was used macrocyclic uranyl salophen **15** was obtained.[14] Cleft or macrocyclic receptors with enhanced π-π stacking abilities in addition to the uranyl coordination exhibited interesting properties. According to the CPK model for the metallocleft **9** the aromatic rings are parallel to each other at distances from 6 Å to more than 10 Å. In the cyclic metalloclefts **15**, rotation around O-CH_2 and CH_2-C_6H_5 bonds is restricted by connecting the two aromatic rings by a spacer, making the cyclic **15** more preorganized than the salophen **9**. The distances between the aromatic rings are 5.7 - 8.1 Å. To still diminish the rotation, metalloclefts **16** were synthesized. In these salophens the only conformational freedom is the rotation of the phenyl groups of the biphenyl unit. The distances between the parallel aromatic rings are 7.5 Å.[14]

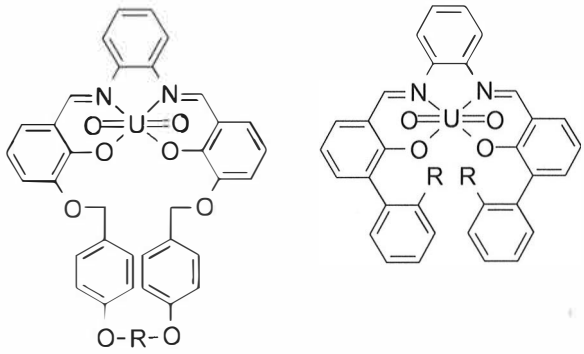

15a) R = $CH_2CH_2CH_2CH_2$
15b) R = $CH_2CH_2OCH_2CH_2$
15c) R = allyl

16a) R = H
16b) R = OMe

Figure 11 Macrocyclic **15** and metallocleft receptors **16** with aromatic side arms allowing π-π stacking with aromatic guest molecules.[14]

The complexation of the receptors shown in Figure 11 with pyridine and related derivatives: 4-*tert*-pyridine, 4-*tert*-butylpyridine, 2,6-dimethylpyridine, pyridine *N*-oxide, isoquinoline, benzamine, benzylamine and aniline, was studied. Strong

complexes were found except for aniline and 2,6-dimethylpyridine. The crystal structure of **16b**-4-*tert*-butylpyridine is shown in Figure 12.[14]

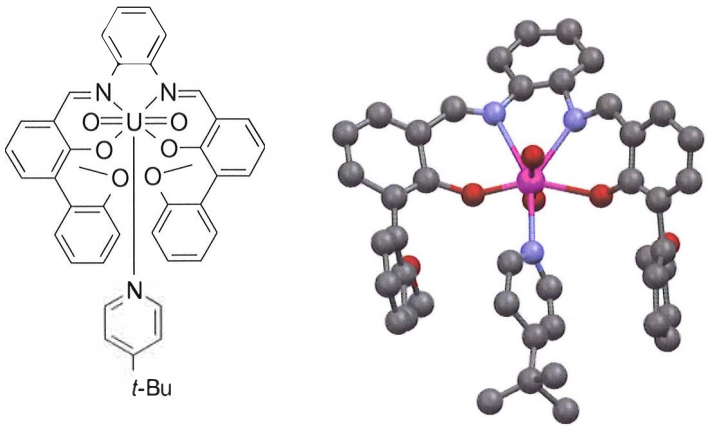

Figure 12 Crystal structure of the complex of **16b** with 4-tert-butylpyridine.[14]

As can be seen from Figure 12, the guest molecule, 4-tert-butylpyridine, lies beautifully between the aromatic "arms" of the uranyl salophen. To prove the effect of π-π stacking the uranyl salophen **17** shown in Figure 13 was synthesized by the Reinhoudt group. Complexation studies with compound **17** showed that the introduction of an extended cleft as in **16** results in more stable complexes.[14]

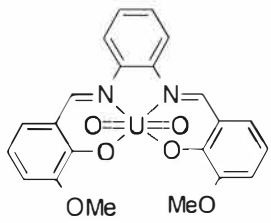

17

Figure 13 Chemical structure of 3-methoxy uranyl salophen.[14]

2.4.2 Recognition of anions

The design and synthesis of neutral receptors that selectively bind anions has not been as popular as that of cation receptors. In earlier studies, macrocyclic and acyclic ligands containing quaternary ammonium ion moieties[48] or Lewis acidic binding sites such as boron,[49] silicon,[50] tin,[51] and mercury[52] to bind anions have been reported, but a lack of binding selectivity and the possibility for subtle structural variations has been a problem with these receptors. In nature anion receptors play a crucial role and the selective complexation of anions takes place primarily by hydrogen bonds. As an example, the selective recognition of phosphate and sulphate by transport proteins is an important process in all living tissues.[53]

Reinhoudt *et al.* were again the first group who in 1992 published uranyl salophen structures capable of binding anions. The binding ability of the core salophen structure **1** towards chloride anion with tetraethyl ammonium or tetrabutyl ammonium as the counter cation was studied first.[54] High binding constants of 4200 M^{-1} and 4000 M^{-1} respectively were determined by ^1H NMR dilution experiments and by conductometric measurements. In the early 1990s receptors were designed only for the anionic parts of the salts, but in the X-ray structures also the cation plays an important role. At that time, ditopic behaviour of these receptors was not recognized. Only after the anion binding ability of the uranyl salophens was discovered, different kinds of structural modifications to the core salophen moiety were introduced to obtain more selective anion binding. Later on these receptors have been developed into ditopic receptors or they have been used as selective structural elements in molecular recognition using membranes.[11]

The aliphatic *viz.* salen moiety, instead of aromatic salophen, is often used to improve the solubility of the complexes to non-polar solvents; the structural modification does not affect their ability to act as receptor to anionic guests. The introduction of sidearms with amido functions into a salen moiety, as in **18 - 19** (Figure 14) improves the complexation power with Cl^-, HSO_4^-, NO_2^-, and SCN^-, and $H_2PO_4^-$ when compared to the core salophen structure **1,** because the amido H-atoms are capable of forming hydrogen bonds with the mentioned inorganic anions.

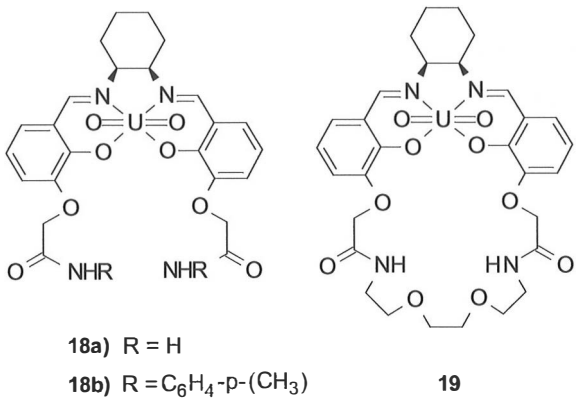

Figure 14 Uranyl amidosalen receptors **18 - 19** for inorganic anions.[54]

The binding constants for the core uranyl salophen **1**, its 3-methoxy derivative **17** and uranyl amidosalens **18 - 19** have been determined conductometrically (Table 1).[54] Increased preorganization and hydrogen bonding power leads to larger binding constants towards the anions mentioned above, the cyclic receptor **19** being the best receptor for all the anions except for HSO_4^-. For HSO_4^- the slightly more flexible receptor **18b** is the best receptor. For Cl^-, HSO_4^-, NO_2^-, and SCN^- the order of magnitude for the binding constant is from 28 to 12 000, dihydrogen phosphate binding being the best, $>5.0 \times 10^6$.[54]

Table 1 Conductometrically determined association constants for receptors **1, 17, 18** and **19**. d = Not determined due to low solubility of free ligand.[54]

anion	**1**	**17**	**18a**	**18b**	**19**
Cl^-	4.0×10^2	6.8×10^1	4.0×10^3	1.7×10^3	1.2×10^4
$H_2PO_4^-$	1.4×10^4	2.0×10^4	1.9×10^4	2.5×10^6	$>5.0 \times 10^6$
HSO_4^-	5.0×10^1	2.8×10^1	d	1.4×10^2	6.8×10^1
NO_2^-	3.1×10^2	6.7×10^1	8.3×10^2	4.5×10^2	1.5×10^3
SCN^-	5.0×10^1	1.4×10^1	d	7.1×10^1	d

Already in this study, a high selectivity of the dihydrogen phosphate anion to the uranyl salophens and salens compared to other common inorganic anions was observed. The binding constant is very high, 1.4×10^4, for the core uranyl salophen **1.** The introduction of the amido groups themselves into the salen moiety is not enough to improve the binding constant (K) for $H_2PO_4^-$, the value of K being the same for receptors **1, 17** and **18a**. Only when the receptor is at the same time highly preorganized, the binding will improve as with receptors **18b** and **19**. The binding strength and the selectivity towards $H_2PO_4^-$ remain high despite the structural modifications to the salen and salophen structures, as shown by Reinhoudt *et al.* for salophens **20 - 21** and salens **22 - 26** shown in Figure 15.[20]

The complexation of $H_2PO_4^-$ was studied both in the solid state and in the solution. All receptors shown in Figures 14 and 15 bind $H_2PO_4^-$. In the solid state different stoichiometries exist depending on the type of the additional binding site; in the DMSO-solution the ratio is 1:1.[55] The dimerization of hydrogen phosphates upon complexation was already known in the solution, but dimerization in the solid state had not been observed before. Receptor **17** complexed with $H_2PO_4^-$ crystallizes out as a 2:2 dimer, whereas receptors with an $-OCH_2C(O)NHR$ moiety (**18**, **19**) instead crystallize as 1:2 complexes.[55]

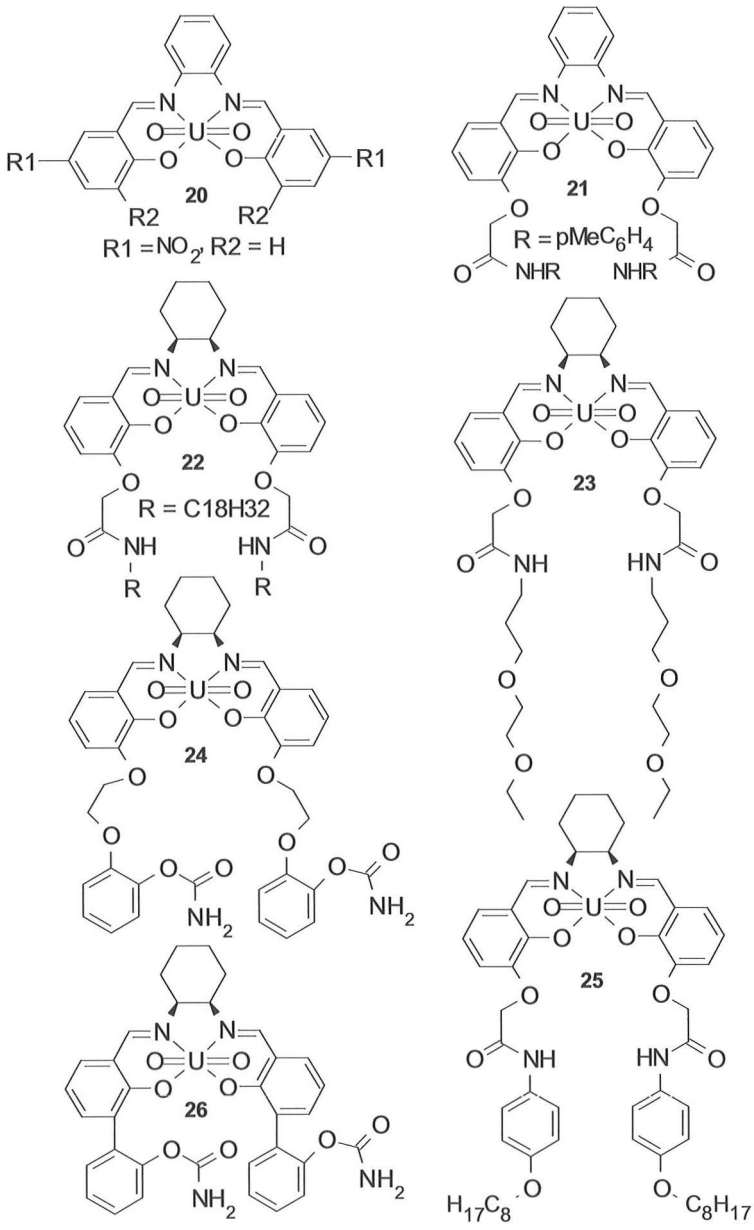

Figure 15 $H_2PO_4^-$-selective uranyl salophen (**20 - 21**) and uranyl salen (**22 - 26**) receptors.[20]

The normal salophen or salen molecule has two imine moieties, one on each side of the aromatic or aliphatic central part, and the resulting uranyl salophen or salen has only one empty site to bind a guest molecule. To be able to bind simultaneously more than one guest molecule Reinhoudt *et al.* designed and synthesized hemi-salophen compounds[20] such as **27** (Figure 16), which have two vacant coordination sites around the uranyl atom.

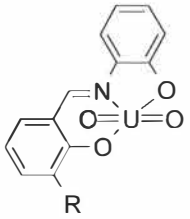

27a) R = H

27b) R = $OCH_2CONHC_6H_4pMe$

27c) R = $OCH_2CH_2OC_6H_4CONH_2$

Figure 16 Chemical structures of hemi-salophens **27**.[20]

As the receptors **27** now have two vacant positions for complexation with the guest, they bind two $H_2PO_4^-$ molecules at the same time. As mentioned above, the $H_2PO_4^-$ anions dimerize easily with each other via hydrogen bonding. With the simplest receptor **27a** with no "arms" this dimerization leads to a ribbon-like structure where there are two $H_2PO_4^-$ anions between the hemi-salophen structures (Figure 17).[20]

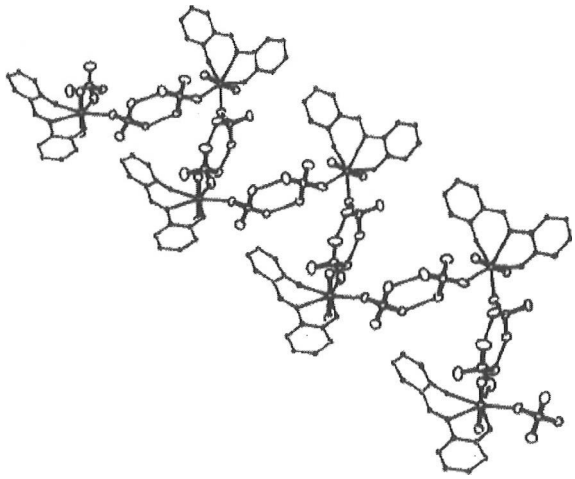

Figure 17 Crystal structure of the H-bonded ribbon of the complex **27a** and 2 x $H_2PO_4^-$. [20]

2.4.3 Recognition of ion pairs

After the complexation properties of the uranyl salophens towards the anionic guests were found, the development of ditopic receptors capable of binding both counter ions of the salt at the same time was initiated.[56-57] NMR titration methods for solution complexation studies were developed at the same time, allowing a reliable determination of binding constants. In many cases the anion binding is provided by hydrogen bonding[58-59] or coordination to the Lewis acid centers[60], and crown ether moieties or multidentate ligands containing oxygen donors are often used for cation binding.[61-62] For quaternary ammonium salts, crown ethers are however ineffective. From the earlier studies with the anions it is well known that chloride binds strongly to the uranyl dication.[54] Also π-π stacking of aromatic guests with aromatic pendant "arms" is known.[14] Mandolini and Rissanen were the first who reported the cation-π interaction[63-66] between aromatic pendants in the uranyl salophen and the cation moiety of quaternary

ammonium salts.[67] The interaction of uranyl salophens **1**, **9** and **28** (Figure 18) was studied towards guest molecules **29 - 36** shown in Figure 19.[68]

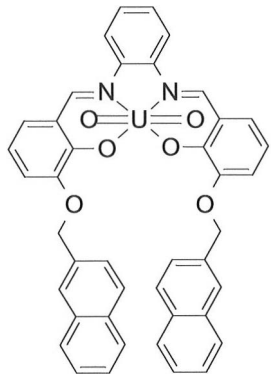

28

Figure 18 Ditopic uranyl salophen receptor capable of cation-π interaction with guest cations.[67]

Uranyl salophens **1**, **9** and **28** form very strong complexes with the ammonium salts shown in Figure 19. The core uranyl salophen **1** was used as a control receptor in this study. The binding constants were determined by NMR-titration technique and it was found that the stabilities of the complexes with the control receptor **1** were always lower than those with the side-armed receptor **28** and, with the sole exception of pyridium ions NMP and NMiQ, also lower than those with the receptor **9**, which demonstrates that cation-π interactions of the counter cation with the aromatic side arms significantly contribute to the complex stability in almost all cases. Binding constant values, with their error percents, for complexes of the quaternary ammonium salts with receptors **1**, **9** and **28** are shown in Table 2. Chloride salts bind best to uranyl salophen receptors.[68]

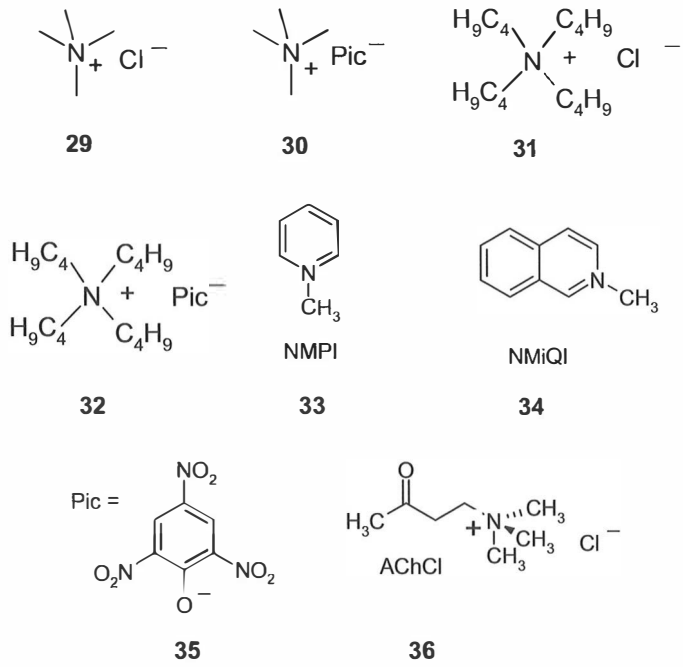

29 30 31 32 33 34 35 36

Figure 19 Chemical structures of the guest molecules studied with receptors **1**, **9** and **28**.[68]

Table 2 Binding constants (K, M^{-1}) for complexes of quaternary ammonium salts with receptors **1**, **9** and **28**.[68]

Salt	**1**	**9**	**28**
TMACl	1000 ± 130	13 600 ± 600	28 000 ± 2000
TMAPic	350 ± 40	660 ± 40	950 ± 80
TBACl	5400 ± 500	22 000 ± 3000	23 000 ± 1800
TBABr	100 ± 20	930 ± 90	1200 ± 180
TBAI	30 ± 4	270 ± 70	190 ± 40
AChCl	660 ± 600	19 000 ± 2600	42 000 ± 5000
NMPI	110 ± 20	130 ± 30	500 ± 100
NMiQI	120 ± 40	110 ± 30	800 ± 120

The TMACl, TBACl and (ACh)Cl complexes of receptors **9** and **28** have binding constants over 10 000. The values of the binding constants are also high (1000 ± 130, 5400 ± 500 and 6600 ± 600 respectively) with the control receptor **1**.[68]

With TBABr the binding constants were much lower (around 100 for receptors **1**, **9** and **28**) and with TBAI even lower. Picrates bind with about the same strength as bromides. Crystal structures of the receptor **9** and **28** complexes show that the binding is mediated by cation-π interactions and simultaneously by weak CH···O/Cl hydrogen bonds to the phenolic oxygen of the ligand and the chloride anion coordinated to the uranium. Crystal structures of receptor **9** with TMACl and TBACl are shown in Figure 20, where the complexes are depicted as 1:1 complexes for the sake of clarity. In the crystalline state, however, the TMACl forms 4:4 assemblies with receptors **9** and **28** (Figure 21), while TBACl forms 2:2 assemblies. In the TMACl complexes four chloride-bound receptors fully enclose four cations inside a tetrameric capsule-like assembly.[68]

Of the pyridium salts studied, only NMP forms a complex with receptor **9** and crystallizes as good quality single crystals (Figure 22). The crystal structure reveals a 1:1 complex where the NMP cation is offset face-to-face π-stacked with one aromatic side arm of the receptor.[68]

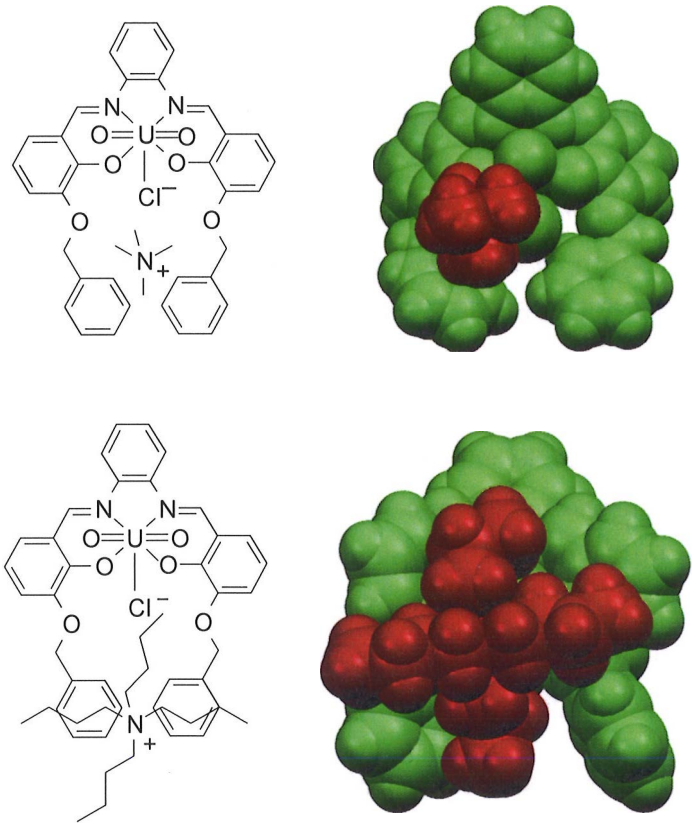

Figure 20 The chemical and crystal structures of **9•29** (top) and **9•31** (bottom) as CPK models.[67]

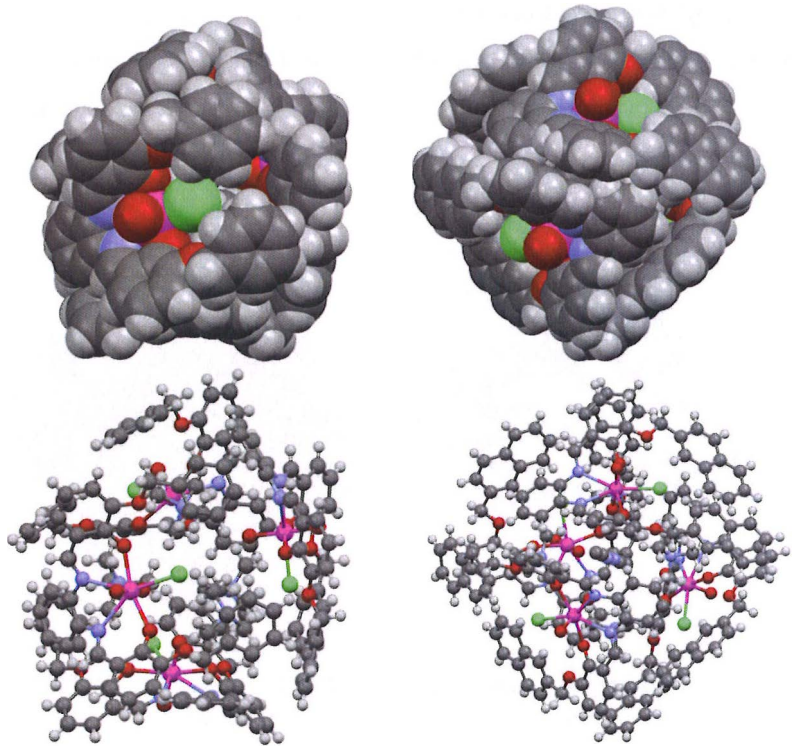

Figure 21 The 4:4 assemblies of **9•29** (left) and **28•29** (right).[68]

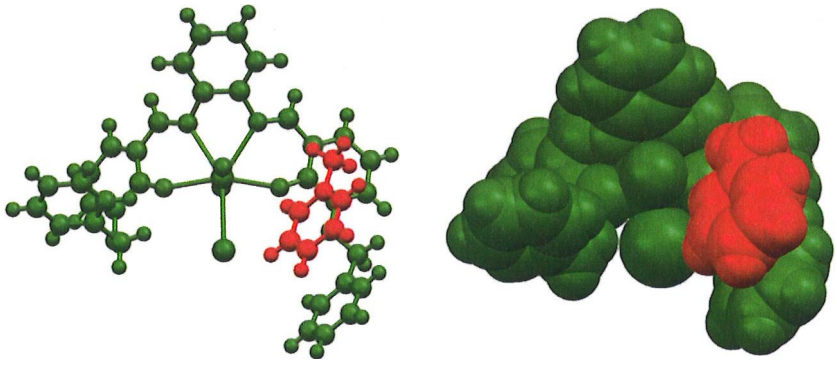

Figure 22 The crystal structure of monomeric 1:1 complex of receptor **9** and an NMP cation.[68]

The core uranyl salophen **1** crystallizes as a 6:6 assembly with TMACl, as shown in Figure 23. The solid state assembly is a star-like structure where the cavity formed by the six chlorine atoms is occupied by disordered acetonitrile molecule.[68]

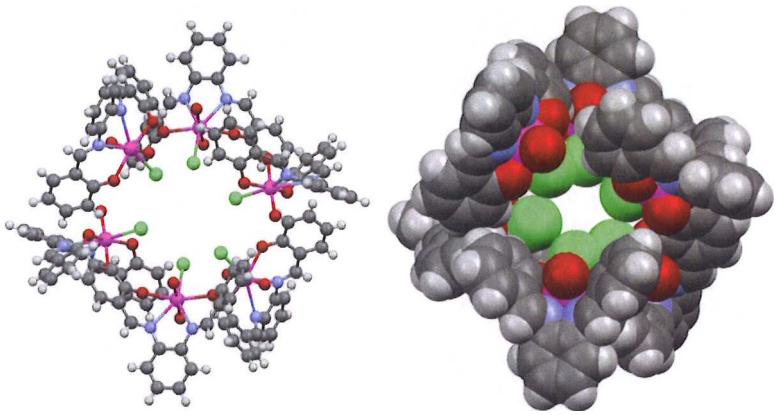

Figure 23 The solid state 6:6 assembly of **1•29**.[68] The disordered acetonitriles in the cavity were removed for clarity.

Acetylcholine is a neurotransmitter and hence a biologically important molecule and an important target in molecular recognition studies. Receptor **28** crystallizes with acetylcholine as a dimer where two acetylcholine units are joined by weak interactions (Figure 24).[68] In the crystal the dimers form a layerlike assembly where dimeric acetylcholine pairs are arranged in rows due to π-π stacking of the naphthalene sidearm to the naphthalene sidearm of the adjacent receptor.[68]

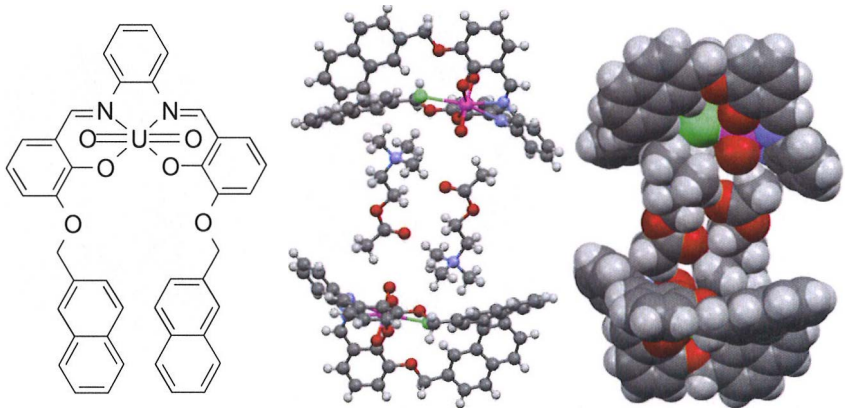

Figure 24 Molecular structure and the 2:2 assembly in the crystal of **28**•**36**.[68]

Alkali metal cations are chemically and biologically relevant and hence the cation-π interactions of alkali metal cations and host molecules are of wide interest.[69-72] Similarly to the quaternary ammonium cations, the uranyl salophens with aromatic sidearms are capable of binding rubidium, cesium and potassium as chlorides and fluorides by cation-π interactions.[73] RbCl, CsCl and CsF all form structurally similar 2:2 complexes with receptor **9** (Figure 25) In the dimers, Rb and Cs cations are coordinated to the six oxygens, three from each receptor. Additionally, each metal cation is coordinated to both halide ions and to two aromatic sidearms, one from each receptor.[73]

Because of the smaller size and more electronegative nature of fluoride compared to chloride, a cavity inside the dimer is larger and in the crystal structure of CsF it is occupied by an acetonitrile molecule. When the salophen structure is changed to salen, the molecule is not so preorganized anymore. The less ordered structure of the salen version compared to the salophen is evidenced by the crystal structures of their salt-free methanol complexes, in which methanol is coordinated to the uranyl center.

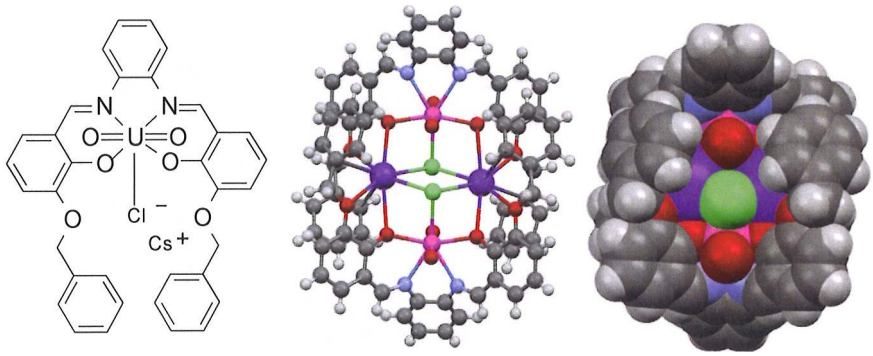

Figure 25 The chemical structure and the dimeric assembly of **9**•CsCl.[73]

In salophen the side arms are turned inward in a quasimacrocyclic arrangement that encloses the methanol guest, while in salen the conformation is more open and the side arms are completely turned away from the core of the receptor. This causes different salt coordination properties of the uranyl salen receptors compared to the salophens shown above. In the crystal structure of the salen version of receptor **9** with CsF two uranyl salen complexes form a dimeric 2:2 arrangement (Figure 26) mediated by the coordination of two cesium cations to two receptors.[74] In contrast to the salophen analogue, in the salen complex only one sidearm of each receptor is in contact with cesium. The second side arm is bent outward from the interior of the dimer and chloroform (used as crystallization solvent) is CH···F hydrogen bonded to the fluoride. This hydrogen bonding orients the chloroform toward the interior of the dimeric assembly and keeps it in close proximity to the cesium cation, to which it is coordinated via a chlorine atom. This unusual Cl···Cs solvent ligation completes the coordination sphere of the cation, which in the case of salophen analogue is filled with cation-π interactions to two aromatic side arms. Organochlorine ligation to an alkali metal ion of this type is extremely rare.[74]

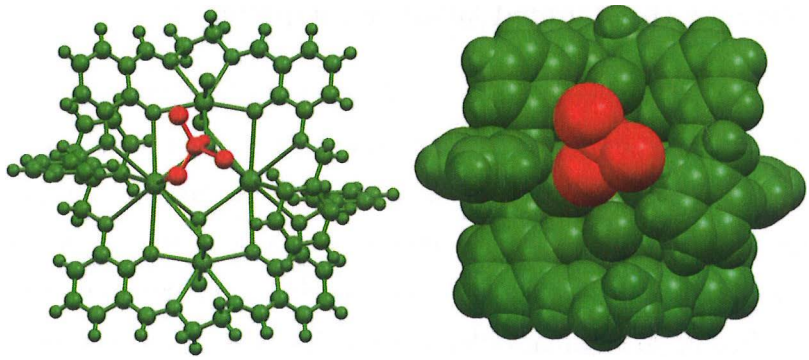

Figure 26 Crystal structure of the dimeric assembly of salen version of receptor **9** with CsF.[74]

An asymmetric receptor **37** with only one phenyl methoxy sidearm also crystallizes with CsCl with two receptors binding one salt molecule.[73] In the crystal this complex exists as a 4:2 assembly. In the structure shown in Figure 27, one receptor binds chloride and another binds a methanol molecule (which was used as a solvent in crystallization), and both participate in cesium complexation. Two dimers of this kind of form a capsule-like arrangement in which both CsCl molecules are enclosed inside the capsule.[73]

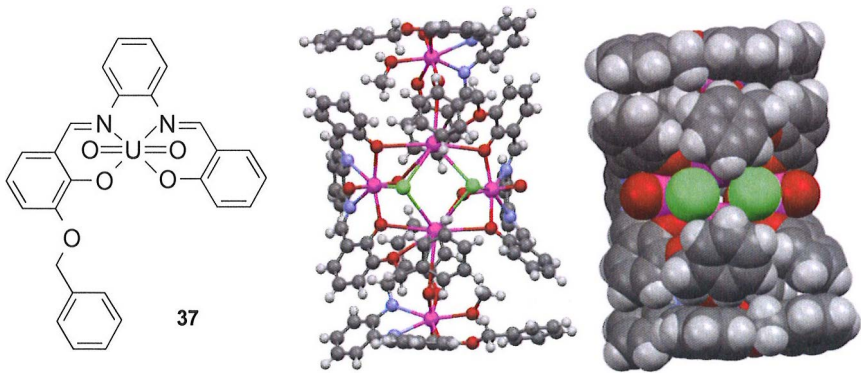

Figure 27 The chemical structure and the 4:2 assembly in a crystal of **37**•CsCl.[73]

2.5 Inherently chiral uranyl salophen complexes

The expression "inherently chiral" was first introduced by Böhmer to indicate calix[4]arenes with an XXYZ or WXYZ substitution pattern at the upper rim of the calixarene structure.[75] According to Dalla Cort, nonsymmetrical uranyl salophens can be related to such calixarenes because of flipping of a curved uranyl salophen unit that, due to an easy rotation around the bonds connecting the phenolic units to the imine carbons (Figure 28), exists as a pair of enantiomers in a solution.[76] In these uranyl salophens the uranium ion is not a stereogenic centre[77] in a strict sense, but because of its steric bulk it distroyes the symmetry of the entire structure thereby forcing curvature into an otherwise planar ligand. This kind of inherent chirality arises from the introduction of curvature into an ideally planar structure that lacks symmetry axes in its bis-dimensional representation. Such a curved structure is chiral in a two-dimensional but not in three-dimensional space because the plane on which it lies is itself a symmetry plane.[76]

Figure 28 The flipping of the phenol rings in uranyl salophen.[13]

According to molecular models the flipping motion is resisted by van der Waals interactions between the hydrogen atoms shown in Figure 28 because these hydrogens are required to pass each other. By substituting these hydrogens with one or more bulky substituents the flipping can be prevented.[13] Compounds **38** and **39** shown in Figure 29 are shown by temperature dependent NMR studies to

exist as a pair of enantiomers in the solution. In the case of the compound **40** the flipping is not prevented and it is too fast in the NMR time scale to observe the different enantiomers.[13]

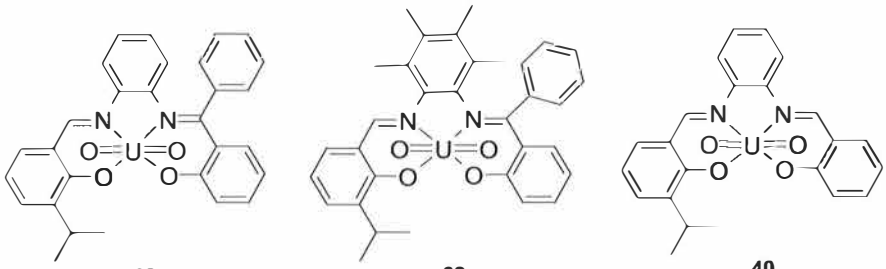

Figure 29 Inherently chiral uranyl salophens **38 - 40.**[13]

A resolution of the enantiomers by chromatography is however impossible because, unlike sterically unhindered uranyl salophens, these compounds do not tolerate chromatographic treatment. However a uranyl salophen with one (*S*)-naproxen sidearm **41** (Figure 30) forms a diastereoisomeric mixture that can be resolved by crystallization.[78] Slow diffusion of di-isopropyl ether into the solution of compound **41** in chloroform gives only one diastereoisomer in high purity. While a solid sample of isolated diastereoisomer of compound **41** is configurationally stable for at least one month at room temperature, a slow epimerization takes place in the solution.[78]

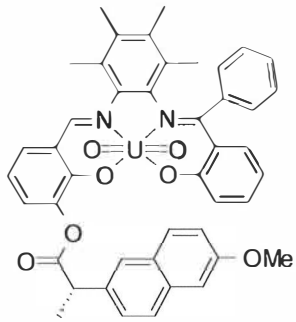

41

Figure 30 Uranyl salophen with one (*S*)-naproxen side arm.[78]

As mentioned above, sterically hindered uranyl salophens do not tolerate chromatographic purification. Instead the complex breaks down to a free uranyl cation and the free ligand. This is due to the internal strain caused by the curvature of the complex that reduces the strength of the bonding between the uranyl cation and the ligand. An analysis of calculated structures of uranyl salophens shown in Figure 29 demonstrates that compounds with steric hindrance in the imine bonds region, such as **38** and **39,** are more distorted than the unhindered ones. This is probably the reason for the decreased thermodynamical stability of the complexes and their chromatographic lability. Without the uranyl cation the free salophen ligand will have a very different conformation and in polar solvents such as DMSO both *cis* and *trans* isomers exist.[79] In apolar solvents such as benzene the *cis* conformer is destabilized with respect to the *trans* one. *Ab initio* computed stuctures of *cis* and *trans* conformers of compound **39** shown in Figure 29 without the uranyl cation are shown in Figure 31.[79]

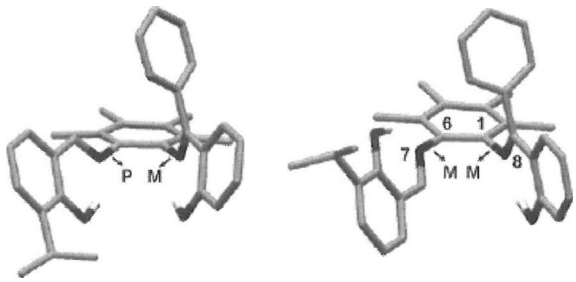

Figure 31 Ab initio calculated structures of the *cis* and *trans* conformers of compound **39.**[79]

A comparison of the height of the barrier for the salophen diastereoisomers with or without the uranyl shows that coordination to the metal center increases significantly, albeit not dramatically, the stereochemical stability of the ligand.[79]

The ability of the uranyl salophens to bind neutral and anionic guest molecules is well known and it was discussed briefly earlier in this text. Besides the Lewis acidic uranyl center, phenyl groups as additional interaction sites have been shown to be important in binding guest molecules via π-π and cation-π interactions.[68] Adding chirality to the salophen skeleton should lead to receptors which should be able to exhibit chiral recognition. Indeed the inherently chiral uranyl salophen **42** is capable of recognizing chiral neutral and charged molecules **43 - 46** shown in Figure 32.[80] The formation of the diastereomeric host-guest complex was studied by ^{1}H NMR. The enantioselectivities obtained with receptor **42** towards α-methylbenzylamine **43**, 1-(2-naphthyl)ethylamine **44**, methyl-p-tolylsulfoxide **45**, and N,N –dimethyl-α-methylbenzylammonium chloride **46** in the configurations shown in Figure 32 were encouraging. A rasemic mixture of receptor **42** shows different binding affinities towards the two enantiomers of the guest.[80]

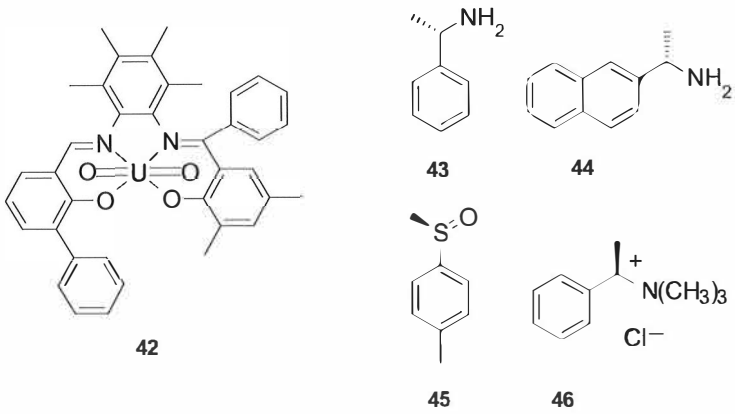

Figure 32 The chemical structures of inherently chiral uranyl salophen receptor **42** and the chiral neutral and charged guest molecules **43 - 46.**[80]

The nonsymmetrical inherently chiral uranyl salophen complexes **42+43-46** dissociate upon chromatographic treatment. By linking the oxygen atoms in the *para*-positions (position 5) with respect to the phenolic oxygens by a polymethylene chain leads to configurationally stable macrocyclic uranyl salophens.[81] Three macrocyclic uranyl salophen complexes **47 - 49** shown in Figure 33 can be synthesized in good yields and purified by normal column chromatography (silica gel). Compounds **48** and **49** can also be resolved into their enantiomers by chiral HPLC. The best chain lengths are those that fit the distance between the 5-position at the phenolic rings without altering the natural curved geometry of the parent uranyl salophen compound. According to calculations, -$(CH_2)_{12}$- and -$(CH_2)_{13}$- chains are the best. To adopt this ideology, stable inherently chiral macrocyclic uranyl salophens **50 - 52** (Figure 33) have been synthetised by Dalla Cort and Mandolini.[82] The calculated structure of the cyclic uranyl salophen **52** is shown in Figure 34.[82]

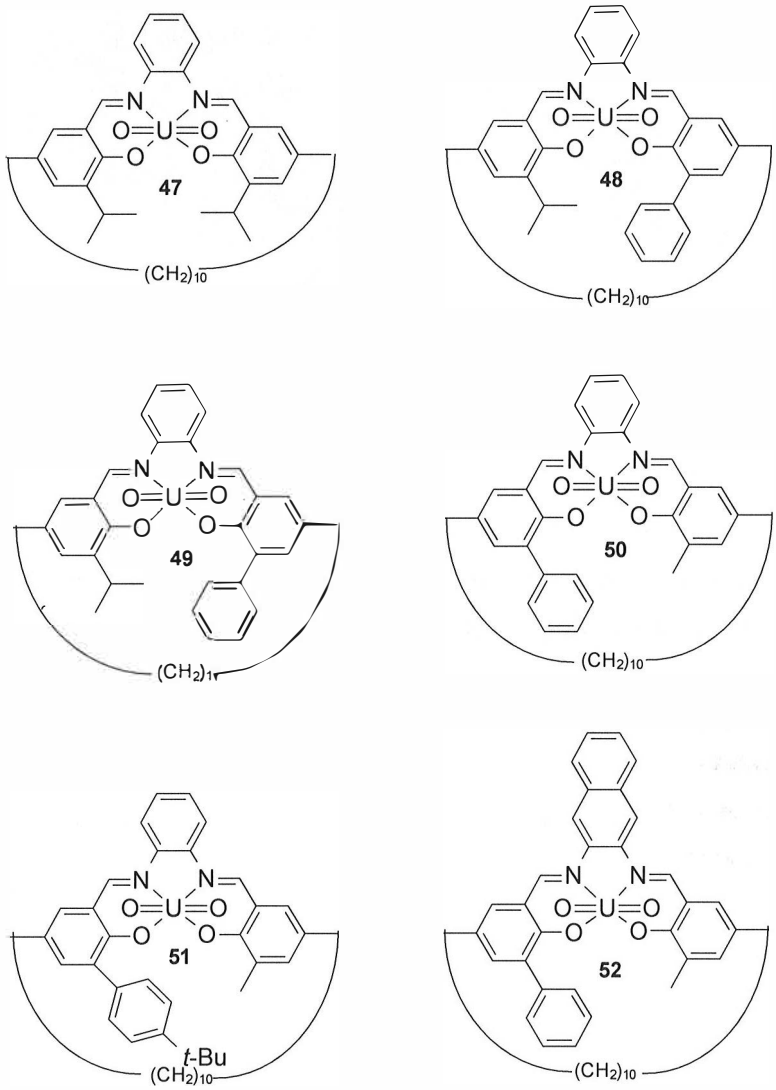

Figure 33 Chemical structures of cyclic uranyl salophens **47 – 52**.[81-82]

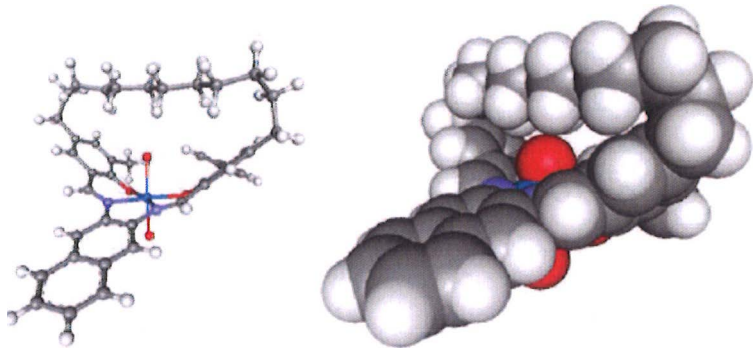

Figure 34 Calculated structure of cyclic uranyl salophen **52.**[82]

Compounds **50-52** (Figure 33) were synthesized to have more configurationally stable macrocyclic uranyl salophens. However, when the temperature of the HPLC column was raised to 80 °C, it was noticed that compound **50** showed flipping of the phenol rings. This flipping can not just be a result from a slightly different structure since compounds **51** and **52** also show the same dynamics. These compounds are stable under chromatographic conditions; hence a dissociation-reassociation process in which the ligand releases the uranyl cation, undergoes free conformational changes, and eventually recombines with the metal, is excluded. Also a simple jump rope-type movement can be excluded because of the strongly hindered structures of compounds **51** and **52**. Although unprecedented for the Schiff base $N_2O_2^{2-}$ tetradentate ligands, hemilability in the complexes **50 - 52** offers a unique key to the intriguing problem of the enantiomerization mechanism.[82] Hemilability of the bidentate or polydentate ligands with metal centers suggests a process where the weakest coordinative bond in a chelate structure undergoes a dissociation process. If the free donor atom of the ligand is easily re-coordinated to a metal ion, the process becomes reversible.[83-85] The proposed mechanism for the uranyl salophens is shown in Scheme 4.[82] At present, there are no conclusive experimental observations to

definitely support either path A or path B in Scheme 4, but there is a hypothesis that the enantiomerization of the inherently chiral uranyl salophen macrocyclic complexes originates from the ligand hemilability.[82]

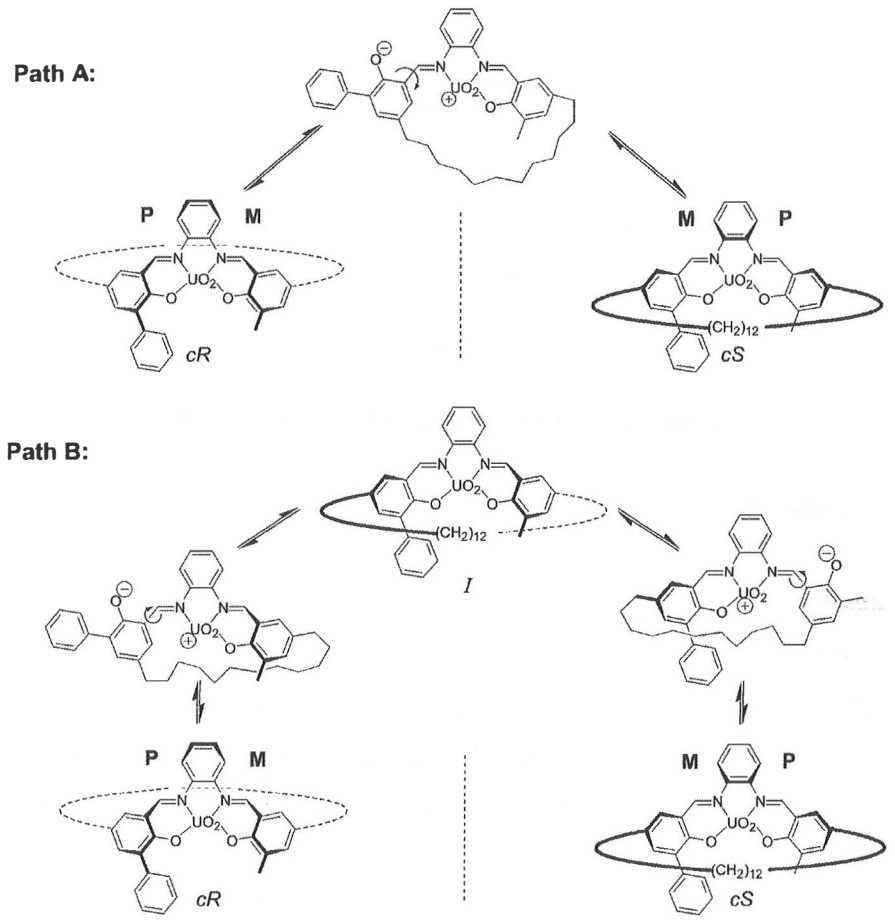

Scheme 4 Enantiomerization of uranyl salophen based on ligand hemilability via a one-step mechanism (path A) and via a two-step mechanism (path B).[82]

A more rigid spacer in compound **53** shown in Figure 35 destabilizes the intermediates involved in the enantiomerization process (Scheme 4) and

therefore extendts the enantiomerization half-life so much that the use of uranyl salophen complexes in enantioselective recognition and catalysis might become possible.[82]

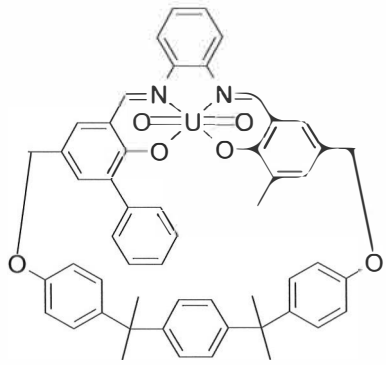

53

Figure 35 Uranyl salophen with a rigid spacer.[82]

2.6 Applications

2.6.1 Uranyl salophens as catalysts

Salophen and salen structures with other metal cations than uranyl, such as Mn^{2+}, have been widely used as catalysts.[86] The hard Lewis acid character of the uranyl center in the salophen complexes has however been exploited in catalytic studies of reactions of carbonyl compounds. The Lewis acid center together with an attractive van der Waals interaction of the guest with the walls of the cleft-like salophens **55** and **56** (Figure 36) catalyzes a conjugate addition of benzenethiol to cyclic and acyclic ketones,[87] Michael addition[88] and Diels-Alder reactions[89] with a high turnover efficiency. The cleft-like salophens have a high degree of substrate specificity compared to core uranyl salophen **1** and its derivative **54**. These catalysts mimic the behavior of a metalloenzyme in that they first bind the

substrate and then promote the reaction to it. A release of the reaction product followed by the preferential binding to another substrate molecule ensures the onset of a catalytic cycle with a high turnover efficiency.[87-89]

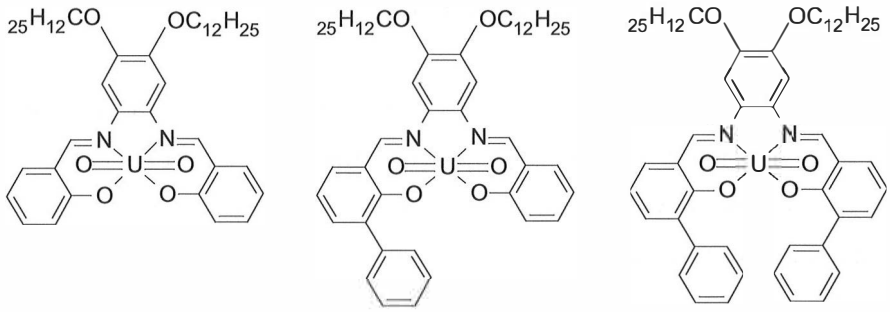

54 **55** **56**

Figure 36 Uranyl salophens that catalyze the conjugate addition of benzenethiol to cyclic and acyclic ketones,[87] Michael addition,[88] and Diels-Alder reactions.[89]

The most carefully investigated reaction has been the conjugate addition of benzenethiol to cyclic and acyclic ketones co-catalyzed by tertiary amines (Scheme 5).[87] All uranyl salophens shown in Figure 36 can act as catalysts in

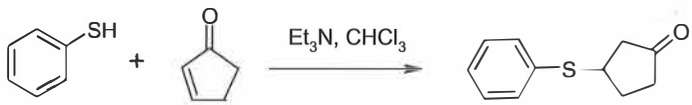

57 **58** **59**

Scheme 5 The conjugate addition of benzenethiol to cyclic and acyclic ketones co-catalyzed by a tertiary amine.[87]

this reaction, the cleft-like compound **56** being superior to compounds **54** and **55** because of its higher degree of specificity and the passive binding due to the van der Waals interaction with the aromatic side arms, giving the reaction of

benzenethiol with 2-cyclopentenone a 420 fold reaction rate compared to the reaction without it. The half-cleft compound **55** makes the catalyzed reactions much less sensitive to the adverse influence of steric effects. There is no large difference between the compounds **54** and **55** in catalytic effects except when using saturated solutions of compound **55**.[87]

In the reaction shown in Scheme 5 the Brönsted base activates the thiol nucleophile while the metal centre provides the enone electrophile with Lewis acid activation through coordination of the carbonyl oxygen to the fifth equatorial coordination site. The reaction proceeds via the activation of the enone by the uranyl salophen catalyst by binding the oxygen atom of the enone, followed by an addition reaction and release of the addition product. Fairly high reaction rates with a high turnover efficiency and low product inhibition are accompanied by a high degree of substrate specificity, which is lacking in the reaction solely catalyzed by amines or by combination of an amine and the unsubstituted core uranyl salophen. The reaction with ketones **58** and **60 - 64** shown in Figure 37 has been studied.[90-91] The α,β-unsaturated ketones are stronger Lewis bases than saturated ketones because of the strong conjugation of the double bond with the carbonyl group; therefore α,β-unsaturated ketones bind more strongly to the uranyl center. The reaction rates of cyclic and acyclic enones are very similar. The only significant difference between the cyclic and acyclic ketones is that unlike the cyclic ketones, the ethyl vinyl ketone does not form a significantly stable complex with the core uranyl salophen **1** and neither does its addition product. No major differences of a mechanistic nature for conjugate thiol addition to the cyclic or acyclic nature of the enone reactant are found. The interaction of the ketone guest with the aromatic cleft walls reinforces the binding.[90]

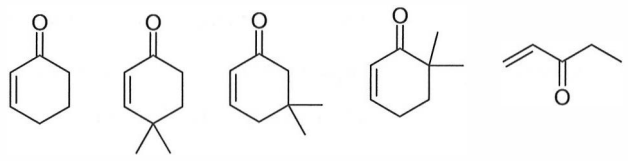

60 **61** **62** **63** **64**

Figure 37 The α,β-unsaturated ketones used in reaction catalyzed by uranyl salophens.[90]

The relative catalytic efficiency of ethyldimethylamine, triethylamine and quinuclidine is essentially related to the differences in their base strength, both in the reactions with and without uranyl salophen catalysis. The size of the base has little or no influence on the reaction rates.[92]

The reaction of methyl 1-oxoindane-2-carboxylate **65** with methyl vinyl ketone **66** is a Michael addition reaction (Scheme 6) that is catalyzed by uranyl salophens.[88] Unlike the conjugate addition of benzenethiol to cyclic and acyclic ketones, this reaction is not catalyzed by the core uranyl salophen **1** and its derivative **54**, but requires the aromatic walls of the cleft-like salophens and is catalyzed with a high turnover efficiency by the phenyl-substituted half-cleft uranyl salophen **55**. The dodecyloxy chains added to 1,2-diaminobenzene moiety of the salophen increase the solubility of the catalyst in chloroform.[88]

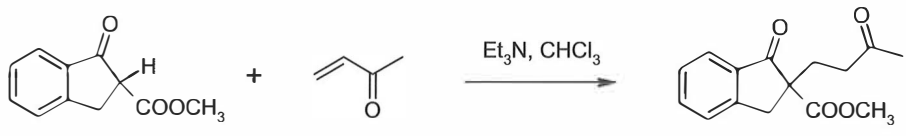

65 **66** **67**

Scheme 6 The uranyl salophen-catalyzed Michael addition reaction of methyl-1-oxoindane-2-carboxylate **65** with methyl vinyl ketone **66.**[88]

Unlike the benzenethiol additions this reaction does not occur with cyclic enones. The much higher reactivity of the open chain enones is to be ascribed to the activation of the enone carbonyl through hydrogen bonding with the neighboring protonated base. A necessary prerequisite for a concomitant nucleophile attack at the β-carbon and hydrogen bonding to the carbonyl oxygen is the s-*cis* conformation of the enone reactant, obviously available for the methyl vinyl ketone, but not for the 2-cyclopentenone (Scheme 7).[88]

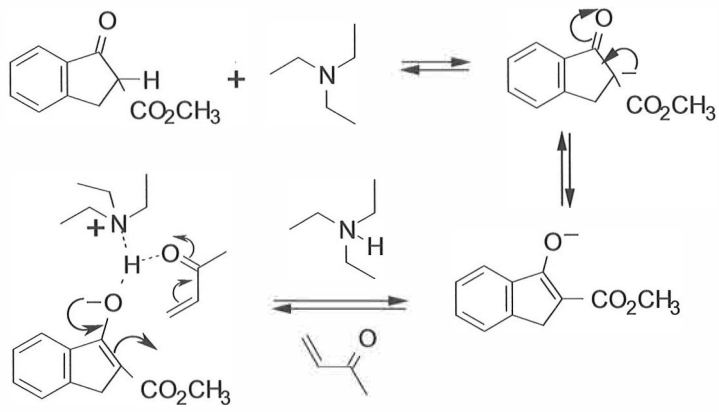

Scheme 7 Proposed mechanism for tertiary amine-assisted addition of methyl 1-oxoindane-2-carboxylate **65** to methyl vinyl ketone **66.**[88]

In the Michael addition reaction the catalysis proceeds via a different mechanism compared to the thiol addition. In this reaction both reactants and the product are all bound to the uranyl salophen. In the proposed mechanism the activation of the Michael acceptor arises from hydrogen bonding between the enone carbonyl and the Et_3NH^+ countercation bound to the salophen framework by means of cation-π/CH-π interactions, as well as by means of a cation – anion electrostatic attraction of the β-ketoester and the uranyl cation (Figure 38).[88]

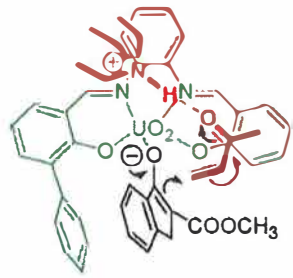

Figure 38 Schematic representation of the proposed mechanism for the addition of methyl 1-oxoindane-2-carboxylate **65** to methyl vinyl ketone **66** catalyzed by uranyl salophen **55.**[88]

Diels-Alder additions of the enone dienophiles are well known to be sensitive to Lewis acid catalysis. The half-cleft compound **55** with dodecyloxy chains behaves as a supramolecular Lewis acid catalyst offering the aromatic sidearm for weak interactions to bind the guest molecule.[89] The core uranyl salophen **1** and its derivative **54** do not catalyze this reaction. The half-cleft salophen is used because the binding efficiency of it is comparable to the cleft-like compound **56**, but with only one sidearm the other face of the bound benzoquinone used in this reaction is available for the reaction with the diene (Scheme 8). The rate of the addition is significantly enhanced by the presence of compound **55**, whereas the core salophen **1** and its derivative **54** have a negligible influence.[89]

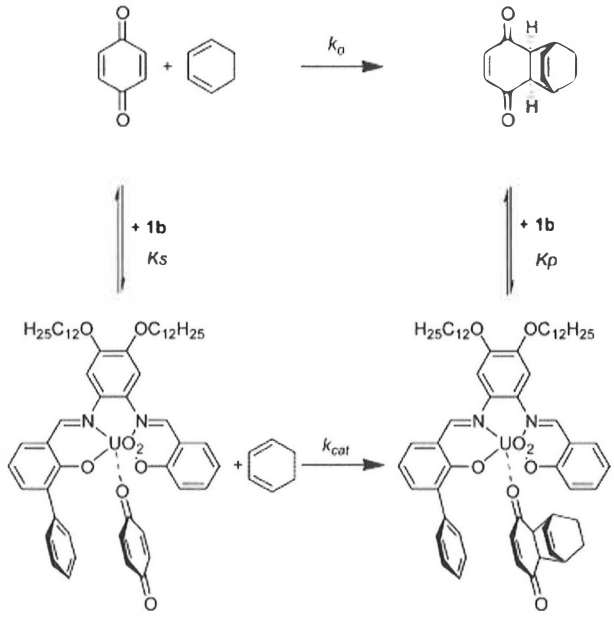

Scheme 8 Diels-Alder addition of benzoquinone to 1,3-cyclohexadiene. Complexation catalysis involving non-covalent binding of benzoquinone to catalyst **55.**[89]

The uranyl cation also plays a role as an electrophilic catalyst in an ester cleavage reaction.[93] This ester cleavage reaction is a base-induced methanolysis or ethanolysis, the latter being the faster reaction when catalyzed by uranyl compounds. In a studied reaction the ester group is situated in a macrocycle containing also a uranyl salophen moiety **68** (Scheme 9). In the alcoholysis reaction the alkoxide ion is first bound by the uranyl cation. The negative charge is transferred from an incoming alkoxide to the ester carbonyl. The oxygen atom of the ester carbonyl becomes a much better donor (stronger Lewis base) in the transition state than in the initial state. Hence, the uranyl center offers electrophilic assistance to the alkoxide ion for the reaction to happen. The reaction rates with the uranyl salophen and with a reference compound **70** were

determined. In the ethanol solution the observed rate accelerations caused by the uranyl centre increased regularly from 9-fold for n = 4 to 310-fold for n = 2 compared to reference compound **70**, which points to a definite role played by the spatially close uranyl centre as a Lewis acid catalyst. Much smaller rate accelerations are observed in methanol solutions.[93]

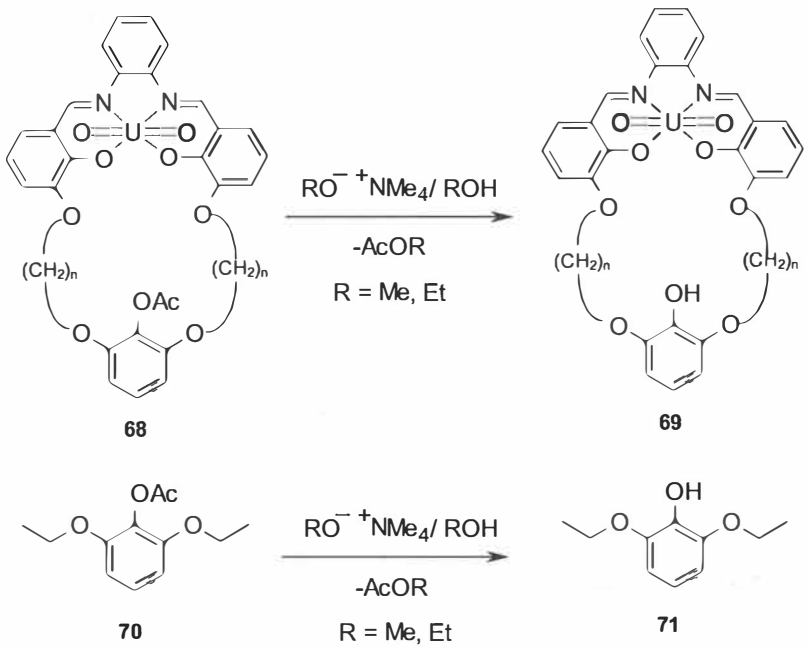

Scheme 9 Base-induced methanolysis or ethanolysis reaction catalyzed by uranyl cation.[93]

2.6.2 Membrane studies

Natural membranes are fluid mosaics of lipids, proteins and carbohydrates, and the traffic across the membrane is either passive diffusion or active transport.[94] In order to mimic these membranes artificial membranes have been developed.[95] These membranes can work either as sensors or filters.[96-98] Anion-sensitive

artificial membranes are usually made of plasticizers and polyvinyl chloride (PVC) and their selectivity pattern follows the Hofmeister series (ClO_4^- > SCN^- > Br^- > NO_2^- ≈ NO_3^- > Cl^- > F^- > AcO^- > HPO_4^{2-} > SO_4^{2-}) which is related to the negative values of the free energies of hydration of the anions, favoring lipophilic anions with a low hydration energy. However, if the membrane contains, in addition to the anion-exchange sites, sensor molecules that are able to bind specific anions, the membrane may become selective towards those anions.[99-100] As the uranyl salophens are shown to be good receptors for anions, they are also observed to function as sensors in membranes. The binding selectivity of the sensor can be influenced by substituents near the uranyl binding site of the sensor component. They will influence the electron density of the uranyl center or, the lipophilicity of the binding cleft or they can provide sites for hydrogen bonding.[99]

Ions attached to the membrane are usually detected by potentiometric techniques. Potentiometric detection of the ions can easily be achieved by modifying ion-selective electrodes (ISE)[101-102] or chemically field effect transistors (CHEMFET)[103] with an ion-exchange membrane. An ion-selective electrode produces a measurable potential that is proportional to the concentration of an analyte. CHEMFETs are very small electronic devices fabricated in silicon that are designed to detect and quantify the presence of a chemical species in a given environment.

A membrane containing 1 wt.% of sensor, 66 wt.% of plasticizer [bis(1-butylpentyl) adipate = BBPA] and 33 wt.% of PVC, using the uranyl salophens shown in Figure 39 as sensors, is a good composition for a nitrite sensing ion-selective electrode (ISE).[99] Selectivity coefficients determined reveal that these PVC/BBPA ISEs with sensors **72 - 76** and core uranyl salophen **1** are highly

selective towards nitrite over all other anions (except perchlorates). This effect is most pronounced for sensors **72** and **75**, sensor **72** being the most selective.

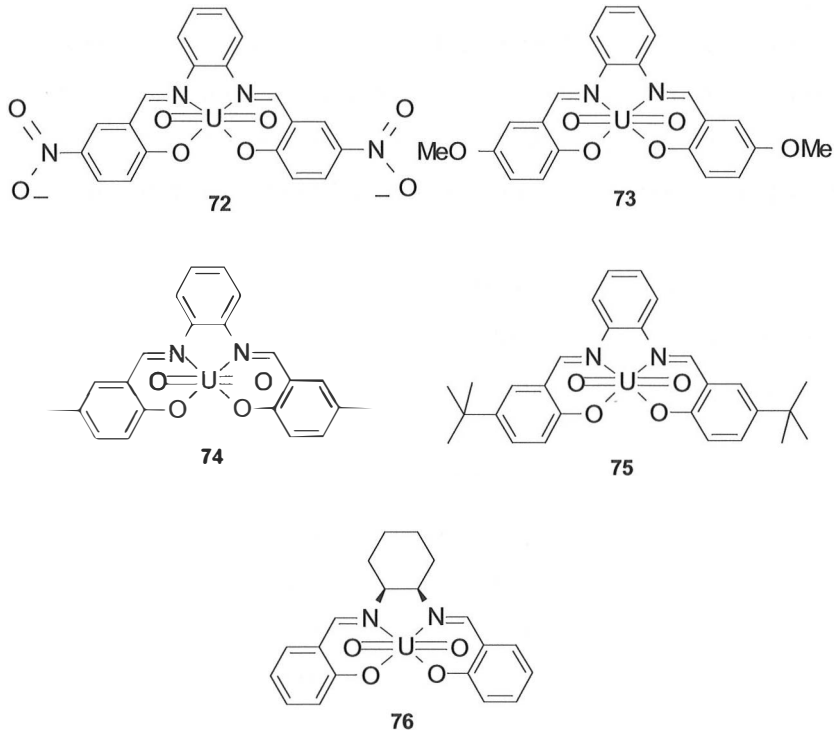

Figure 39 Sensors for nitrite-selective membranes.[99]

This highest selectivity for nitrite of sensor **72** can be explained by the presence of an electron-withdrawing substituent present in **72**, other compounds instead containing electron donating groups or a hydrogen atom. Electron-withdrawing substituents increase the Lewis acidity of the uranium atom improving the complexation of the nitrite anion, which is a relatively hard Lewis base.[99]

The sensor complexes shown in Figure 39 are polar and hence they are not easily soluble in PVC-membranes, the cyclohexyl salen derivative **76** being the best soluble. If the plasticizer is changed to more polar o-nitrophenyl *n*-octyl ether (o-NPOE) to make the membrane more polar, the selectivity towards NO_2^- over ClO_4^- and Br^- is lowered. Another option to make more polar membranes is to add ammonium salts to the membrane. Already a low amount (10 mol%) of the lipophilic ammonium salt makes the membrane sufficiently polar to dissolve the uranyl salophen sensors shown above. Lipophilic salts with different sizes added to the PVC/BBPA/sensor **72** membrane have been studied and in contrast to the membranes without salts, selectivity for nitrite over perchlorate is observed. The best selectivity is found with a membrane containing 10 mol% of tridodecylmethylammonium chloride.[99-100]

Phosphorus is a key nutrient in living organisms and it is involved in several biological and environmental processes[104-106] and hence there is a need for good phosphate sensors. Fluoride anion is also of great interest in sensor research because of its high levels in municipal water supplies and dental hygiene products.[107-109] PVC membranes plasticized with 65 wt % of o-NPOE and containing 1 wt % of one of the uranyl salophen receptors **54**, **77** or **78** (Figure 40) and 20 mol% tetraoctylammonium bromide (with respect to the receptor) show a high selectivity for either dihydrogen phosphate[110-113] or fluoride[114] depending of the sensor chosen.

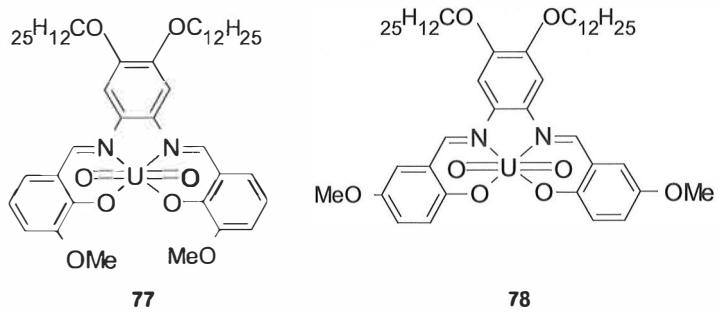

Figure 40 Sensors for phosphate-selective membranes.[110]

The lipophilic core uranyl salophen structure **54** in the membrane renders the sensor sensitive and selective for hydrophilic monovalent dihydrogen phosphate over many other and much more lipophilic anions, and this sensor can be successfully applied in CHEMFETs with the selectivity towards this hydrophilic anion.[110] This sensor is 20 times more sensitive to $H_2PO_4^-$ over nitrate, which was used as one control anion in this study. This is in strong contrast with normal ion-exchange sensors, where the situation is reversed. In the presence of methoxy substituents in the uranyl salophen derivative **77** the additional hydrogen bond formation of an $H_2PO_4^-$ anion towards the methoxy groups enhances the sensitivity and selectivity for $H_2PO_4^-$ in the presence of halides and sulfate. The presence of electron-donating methoxy substituents however reduces the electrophilicity of the uranyl center thereby affecting its anion binding strength. This electronic effect causes the reduced selectivity of the "hard" $H_2PO_4^-$ over the "softer" nitrate anion. The detection limit for $H_2PO_4^-$ is lowered and selectivity over halides is improved. The sensor **78** can not form additional hydrogen bonds with $H_2PO_4^-$. This results in a reduced selectivity for $H_2PO_4^-$ over nitrate.[110-112]

A fluoride anion is a strong hydrogen bond acceptor and this makes the ion very hydrophilic and difficult to extract into organic media. Fluoride selectivity is

observed with uranyl salophens with hydrogen bond donating sites in a close proximity to the uranyl centre that itself has a strong interaction with the fluoride anion.[113]

Fluoride anion is selectively sensed over many lipophilic anions by the simple uranyl salophen receptor **54** (Figure 36). Only nitrate ions interfere when present at equal or higher concentrations. In the methoxy derivative **77** the selectivity toward fluoride is improved over larger chloride and bromide ions. The presence of acetamido groups (Figure 41) reduces the $H_2PO_4^-$ binding strength, but these hydrogen bond donating substituents induce an excellent fluoride sensitivity and selectivity. All the amido substituted uranyl salophen sensors **79 - 83** (Figure 41) in the membranes show increased selectivity towards fluoride. The more lipophilic is the receptor, the better selectivity it shows over the other hydrophilic anions and ClO_4^- . Lipophilic SCN^- interferes at equal or higher concentrations, but by increasing the number of hydrogen bonding donor sites as in sensor **79**, selectivity against this generally strongly interfering anion is obtained.[113-114]

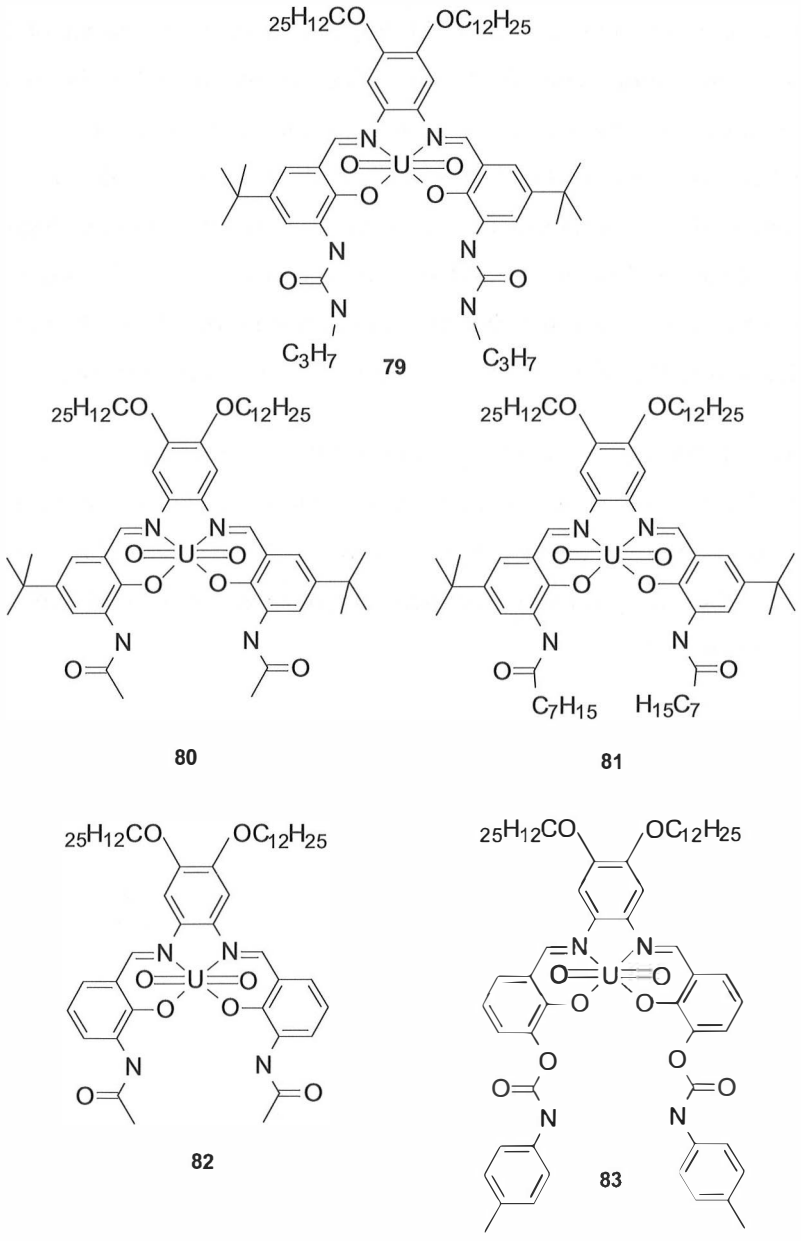

Figure 41 Uranyl salophen-based sensors for fluoride-selective membranes.[113]

The detection limit of lipophilic salophen **54** for fluoride is 1.3 x 10^{-3} M. Its selectivity is nearly the same as to $H_2PO_4^-$ and higher by a factor of 10 with respect to the more lyophilic halides. The membrane with the sensor **80** demonstrates a better performance as its detection limit is smaller than 0.001 M. This is because of its capability of forming hydrogen bonds with fluoride. The selectivity of these membranes towards fluoride is about two orders higher than that for other halides, sulfate and nitrate. The sensor **81** with longer carbon chains provides even a better detection limit for fluoride, 10^{-4} – 10^{-1} mol/l. Also with this sensor, the selectivity against nitrate and chloride is increased.[113]

Also phenyl- (**56**, Figure 36), t-butyl- (**84**) and fluoro- (**85**) (Figure 42) substituted uranyl salophens show an increased selectivity towards fluoride. In phenyl- and t-butyl-substituted salophens selectivity towards SCN^- is also observed. In the electron-withdrawing fluoro-substituted salophen the sensor sensitivity towards NO_3^- is lowered.[113]

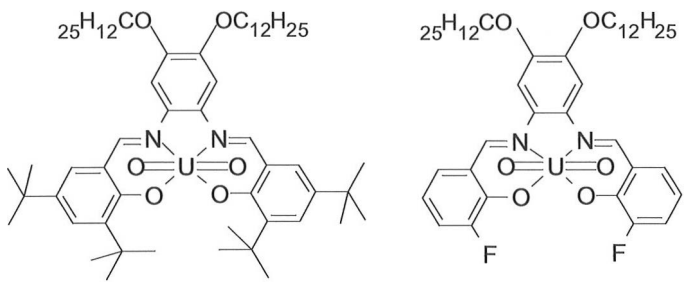

84 **85**

Figure 42 Sensors selective towards fluoride (**84 - 85**), thiocyanate (**84**) and acetate (**85**).[113]

The phenyl-substituted uranyl salophen **56** (Figure 36) also shows increased selectivity towards acetate ion, a very hydrophilic anion situated between

fluoride and phosphate in the Hofmeister series. Receptor **56** shows an over 250-fold selectivity towards acetate over phosphate.[113]

Knowledge about the complex stoichiometry in the membrane is required to obtain optimal sensor selectivity. When a counter ion concentration exceeds the maximum complex concentration, a reduction of the sensor selectivity is observed. In the PVC/NPOE ion-selective membranes of potentiometric sensors the guest –host stoichiometry of the anion complex of $H_2PO_4^-$ and F^- selective uranyl salophen derivatives is 2:1. The same stoichiometry is observed in nonpolar solvents such as chloroform. In contrast, the softer Cl^- is bound in a 1:1 stoichiometry.[55]

The durability of the membrane sensors varies. It is most important that the sensor used must be soluble to the membrane. Electrode durability can also be improved by decreasing the amount of the ammonium salt in the membrane to 5 mol%. The small decrease in the selectivity is compensated by a significant increase in durability. This way the durability of the membrane sensors can be extended to seven months.[115-117]

The uranyl salophens and salens can also be used as carrier molecules through supported liquid membranes.[118] Uranyl salophens **13 - 14** (Figure 10) and salen **12** (Figure 8) can be used as carriers for urea in its neutral form in the membrane composed of porous polymeric support (Accurel) impregnated with *o*-nitrophenyl *n*-octyl ether (NPOE).[119] High fluxes of urea can be obtained with these carriers because these compounds have a strong interaction with urea via hydrogen bonds, as well as trhough coordination of the urea carbonyl to the uranyl cation. In addition, these compounds possess a cavity in which the guest molecule fits well.[118-119]

Uranyl salophens **86 - 87** and salens **88 - 90** shown in Figure 43 can be used as anion carriers through supported liquid membranes.[120] $NPr_4H_2PO_4$ and NPr_4Cl can be transported from water trough NPOE using uranyl salophens **86 - 87** and salens **88 - 90**. The rates of salt transport by these anion carriers are much lower than those of transport by common cation carriers due to the low values of diffusion coefficients of uranyl salophens in the membranes used.[120]

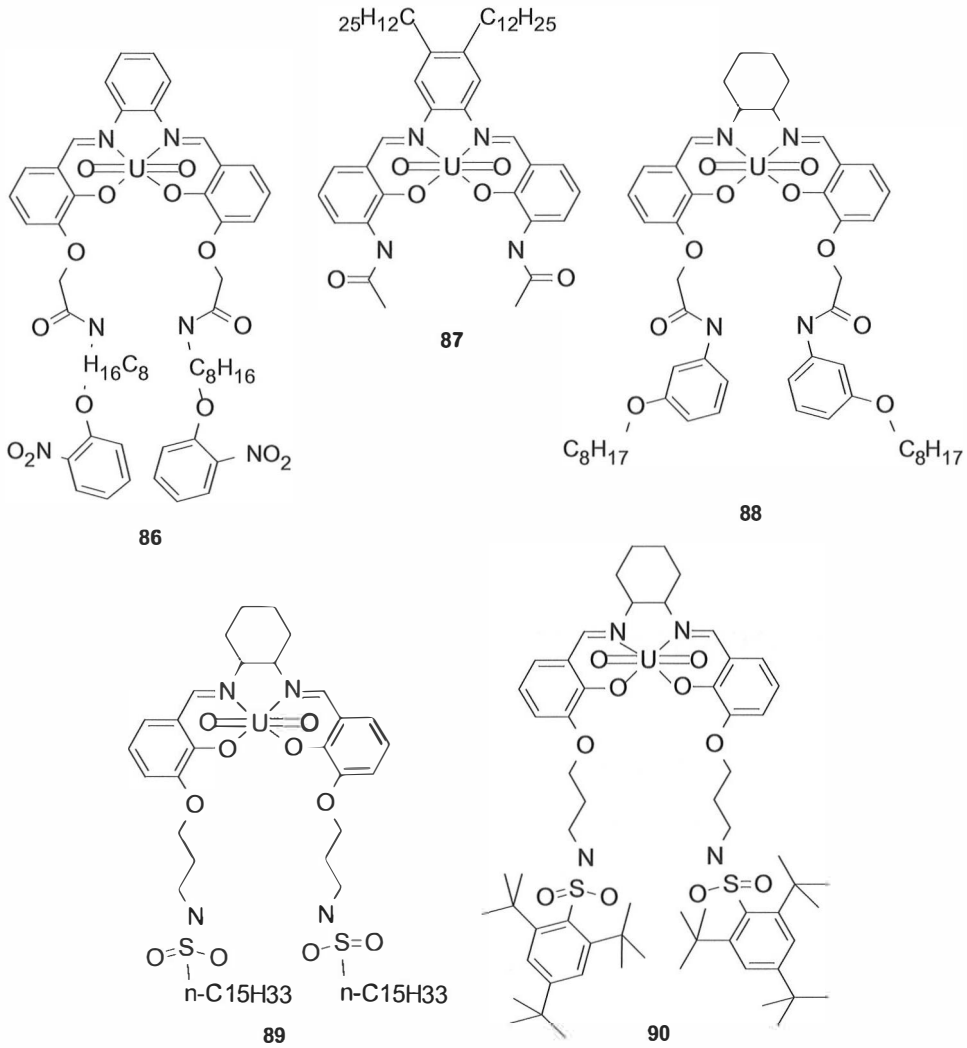

Figure 43 Uranyl salophens and -salens used as anion carriers in supported liquid membranes.[120]

3. AIM OF THE STUDY

The aim of this Ph.D. thesis has been the design, synthesis and structural characterization of ditopic uranyl salophen receptors and their complexation studies with various quaternary ammonium salts (R_4NX) in solution and in the solid state. The synthesis chemistry deals with the synthesis of the starting aldehydes for the phenylmethoxy salo- and salothiophens, the core or modified salo- and salothiophens, and the target salo- and salothiophens. The ditopic receptor behavior and the complexation of the phenylmethoxy salo- and salothiophens have been studied in solution using NMR spectroscopy, while the solid state structures of the salo- and salothiophen R_4NX complexes and solvent complexes have been determined by single crystal X-ray crystallography.

4. RESULTS AND DISCUSSION

4.1 Phenylmethoxy uranyl salophens

The 3-phenylmethoxy uranyl salophen **9** was first reported by Reinhoudt in 1991.[14] Later the same compound was used in the complexation studies in a collaboration between the research groups at the University of Jyväskylä and the University of Rome, La Sapienza, where its complexation properties with alkali halides[73-74] and tetraalkyl ammonium halides[67-68] were studied. To form a full picture of the ditopic nature of phenylmethoxy salophens, 4-phenylmethoxy uranyl salophen **95** was prepared and complexation studies both in the solid state and in the solution with tetraalkyl ammonium salts of different size were carried out for all isomers of the phenylmethoxy salophen, namely 3-, 4-, and 5-phenylmethoxy uranyl salophens (**9**, **95** and **100**, respectively).

4.1.1 Synthesis and characterization of 95

Following a common procedure, all salophens were prepared by one-pot synthesis from a corresponding aldehyde and diaminoarene by the Schiff base reaction. The starting aldehyde, 2-hydroxy-4-(phenylmethoxy)-benzaldehyde **93** (Scheme 10), was prepared from 2,4-dihydroxy-benzaldehyde **91** and benzyl bromide **92** with K_2CO_3 and 18-crown-6 in acetone at room temperature under nitrogen by a Williamson ether synthesis in a moderate 26 % yield.[121-122] For the synthesis of 4-phenylmethoxy uranyl salophen **95** 2-hydroxy-4-(phenylmethoxy)benzaldehyde **93** and 1,2-diaminobenzene **94** were added to uranyl acetate in methanol under reflux. Salophen **95** was isolated as a red powder in a 93 % yield.

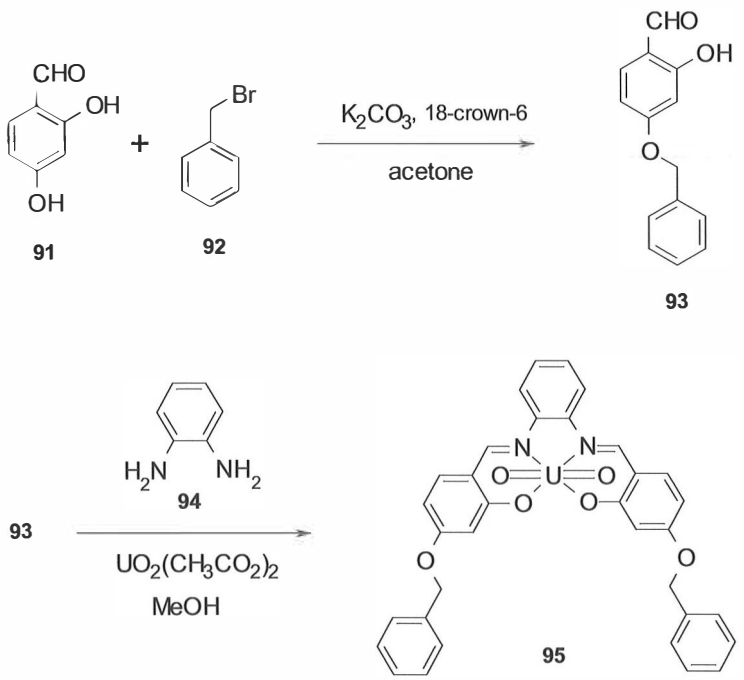

Scheme 10 Synthesis of 4-phenylmethoxy uranyl salophen **95**.[121-122]

The products were characterized by ^{1}H NMR, ^{13}C NMR, mass spectrometry (MS) and elemental analysis (EA). The ^{1}H NMR spectrum of 2-hydroxy-4-(phenylmethoxy)-benzaldehyde **93** shows a singlet of the aldehyde proton at 11.48 ppm and a singlet of the hydroxyl proton at 9.76 ppm. Both singlets disappear in the spectrum of 4-phenylmethoxy uranyl salophene **95** and a singlet at 9.49 ppm appears due to the imine protons. A more detailed analysis of ^{1}H NMR spectrum of the receptor **95** is presented in Figure 44. In the MS-spectrum of aldehyde **93**, M-1 peak is observed at m/z = 227.1, and in case of **95**, M-1 peak is observed at m/z = 795.2. The exact synthetic procedure and characterization data of ^{1}H NMR, ^{13}C NMR, MS, and EA for **93** and **95** are given in the experimental section (page 147).

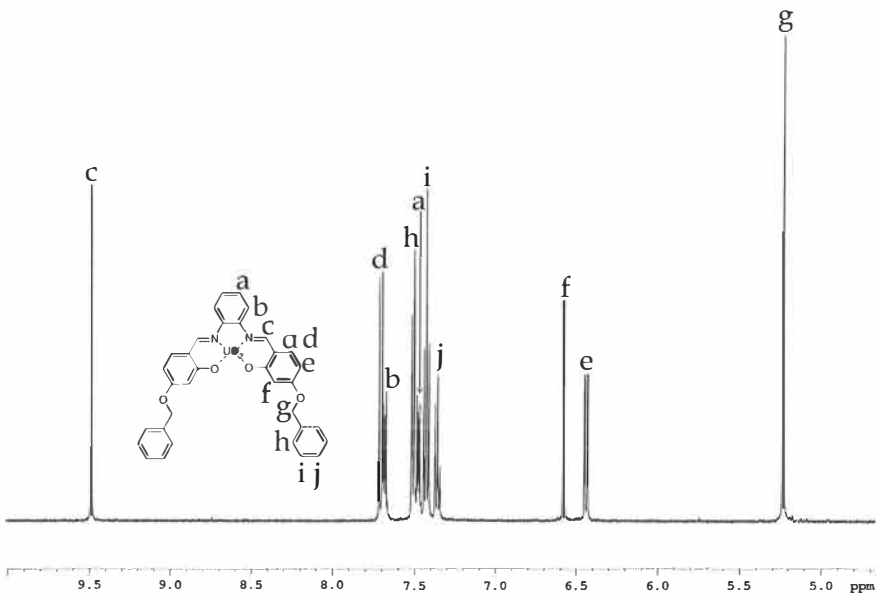

Figure 44 ^{1}H NMR spectrum of receptor **95** in D_6-DMSO.

4.1.2 Crystallization experiments with salophens 9, 95 and 100

4.1.2.1. Crystal structures of the solvent complexes of 9 and 95

The 4-phenylmethoxy uranyl-salophen **95** was crystallized as a solvent complex with water and methanol (Figure 45, Appendices 1 and 2). Crystals of good quality were obtained by slow evaporation of the methanol or, in the case of the water complex from moist acetone.

As is known, the seventh coordination site in a uranium atom is never empty. Hence, in solvent complex structures, when the solvent used in the crystallization experiment is a coordinative molecule, it is always bound to the uranyl cation in the salophen, at least in the solid state. In the water complex (Figure 45, top) the distances from uranium to the oxygen and nitrogen atoms of the salophen are 2.25 – 2.56 Å. The U-O distance is around 2.3 Å and the U-N around 2.5 Å in all uranyl salophen compounds. The distance between uranium and oxygen of the water molecule is about the same, 2.43 Å. In the structure there are two uranyl salophen units joined to each other by two hydrogen bonds from bonded water to phenolic oxygen in the other salophen molecule (O-H···O distances of 1.96 Å and 1.86 Å). Also, uranyl oxygen of the adjacent complex is hydrogen bonded to the methylene hydrogen of the arm of the salophen molecule (2.56 Å). In the methanol complex structure (Figure 45, bottom), the distances from uranium to oxygen and nitrogen atoms of the salophen are 2.26 – 2.53 Å. The distance between uranium and the oxygen of the methanol molecule is about the same, 2.46 Å.

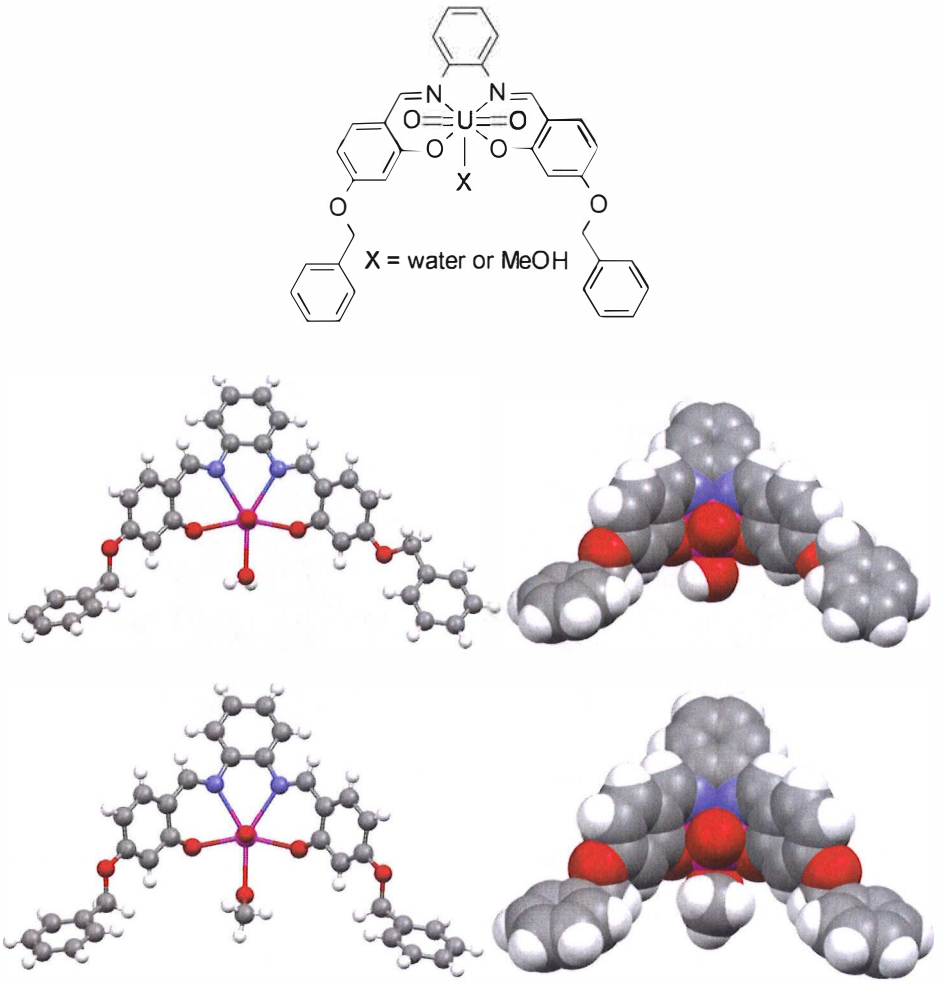

Figure 45 The chemical structure, ball stick and CPK plots of **95**•H_2O (top) and **95**•MeOH (bottom).

Uranyl salophen **9** crystallizes as a solvent complex with methanol (Figure 46, Appendix 3). Crystallization was done by slow evaporation of the methanol.

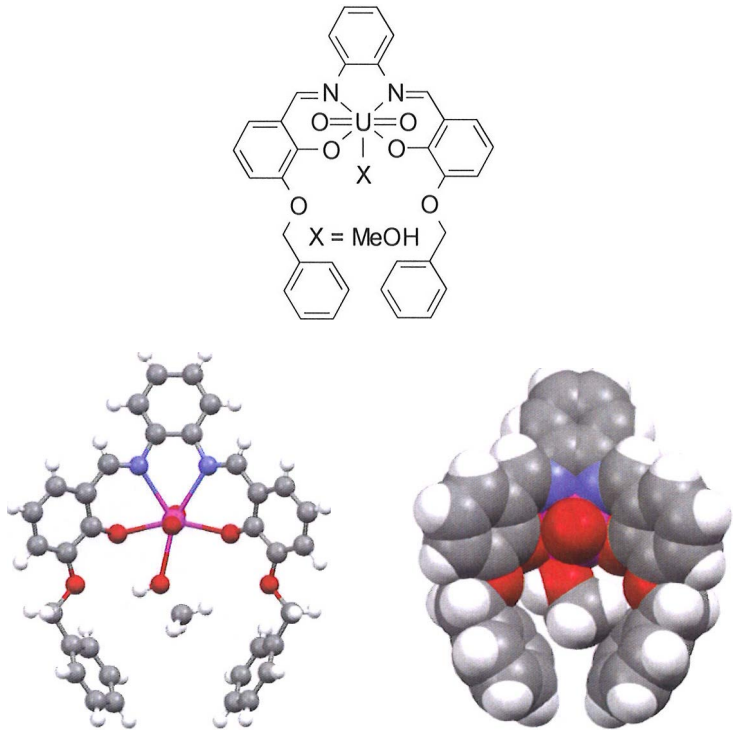

Figure 46 The chemical structure, ball stick and CPK plots of **9**•MeOH.

Unlike **95** the phenylmethoxy arms in **9** form a small pocket into which the methanol molecule fits tightly. In the methanol complex of **9** the distances from uranium to oxygen and nitrogen atoms of the salophen are 2.25 – 2.55 Å and that to the oxygen of the methanol molecule is about the same, 2.54 Å. The overall shapes of the isomeric phenylmethoxy salophens **9** and **95** are markedly different, but in spite of that, all oxygen containing solvents (here H_2O or MeOH) show very similar bond distances to the uranium atom. This overall shape difference of the phenylmethoxy salophens **9** and **95** is an important feature in their R_4NX complexation behavior.

4.1.2.2 Solid state complexation studies of 9, 95 and 100 with R_4NX

As is known from the literature, the uranyl salophens are good receptors for neutral molecules and anions and they can also act as ditopic receptors that simultaneously bind both ions of a salt.[11] Complexation studies of the isomeric phenylmethoxy uranyl salophens **9**, **95** and **100** with R_4NX (X = Cl and F) were made in the solid state by mixing the salophen in a suitable solvent with the R_4NX salt and subsequent evaporation. The crystallization experiments produced six different crystal structures of the corresponding R_4NX complexes which are discussed below.

The 3-phenylmethoxy uranyl-salophen **9** binds tetraalkyl ammonium salts[67-68] and alkali metal halides[73] as ion pairs and hence the binding ability of the receptors **95** and **100** towards the alkali chlorides was studied first. Despite several different crystallization methods and solvents used, no suitable crystals for X-ray diffraction analysis were obtained.

To obtain a full family of structurally different tetraalkyl ammonium salts for the complexation studies, the unsymmetrical dimethyldiethyl- (DMDE) dimethyldipropyl- (DMDP) and dimethyldibutyl- (DMDB) ammonium chlorides **98a-c** were prepared in yields of about 30 % from dimethylformamide **96** and alkylbromide **97** with alkyl chains of different lengths at 70 °C using K_2CO_3 as a base in the reaction (Scheme 11).[123-125] The use of alkyl bromides gave the best yields. Because the uranyl cation is known to bind the chloride anion better, ion exchange[126] was done by using a column filled with Dowex 2x8(Cl), 20-50 mesh and HCl 6 mol/l leading to R_4NCl, viz. tetraalkyl ammonium chlorides, which were then used in the crystallization studies. Experimental details are given on page 148.

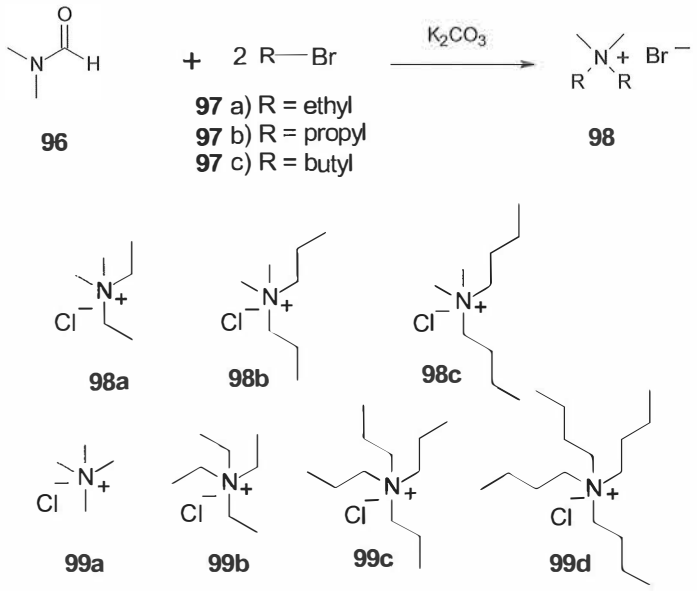

Scheme 11 Synthesis of the unsymmetrical tetraalkyl ammonium salts.[126-125] and the chemical structures of R_4NCl -salts **98a-99d**.

The solid state complexation of 3-phenylmethoxy uranyl salophen **9**, 4-phenylmethoxy uranyl salophen **95** and 5-phenylmethoxy uranyl salophen **100** with dimethyldiethyl- (DMDEACl **98a**), dimethyldipropyl- (DMDPACl **98b**), dimethyldibutyl- (DMDBACl **98c**), tetramethyl- (TMACl **99a**), tetraethyl- (TEACl **99b**), tetrapropyl- (TPACl **99c**), and tetrabutyl ammonium chlorides (TBACl **99d**) was studied in a large number of cocrystallization experiments of all the receptors with all tetraalkyl ammonium salts mentioned above. A large variety of different crystallization methods and solvents were tested and a slow evaporation of the solvent used proved to be the best technique. When the uranyl salophen acts as a ditopic receptor, the anion part of the salt is bound by the uranyl cation and the cation part is bound by the salophen's large π-system primarily by a cation-π –interaction.

Crystals of good quality were obtained of the 1:1 complexes of receptor **9** with DMDPACl **98b** and DMDBACl **98c** (Figures 47 and 48, Appendices 4 and 5). Interactions and their distances between receptor **9** and DMDPACl **98b** (in short **9•98b**) are collected in Table 3 and those of **9•DMDBACl**, *viz.* **9•98c**, in Table 4. Structures of **9•TMACl** and **9•TBACl** have been published before.[67-68] Crystallization experiments were done by adding an excess amount of the salt to the acetone solution of the receptor and slowly evaporating of most of the acetone. All uranyl salophen-salt complexes were analyzed according to the method below; the results are presented in the form of a table of interactions. The intermolecular distances are reported when they are shorter than the sum of the van der Waals (vdW) radii of the interacting atoms, except for the $N^+\cdots$ π (centroid) and $N^+\cdots Cl^-$ distances, (see below), which are used to incidate the position of the tetraalkyl cation relative to the uranyl atom of the salophen. The distances between the uranium and the oxygen and nitrogen atoms of the salophen ligand were measured and reported in the table as U-O/N. The distance between uranium and the bound anion is denoted $U\cdots Cl^-$ and the contact distance between the anion and the nitrogen of the ammonium salt as $N^+\cdots Cl^-$. The possible cation- π interactions are reported as the shortest distance of a hydrogen atom of the alkyl chains of the tetraalkyl ammonium salt and the closest carbon atom of the aromatic side arm, and reported as C-H···π(C). The shortest distance between the calculated centroid of the aromatic ring in the side arm and a hydrogen atom of the alkyl chain was also measured and reported as C-H···π (centroid). In addition to these, the distance between the nitrogen atom of the salt and the centroid of the aromatic ring was measured and denoted as $N^+\cdots$ π (centroid). Besides the cation- π interaction, the tetraalkyl cation is hydrogen bonded from the hydrogen atoms of the cation to the chloride anion (reported as $C\text{-}H\cdots Cl^-$), to the uranyl oxygen atoms (reported as C-H···O=U) and to the

phenolic oxygen atom of the salophen ligand (reported as C-H···O$^-$-Ph). These interactions for **9•98b** are given in Table 3.

In the structure of receptor **9** complexed with DMDPACl **98b** (Figure 47), the R_4N^+ cation lies close to the chloride anion. Alkyl chains of the cation fit nicely in the cleft inside the salophen molecule. In the structure the chloride anion is bound to the uranium at a distance of 2.74 Å, which is clearly longer than the bond lengths from the uranium to the O and N atoms of the salophen ligand (2.26-2.64 Å). There are no obvious C-H···cation or CH···π interactions since these distances are longer than the sum of the vdW radii of H and C atoms. A weak hydrogen bond between the chloride and the hydrogen of the CH_2 next to the nitrogen (2.66 Å) exists. Two hydrogen atoms of the middle carbon of the other propane chain are bound by the uranyl oxygen (2.47 Å) and the phenolic oxygen of the salophen ligand (2.64 Å). The closest distance for N···π (centroid) is 4.95 Å. The distance between the chloride and the nitrogen is 4.15 Å. The conformation of the salophen skeleton in **9•98b** is clearly different that of **9**•MeOH (Figure 46); it is caused by the complexation of **98b** into it.

Table 3 Interactions and their distances for **9•98b**.

Interaction	Distance [Å]
C-H···π (C)	-
C-H···π (centroid)	-
C-H···Cl$^-$	2.66
C-H···O=U	2.47
C-H···O$^-$-Ph	2.64
N$^+$··· π (centroid)	4.95
N$^+$··· Cl$^-$	4.15
U··· Cl$^-$	2.74
U-O/N	2.26 - 2.64

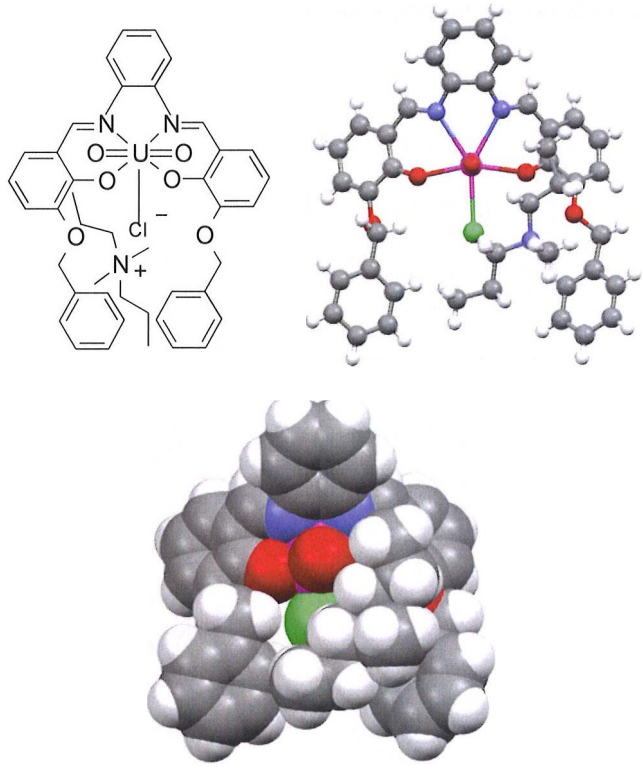

Figure 47 The chemical structure, ball stick and CPK plots of **9•98b**.

As in the structure of **9•98b**, **9•98c** (Figure 48) shows no obvious C-H··· cation or CH···π interactions. The positive nitrogen lies slightly more distant from the chloride anion than in **9•98b**, but the overall position of the R_4N^+ cation and the bond or interaction distances are very similar. A hydrogen atom in the methyl carbon is weakly bonded to the ether oxygen of the other arm (2.56 Å) of the salophen unit, and the hydrogen atoms in both carbons next to the nitrogen atom in the butyl chains are H-bonded to the uranyl oxygen (2.63 Å and 2.53 Å). The other oxygen is weakly interacting with the chloride atoms (2.76 Å). The closest distance for N···π (centroid) is 5.04 Å and that for chloride to nitrogen is 4.35 Å. The overall structures of **9•98b** and **9•98c** are very similar; thus the elongation of

the length of two of the alkyl chains in the R_4N^+ moiety does not affect the structure of the complex.

Table 4 Interactions and their distances in **9•98c**.

Interaction	Distance [Å]
C-H···π (C)	-
C-H···π (centroid)	-
C-H···Cl$^-$	2.76
C-H···O=U	2.63/2.53
C-H···O-Ph	2.70
N^+··· π (centroid)	5.04
N^+··· Cl$^-$	4.35
U··· Cl$^-$	2.74
U-O/N	2.27 – 2.61

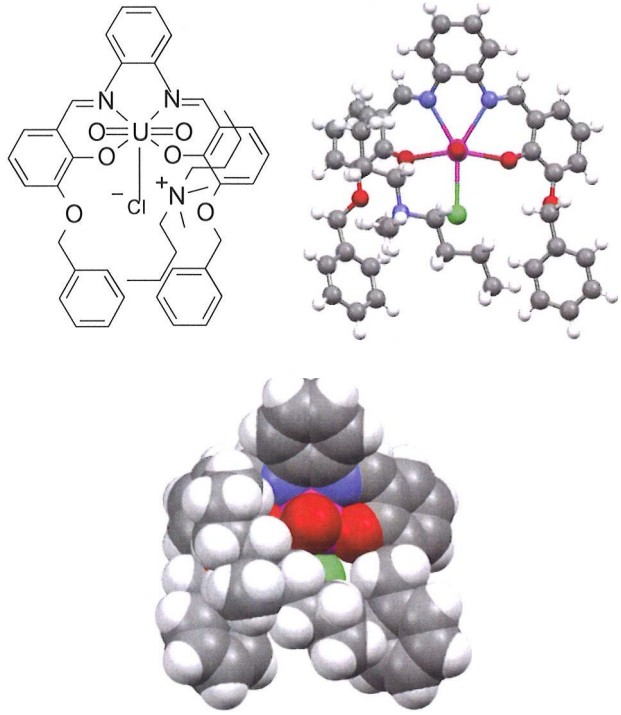

Figure 48 The chemical structure, ball stick and CPK plots of **9•98c**.

The isomeric 4-phenylmethoxy uranyl salophen **95** cocrystallized with TMACl **99a** and DMDEACl **98a** (Figures 49 and 50, Appendices 6 and 7). The interactions and their distances of **95•99a** are shown in Table 5 and those of **95•98a** in Table 6. Crystallization experiments were done by the same procedure as with receptor **9**. These crystals were also obtained from acetone by evaporation.

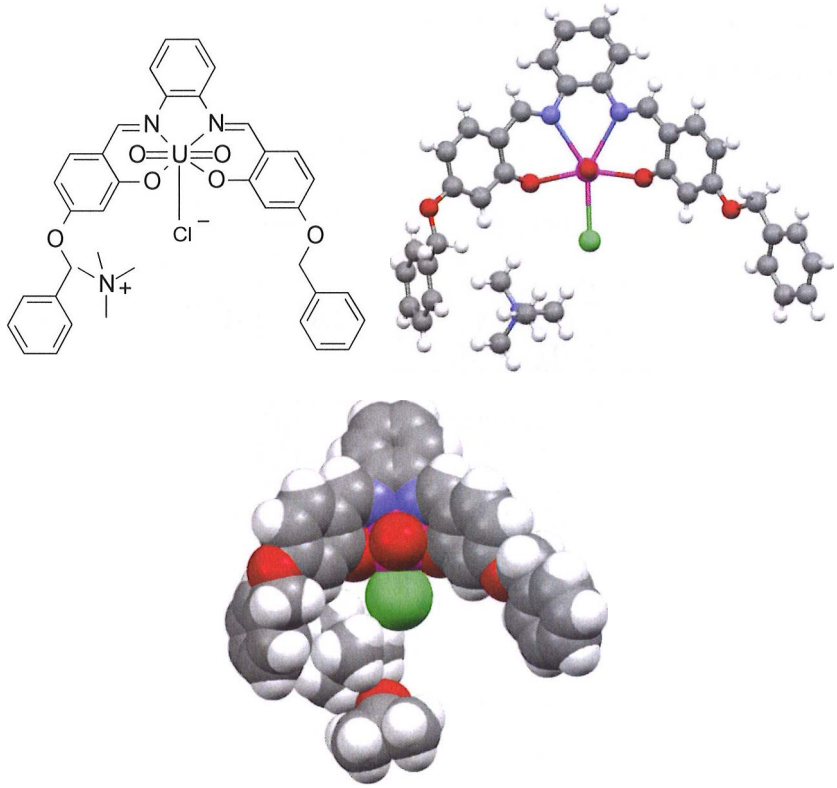

Figure 49 The chemical structure, ball stick and CPK plots of **95•99a**. The acetone molecule seen in the CPK is omitted from the ball and stick picture for the sake of clarity.

In **95•99a** the cation fits very nicely inside the cleft formed by one of the phenylmethoxy arms and the chloride atom is coordinated to the uranium atom. The cation lies close to the other aromatic side arm with clear C-H···π interactions

and there is no connection to the other arm. In the structure the chloride anion is bound to the uranium at the distance of 2.75 Å, which is clearly longer than the bond lengths from the uranium to the salophen ligand (2.24-2.60 Å). The cation is connected to the other aromatic arm from one methyl hydrogen by CH_3··· π (C) interaction (2.90 Å). The chloride binds the hydrogen atoms of the two methyl groups (2.67 Å and 2.92 Å). The closest distance for CH···π (centroid) is 2.79 Å and the closest distance for N···π (centroid) is 4.41 Å. The distance between the chloride and the nitrogen is 4.05 Å.

Table 5 Interactions and their distances in **95•99a**.

Interaction	Distance [A]
C-H···π (C)	2.90
C-H···π (centroid)	2.79
C-H···Cl^-	2.67 + 2.92
C-H···O=U	-
C-H···O^--Ph	-
N^+··· π (centroid)	4.41
N^+··· Cl^-	4.05
U··· Cl^-	2.75
U-O/N	2.24-2.60

In the complex structure of **95•98a** the chloride anion is bound to the uranyl cation at the distance of 2.75 Å, the same as in the complex with TMACl **99a**. The bond lengths from the uranium to the salophen ligand are 2.26-2.60 Å. The cation is only connected to one aromatic arm by connections from another CH_2 hydrogen atom next to the nitrogen atom to the two aromatic carbons in the arm (2.88 Å and 2.74 Å). Also one hydrogen atom in the other methyl carbon is connected to the chloride anion (2.77 Å). The closest distance for CH···π (centroid) is 2.95 Å and the closest distance for N···π (centroid) is 4.79 Å. The distance between the chloride and the nitrogen is 4.36 Å.

Table 6 Interactions and their distances in **95•98a**.

Interaction	Distance [A]
C-H···π (C)	2.88/2.74
C-H···π (centroid)	2.95
C-H···Cl$^-$	2.77
C-H···O=U	-
C-H···O$^-$-Ph	-
N$^+$··· π (centroid)	4.79
N$^+$··· Cl$^-$	4.36
U··· Cl$^-$	2.75
U-O/N	2.26 – 2.60

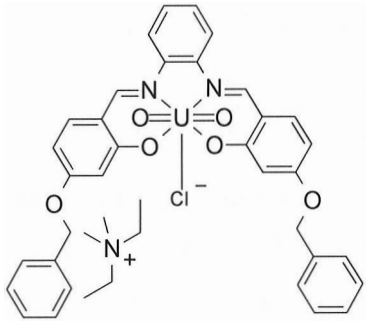

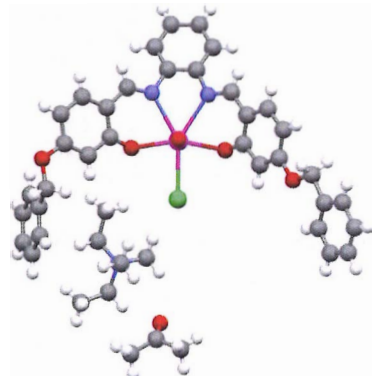

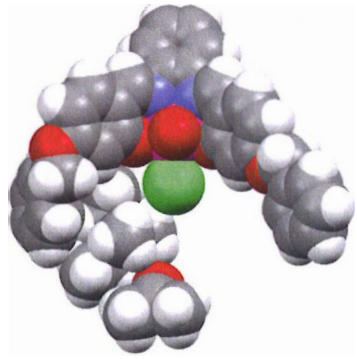

Figure 50 The chemical structure, ball and stick and CPK plots of **95•98a**.

The 5-phenylmethoxy analogue **100** cocrystallized with DMDBACl **98c** (Figure 51, Appendix 8). The interactions and their distances in **100•98c** are shown in Table 7. Crystallization was done by adding an excess amount of the salt to the acetone solution of the receptor and then slowly evaporating the solvent.

Table 7 Interactions and their distances in **100•98c.**

Interaction	Distance [Å]
C-H···π (C)	-
C-H···π (centroid)	-
C-H···Cl^-	2.77
C-H···O=U	2.77
C-H···O^--Ph	2.67
N^+··· π (centroid)	-
N^+··· Cl^-	4.30
U··· Cl^-	2.76
U-O/N	2.26-2.61

The structure of the complex **100•98c** differs substantially from the structures of the complexes of receptors **9** and **95**. The bond lengths from the salophen to the uranium are about the same (2.26 - 2.61 Å); also the bond length from the uranium to the chloride is about the same (2.76 Å) as with receptors **9** and **95**. The guest cation is instead bound to the chloride anion with a C-H···Cl^- interaction (2.77 Å), to one of the uranyl oxygens with a C-H···O=U interaction (2.77 Å), and to the phenolic oxygen of the salophen ligand by C-H···O^--Ph (2.67 Å). No cation-π interactions were observed. The distance between nitrogen and chloride is 4.30 Å.

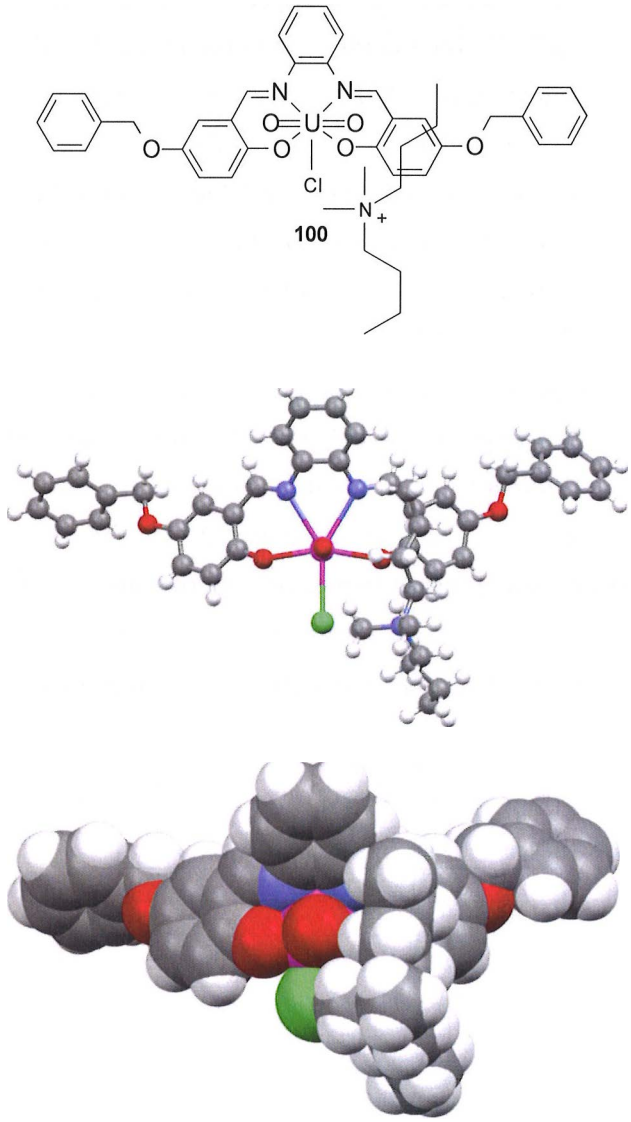

Figure 51 The chemical structure, ball and stick and CPK plots of **100•98c**.

Compared to the chloride anion a fluoride anion binds much more strongly to the uranyl cation.[127-128] Tetramethyl ammoniumfluoride **101a** (TMAF) and tetrabutyl ammoniumfluoride **101b** (TBAF) were used in cocrystallization experiments with uranyl salophens **9, 95** and **100**. With TBAF, no crystals with good quality with any of the receptors were obtained, even though the color of the solution in the experiment always changed from red to yellow, thus indicating the formation of the complex. Contrary to TBAF, TMAF **101a** cocrystallized with receptor **95** as good quality crystals. Crystallization was done by adding an excess amount of the salt to the acetone solution of the receptor and then slowly evaporating the solvent. Unlike tetraalkyl ammonium chlorides, where receptor **95** forms 1:1 adducts, the fluoride anion binds simultaneously to two uranyl salophens in the crystal (Figure 52, Appendix 9) leading to a 2:1 complex. Interactions and their distances of **(95)$_2$•101a** are shown in Table 8.

Table 8 Interactions and their distances in **(95)$_2$•101a**.

Interaction	Distance [A]
C-H···π (C)	2.89
C-H···π (centroid)	2.30
C-H···F$^-$	-
C-H···O=U	-
C-H···O$^-$-Ph	-
N$^+$··· π (centroid)	4.71
N$^+$··· F$^-$	-
U··· F$^-$	2.32, 2.32
U-O/N	2.25 - 2.58

In the **(95)$_2$•101a** the distances between the salophen ligand and the uranium are 2.25 - 2.58 Å and the distances between the two uranium atoms and the bridging fluoride are 2.32 Å. The cation sits in the cleft formed by interwined aromatic side arms, where it fits perfectly. The closest distance for CH···π (centroid) is 2.89 Å and for C-H···π (C) also 2.89 Å. The closest distance for N···π (centroid) is 4.71 Å.

The cation is also bound by weak hydrogen (2.65 Å) bonding between two methyl hydrogen and two etheral oxygen atoms of both aromatic side arms forming the cleft.

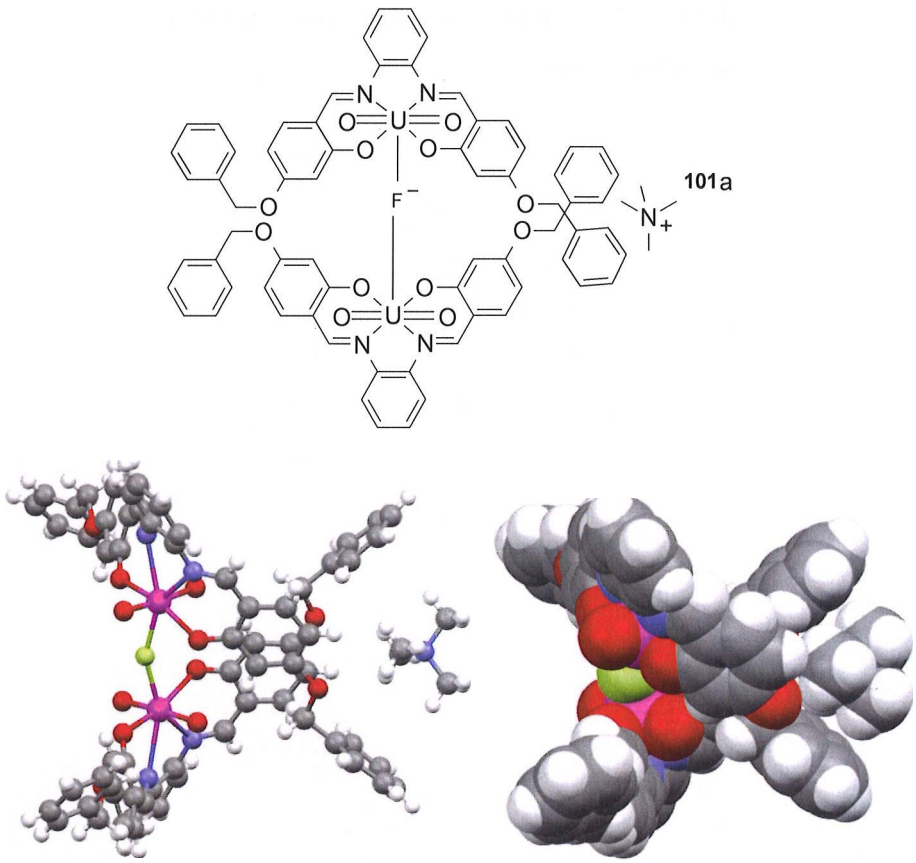

Figure 52 The chemical structure, ball and stick and CPK plots for (**95**)$_2$•**101a**.

In addition to the R_4NX complexation studies, some organic bases, especially amines, were tested for complex formation. The initial idea was to see weather the nitrogen atoms of the amines would directly coordinate to the seventh coordination site of the uranium atoms. 1,4-diazabicyclo[2.2.2]octane (DABCO,

102) is a cyclic compound with two tertiary nitrogens on both sides of the cycle. Receptor **95** cocrystallizes with water and DABCO **102** as good quality crystals (Figure 53, Appendix 10), where a water molecule works as an intermediate between uranium and the DABCO. Crystallization was done by adding an excess amount of DABCO to the acetone solution of the receptor and then slowly evaporating most of the acetone.

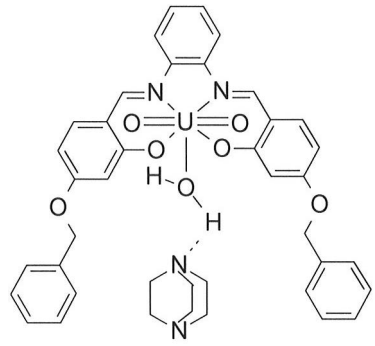

102

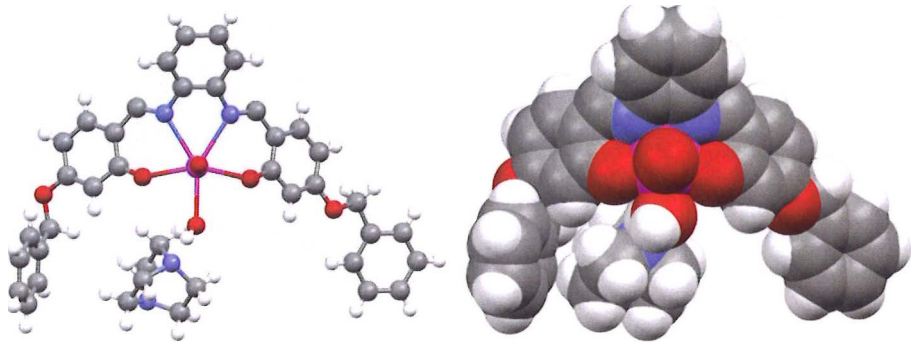

Figure 53 The chemical structure, ball and stick and CPK plots for **95**•H_2O•**102**.

In the complex structure of the receptor **95**•H_2O•**102** the distances between uranium and the salophen ligand are 2.26-2.58 Å. The distance between uranium and the oxygen atom of the water molecule is 2.42 Å. The distance between the

nitrogen atom of the DABCO and the oxygen atom of the water is 2.48 Å. One interaction between the methylene hydrogen and the aromatic side arm is observed as C-H···π (C) (2.89 Å). Both water hydrogen atoms also hydrogen bond to the nitrogen atom of the DABCO (1.66 and 2.71 Å).

4.1.3 Complexation studies in solution for 9, 95, and 100

The thermodynamic stability of a host-guest complex in a given solvent is gauged by a measurement of the binding constant K (or synonyms equilibrium constant, rate constant or stability constant). Because the binding constant is a thermodynamic parameter, it is related to the free energy of the association process according to the Gibbs equation $\Delta G° = -RT \ln K$. Thus the general affinity of a host for a guest under specific conditions (solvent, temperature etc.) may be given either in terms of K or - $\Delta G°$ values.[129-130] The use of K has been more popular and has become a normal practice. The basic equation for host-guest complexation is the following:

$$K = \frac{[complex]}{[host]^a \cdot [guest]^b},$$

where superscripts *a,* and *b* show the stoichiometry of the host and guest molecules. A host-guest complexation can either have a very slow or a very fast exchange rate on the NMR time scale.[131-135] With the uranyl salophens and tetraalkyl ammonium salts the complexation is fast. That means that in the NMR spectrum the average of the free guest and the complexed guest is observed instead of two individual peaks. The signals of the host salophen do not change but the signals of the guest instead move downfield (to the left on the ppm-scale)

during a dilution NMR experiment of a totally complexed guest. (At the start point, the amount of the host was 14 times that of the guest. See page 161).

The binding ability of the phenylmethoxy uranyl salophens **9**, **95** and **100** towards the quaternary ammonium salts **98a-99d** was studied in the solution using the NMR-titration technique. Due to the different complexation behavior of **9** and **100** *vs.* **95**, the binding constants for 1:1 complexes for the receptors **9** and **100** are listed in Table 9. The ^{1}H NMR-measurements were made by Bruker Advance DRX 500 MHz in $CDCl_3$ at 30 °C. $CDCl_3$ was used as solvent because in apolar organic solvents R_4NX-salts exist mostly as ion pairs, not as independent ions. The initial salophens used were water complexes[136], *viz.* **9**•H_2O, **95**•H_2O and **100**•H_2O. Very dilute solutions of the uranyl salophen-water complexes were used due to the low solubility of the uranyl salophen- R_4NX complexes into $CDCl_3$ causing precipitation at higher concentrations. The salophen used was weighed into an empty NMR tube and dissolved into an R_4NX-containing $CDCl_3$ solution of a known concentration. The R_4NX-$CDCl_3$ solution was then sequentially added to the subsequent NMR measurement decreasing the concentration of the host salophen while the concentration of the R_4NX remained the same. The concentrations of the salts varied between 0.4 - 0.8 mmol/l and the starting concentrations of the salophens were between 3.0 – 8.3 mmol/l. At the end of the titrations, concentrations of the salophens were 0.034 – 0.18 mmol/l. Volumes of R_4NX-$CDCl_3$ solution additions were 100 - 500 µl and additions were made using an air-tight glass syringe. In all R_4NXs the CH_2-protons closest to the nitrogen atom were monitored because unlike protons at the end of the carbon chains, their signals did not overlap with neither water signals (water come from the initial salophen•H_2O complex used and from chloroform used). A typical titration curve is shown in Figure 54. Titration data were fitted to an isotherm to correspond to an 1:1 complex using an iterative procedure. Binding constants (K,

M^{-1}) and limiting shifts ($-\Delta\delta_{\infty}$, ppm) were obtained as best fit parameters (Table 9). The experimental procedure and the curve fitting equation are presented in the experimental section (page 161).

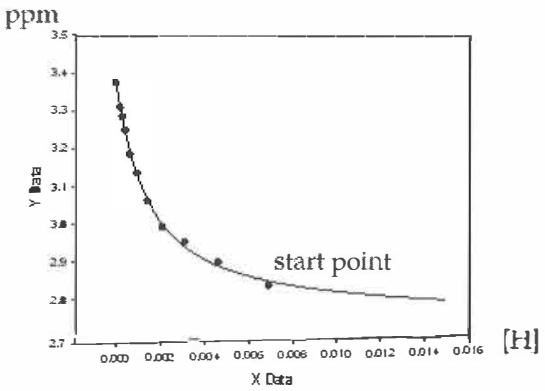

Figure 54 ^{1}H NMR titration curve of 0.4 mM DMDEACl, **98a** with receptor **100** in $CDCl_3$ at 30 °C.

The 1:1 isotherm was used and not confirmed via a Job plot, due to earlier results with the same salophen[67-68]. In the case of receptors **9** and **100** unambiguous results were obtained. Earlier published results[67-68] show that TBA with Cl as the counter anion binds best to receptor **9** (K = 22 000 M^{-1}, Table 9, entry **7**, **9**). In the same study a binding constant of 13 600 M^{-1} was observed for TMACl.[67-68] Being only slightly larger in size, yet asymmetrical ($R^1{}_2R^2{}_2NX$, where $R^1 \neq R^2$), DMDEACl **98a** binds equally (K = 13 800 M^{-1}) when compared with TMACl **99a** and only slightly more strongly than symmetrical TEACl **99b** and TPACl **99c**. The two intermediate-sized salts DMDPACl **98b** and DMDBACl **98c** bind slightly more weakly (Table 9, entries 3 and 4). The large difference in the binding constants for TBA *vs.* TMA, DMDE, TEA and TPA make it difficult to correlate

the size and shape of these strongly binding cations, especially as the symmetric cations tend to bind more strongly with salophen **9**.

Table 9 Binding constants (K, M^{-1}) and limiting shifts ($-\Delta\delta_\infty$, ppm) for compelexes of quaternary ammonium salts with receptors **9** and **100**.

entry	R_4NCl	**9**	**100**
1	TMA	**13 600 ± 600**[68]	Not determined
	$-\Delta\delta_\infty$	0.65 (NCH_3)	
2	DMDEA	**13 800 ± 2400**	**830 ± 63**
	$-\Delta\delta_\infty$	0.44 (NCH_3)	0.47 (NCH_3)
3	DMDPA	**8390 ± 1100**	**960 ± 96**
	$-\Delta\delta_\infty$	0.44 (NCH_3)	0.39 (NCH_3)
4	DMDBA	**6920 ± 1400**	**840 ± 110**
	$-\Delta\delta_\infty$	0.34 (NCH_3)	0.35 (NCH_3)
5	TEA	**11 600 ± 2000**	**640 ± 59**
	$-\Delta\delta_\infty$	0.46 (NCH_2)	0.43 (NCH_2)
6	TPA	**11 300 ± 2000**	**880 ± 73**
	$-\Delta\delta_\infty$	0.31 (NCH_2)	0.35 (NCH_2)
7	TBA	**22 000 ± 3000**[68]	**850 ± 120**
	$-\Delta\delta_\infty$	0.30 (NCH_2)	0.23 (NCH_2)

In general, all cations studied bind quite strongly (K > 6900 K-1) to receptor **9** due to the spatial orientation of the phenylmethoxy arms at the 3-position creating a suitable cleft for C-H···π and cation···π interactions. When the binding constant has a value over 10 000 M^{-1}, NMR-titration is not the best method to use due to its large error (< 10 % is excellent, < 15 % is good and < 20 % is adequate). The critical part (dogleg) of the titration curve is too steep and causes large errors in calculations.[134-135]

Receptor **100** has a spatial structure different form that of receptor **9** because the phenylmethoxy arms are situated at the periphery of the salophen skeleton at the 5-position. In receptor **100** both arms (see Figure 51) are far away from the uranyl center and there is no cleft for the cation to fit in. Previous studies with core salophen **1** have shown that the cation binding is markedly weaker than with receptor **9** due to the absence of suitably situated aromatic arms. Although receptor **100** is not as good a receptor as receptor **9**, it still binds all ammonium cations used. The binding constants vary from 640 M^{-1} to 960 M^{-1}, being about 10 - 20 times smaller than those of receptor **9**. The probable errors in the measurements were excellent or good (from 7.6 % to 13.8 %) due to the weaker binding leading accurate measurements. The binding of TEACl is the weakest while all others have almost equal binding constants. No differences in the binding between symmetrical and unsymmetrical salts can be observed, contrary to receptor **9**. Previous results of Cametti et al.[67-68] show that core salophen **1** binds TMACl with a constant of 1000 M^{-1} and TBACl by 5400 M^{-1}. The reason for the slight difference between the unsubstituted salophens and receptor **100** (see Table 9) can be explained by the dimer formation of receptor **100** presented later in this chapter.

Clearly differing from receptors **9** and **100**, receptor **95** gave doubly sigmoidal titration curves which indicates that two processes were happening at the same time. Fitting with an isotherm corresponding to a 1:1 complexation gave very poor results. Takao and Ikeda[21] have shown that uranyl salophens can exist as dimers in all non-coordinative solvents such as chloroform that was used in titrations. In such a dimer one of the phenolic oxygen is bound to the uranyl cation of another uranyl salophen molecule and vice versa, which fills up the empty binding position of the uranyl cation and prevents the salophen from binding to the guest (Scheme 3, p 21).

In order to prove the idea of dimer formation of **95** in $CDCl_3$, low-temperature ^1H NMR measurements were performed for receptors **9**, **95** and **100** in $CDCl_3$. Nine measurements were started at 30 °C and the temperature was reduced in steps of 10 °C until -50 °C was reached. The salophens were used as water complexes.

The ^1H NMR spectra between 4 and 10 ppm of receptor **95** in $CDCl_3$ at different temperatures are shown in Figure 55. At +30 °C the peaks appear as broad signals due to the fast dynamics on the NMR time scale. Lowering the temperature resulted in sharper and well defined peaks. In contrast to the ^1H NMR in DMSO there are double the number of peaks for the aromatic protons, excluding the 1,2-diaminobenzene moiety, and the benzyl protons appear as four doublets. According to this ^1H NMR receptor **95** is either unsymmetrical in $CDCl_3$ or there are two different types of salophen present. ^1H, ^1H NOESY and ^1H, ^1H GS COSY 2D measurements were carried at -50 °C to aid the assignment of the heavily split spectrum. Couplings seen in the 2D-spectra reveal that the benzyl protons are coupled to the phenyl ring highest in the molecule (from 1,2-diaminobenzene). According to molecular modeling, the benzyl protons are too far from that phenyl ring for coupling to be possible, but if the molecule self - organizes as a dimer, it is possible for the benzyl protons to couple with the aromatic ring of the second salophen molecule. According to Takao and Ikea,[21] an imine singlet of the dimer structure is split from the tail at cold temperatures in $CDCl_3$ because of two chemically different environments for azomethine groups closest and farther from the bridging phenoxides. When the dimerization reaction is in equilibrium, both the imine singlets, the dimer and the solvent complex, could also be independently observed in all measurements. In the spectra of receptor **95** only one imine singlet is observed and it is split from the tail at cold temperatures. Hence it is assumed that receptor **95** is self-organized as a dimer in a quantitative yield already at 30 °C and no water complex exists in

$CDCl_3$ that prevents the complexation of the guest molecule. The diastereotopic nature of the benzyl protons is easily identified as two doublets. The presence of four doublets also supports the fact that the compound is a dimer in $CDCl_3$. The absence of the other imine singlet of the water complex and the existence of only water from $CDCl_3$ and not bound water also supports the stable dimer structure in $CDCl_3$ at 30 °C.

After several crystallization attempts to prove the dimer formation of **95** the dimer (**95**)$_2$ was obtained by very slow evaporation of the solvent acetone. The X-ray structure of (**95**)$_2$ is shown in Figure 56 (Appendix 11).

In the dimeric structure of receptor **95** the phenylmethoxy arms at the other side of the dimer cross each other making the structure unsymmetrical; that can also be seen from the NMR spectra measured at -50 °C. The distances from the uranium to the oxygen and nitrogen atoms of the salophen units are 2.24 – 2.56 Å. The distances from the uranium to the phenolic oxygen of the other salophen unit are 2.44 Å and 2.46 Å. The dimeric U-O-U (Figure 56) units block the seventh coordination site and hence the binding of the anion to the uranium cation is prohibited.

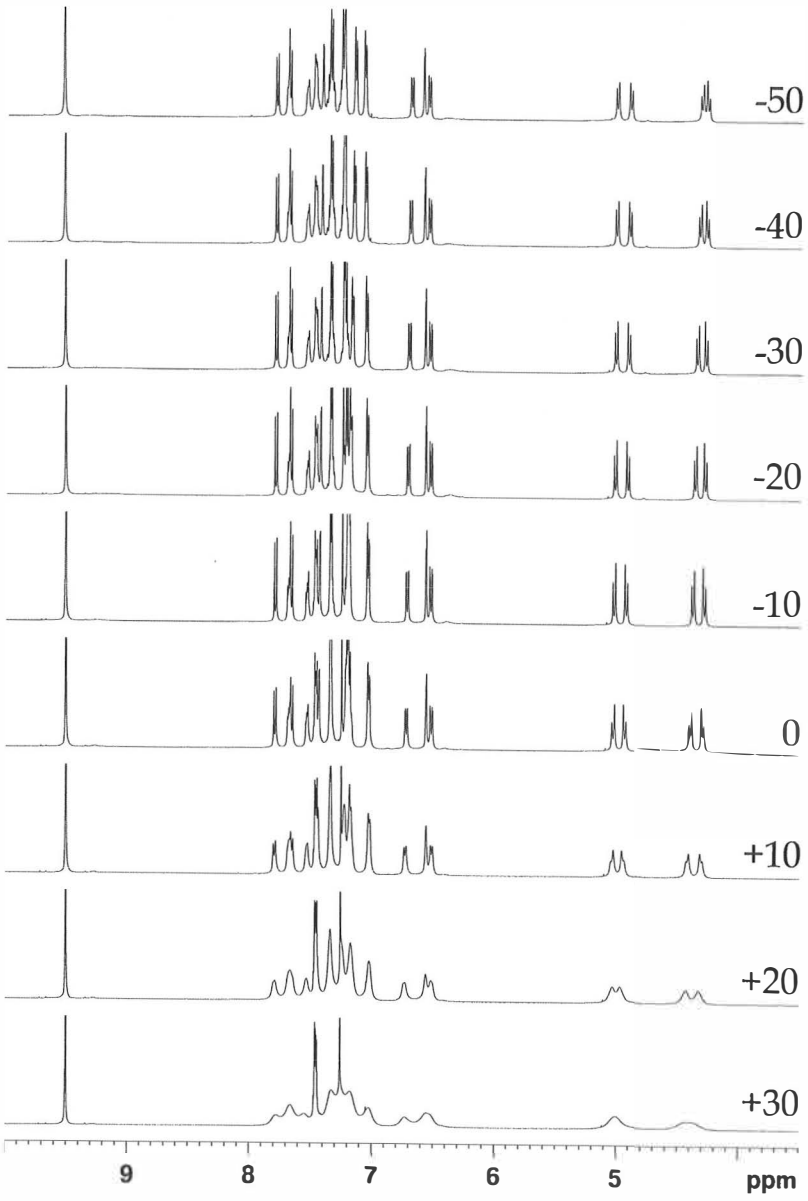

Figure 55 ^{1}H NMR measurements of receptor **95** in $CDCl_3$ at different temperatures (°C).

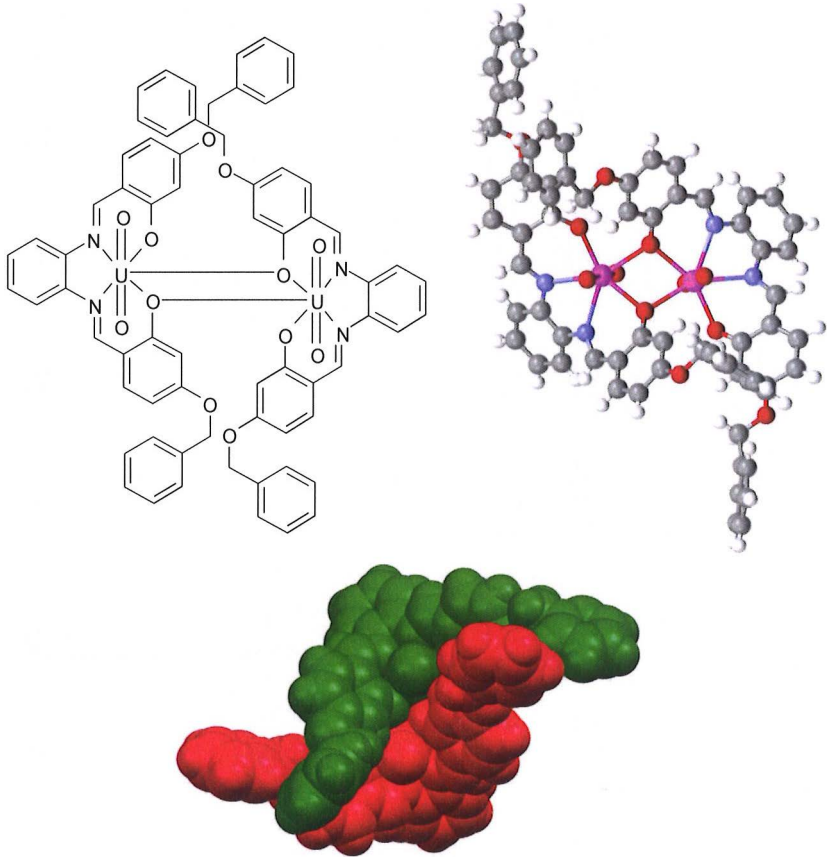

Figure 56 The chemical structure, ball and stick and CPK plots for (**95**)$_2$.

The same variable temperature measurements were done also for receptors **9** and **100**. The spectra of receptor **9** are very similar in $CDCl_3$ and DMSO[14]. There is only one imine singlet and it is not split at all. Also only one singlet for the benzylic protons is observed. When the temperature reaches -50 °C, the spectrum only gets sharper, but no new peaks or dynamics can be observed (Figure 57). Only the signal of the uranyl-bound water moves to a lower field during the measurements and finally it disappears due to freezing.

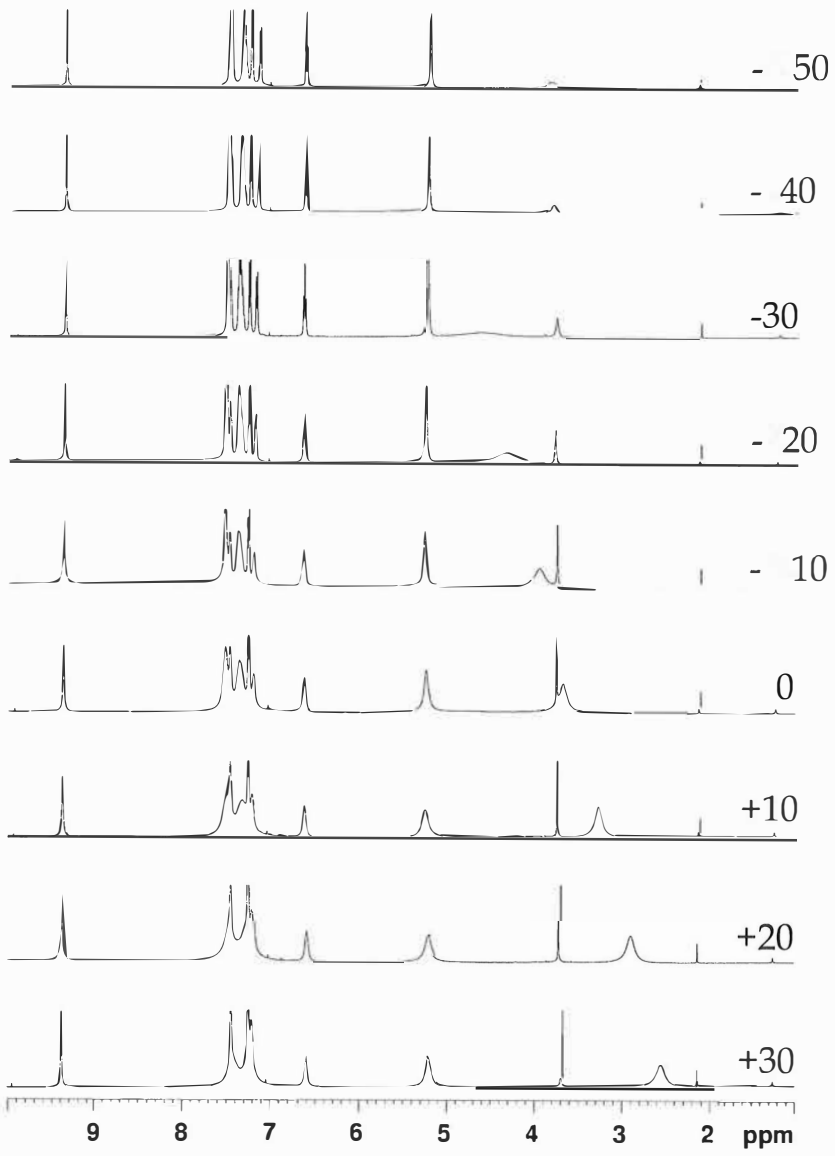

Figure 57 ^{1}H NMR measurements of receptor **9** in $CDCl_3$ at different temperatures (°C).

This behavior is probably due to the overall structure of **9**. Two arms at 3-positions are in close proximity to the uranium atom and act as spatial blockers preventing the dimerization and thus making the uranium accessible to binding of anions (such as chloride and fluoride)

In a spectrum of receptor **100** in $CDCl_3$ two imine singlets, another being split, one benzylic singlet and one doublet are observed at 30 °C (Figure 58). This refers to the equilibrium between the dimer and water complex in $CDCl_3$. The split imine singlet vanishes at lower temperatures and the singlet of the complexed water remains. Also the dimeric benzyl doublet disappears during freezing, which indicates that the water complex is more stable than the dimer and that the complexation of the other guest molecules (anions) is possible, although not as effective as with receptor **9**. The overall reaction, including the water and chloride exchange during the complexation, the formation of dimer and enantiomer exchange of dimer, is shown in Scheme 12.

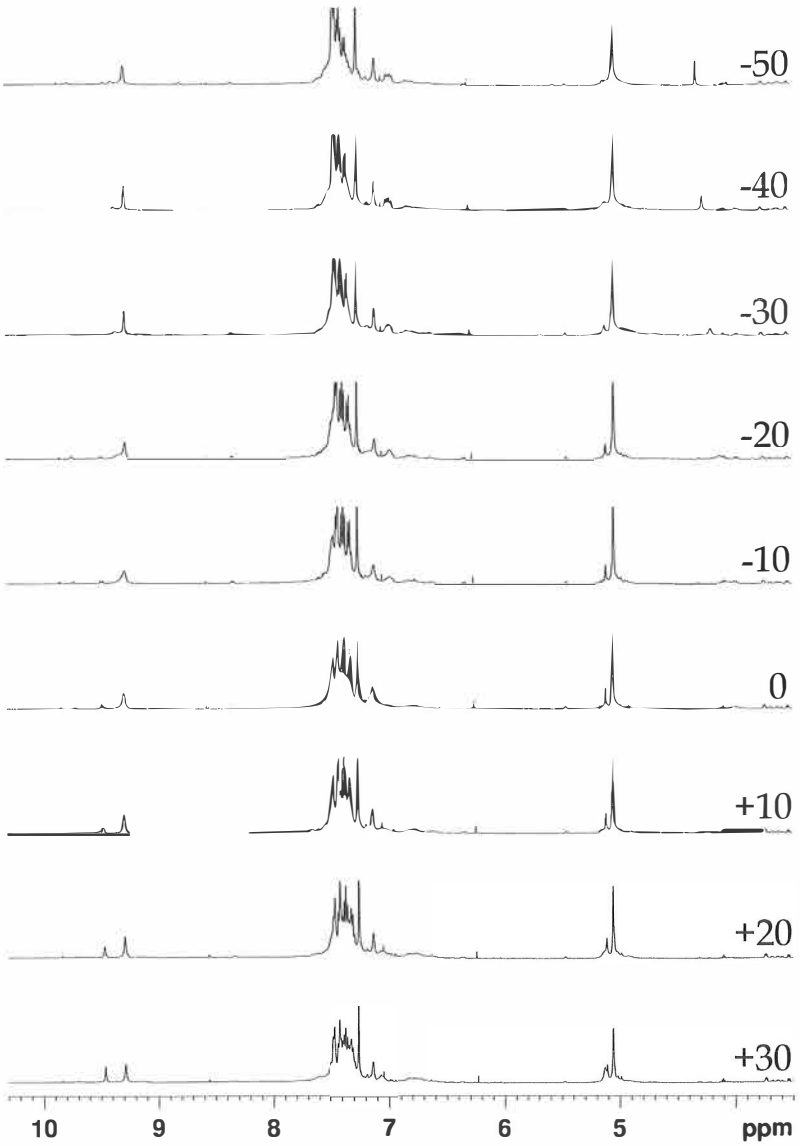

Figure 58 ^{1}H NMR measurements of receptor **100** in $CDCl_3$ at different temperatures (°C).

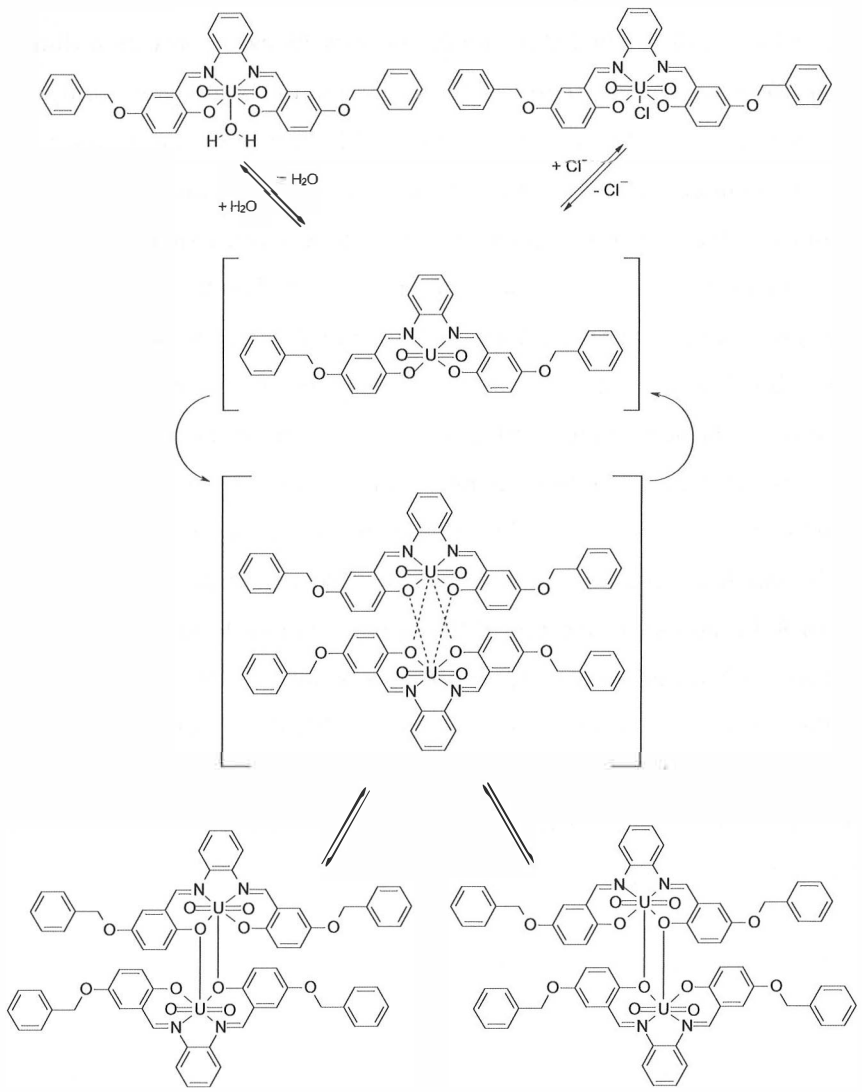

Scheme 12 Overall reaction including water and chloride exchange, the formation of dimer and enantiomer exchange of the dimer during the complexation.

As a conclusion, the results at different temperatures indicate that receptor **9** does not form a dimer in $CDCl_3$, while receptor **95** exists only as a dimer and receptor **100** exists as in a mixture of the dimer and the initial water complex. The structure of receptor **9** makes it suitable for binding the anion to the uranium atom and simultaneously the cation to the cleft via C-H···π interactions. Receptor **95** is not capable of binding anions in its dimeric form. However, at high salt concentrations **95** does show some binding, manifested by the downfield shifting of the signals during titration. Obviously, high salt concentration can force the dimer to break down and some binding do happen. As these two processes are happening at the same time, a reliable determination of the binding constant is not possible. Receptor **100** shows a mixed complexation behavior possibly due to the exchange from the non-binding dimer to the monomeric free UO_2-binding site. The binding constant values for receptor **100** are much lower than those of receptor **9**. In the case of receptor **9** the cation is bound to the cleft between the salophen's side arms. With receptor **100** this is not possible because both arms are oriented away from the uranyl center. In **100** the cation is quite probably bound to the upper π-system as in the core salophen **1**. This is supported by the similar TMACl binding constants of the core salophen **1**, K ~ 1000 when it is ~ 800 for the receptor **100**.

4.2 Phenylmethoxy uranyl salothiophens

A change of the phenylmethoxy group from 3-position to 4- or 5-position of the salophens gave too open structures and the cleft between sidearms was lost. Hence another way to obtain cleft-like structures was needed. The route to this is to change the 1,2-diamino benzene moiety in the salophen into another, yet structurally similar, moiety. The first try was 1,8-diamino naphthalene,[137] but it turned out that due to sterical reasons only one of the amino groups will react

and no uranyl salophen-type of receptor can be obtained. Instead, a structurally similar five-membered ring compound, 3,4-diaminothiophene **104,** was used in place of 1,2-diaminobenzene **94** due to the easy uranyl complexation and the slightly different amino-ring-amino angle and N···N distance of **104**. In **94** (CCDC BAGFIY, Cryst. Struc. Commun. 10 (1981), 1081) this angle (measured as H_2N-ring centroid-NH_2) is 58.8 deg. and N···N = 2.75 Å, while in **104** (CCDC NISTAL, Sol. energy Mater. Sol. Cells 91 (2007), 996) the corresponding values are 65.5 deg. and 2.84 Å, which should make the resulting uranyl thiosalophen slightly more open at the uranyl center. In addition the sulfur atom also offers an opportunity to bind these uranyl salothiophens into a silver[138-139] or copper[140] surface.

4.2.1 Synthesis and characterization of 105 and 106

3-phenylmethoxy- (**105**) and 4-phenylmethoxy salothiophens (**106**) were prepared by adding 2-hydroxy-3-(phenylmethoxy)-benzaldehyde **103** or 2-hydroxy-4-(phenylmethoxy)-benzaldehyde **93** and 3,4-diaminothiophene **104** to uranyl acetate in methanol under reflux (Scheme 13). Yields for **105** and **106** were respectively 60 % and 88 %.

The thiosalophens were characterized by ^{1}H NMR, ^{13}C NMR, mass spectrometry and elemental analysis. The ^{1}H NMR spectrum of **105** shows a singlet at 9.71 ppm due to imine protons and a singlet at 7.82 ppm due to aromatic protons in the thiophene moiety. In the ^{1}H NMR of **106**, a singlet due to imine protons is at 9.59 ppm and a singlet due to aromatic protons in the thiophene moiety is at 7.96 ppm. In the MS-spectrum of **105**, M+CH_3O^- peak is observed at m/z = 833.4, and in case of **106**, M+CH_3O^- peak is observed at m/z = 833.5. The exact synthetic procedures and characterization data of ^{1}H NMR, ^{13}C NMR, MS, and EA for both uranyl thiosalophens are reported in the experimental section (page 149).

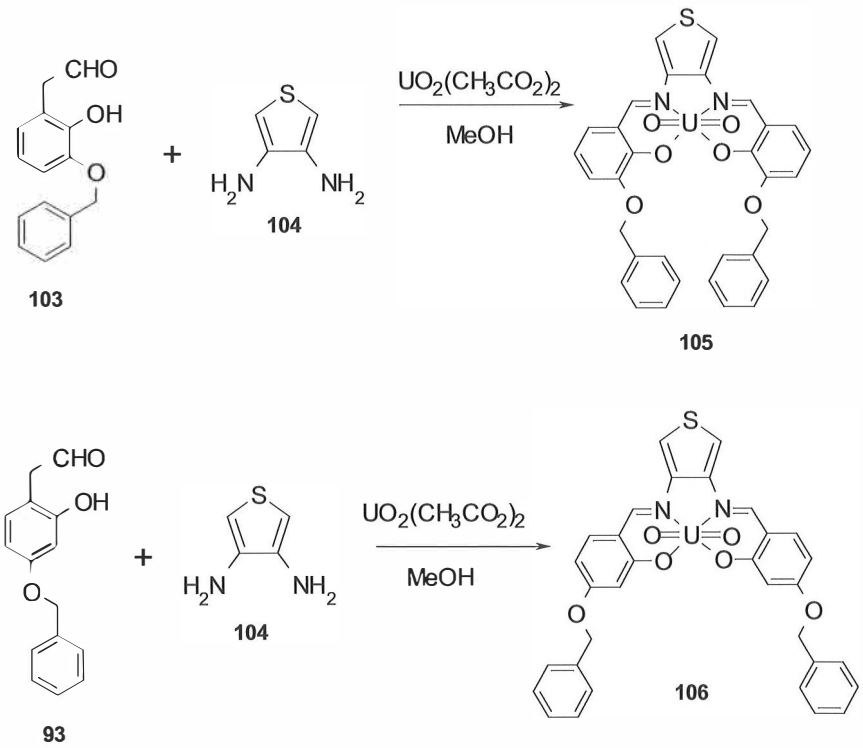

Scheme 13 Synthesis of **105** and **106**.

4.2.2 Crystallization experiments

4.2.2.1 Crystal structures of the solvent complexes of 106

4-phenylmethoxy uranyl salothiophen was crystallized as a solvent complex with methanol and water (Figure 59, Appendices 12 and 13). Crystals in good quality were obtained by a slow evaporation of methanol and, in the case of the water complex, from moist acetone. The 3-phenylmethoxy uranyl salothiophen

105 unfortunately did not crystallize as a solvate complex despite several attempts. The original objective of more open structures was not attained even though 3,4-diaminothiophene **104** should lead to a more open structure than 1,2-diaminobenzene **94**, its U-O and U-N distances and angles in uranyl salothiophenes being very similar to the corresponding values in uranyl salophens. Obviously the uranyl cation binds the organic salophen structure tightly to itself and forces **104** to adopt very similar bond distances and angles around the U-atom as in the case of **94**.

In the X-ray structure (Figure 59) of the methanol complex, **106**•MeOH, the distances between the salothiophen ligand and uranium are 2.22-2.54 Å and the distance between uranium and the oxygen atom of methanol is 2.51 Å. In the structure of the water complex, **106**•H_2O, the distances between the salothiophen ligand and uranium are 2.25-2.55 Å and the distance between uranium and the oxygen atom of water is 2.45 Å. These bond distances are about the same as in a normal salophen ligand with a diaminobenzene moiety. In both **106**•MeOH and **106**•H_2O two of the uranyl salothiophen solvent complexes are joined together by hydrogen bonds between the phenolic oxygen of the adjacent salothiophen ligand and the hydrogen atom of the complexed solvent molecule.

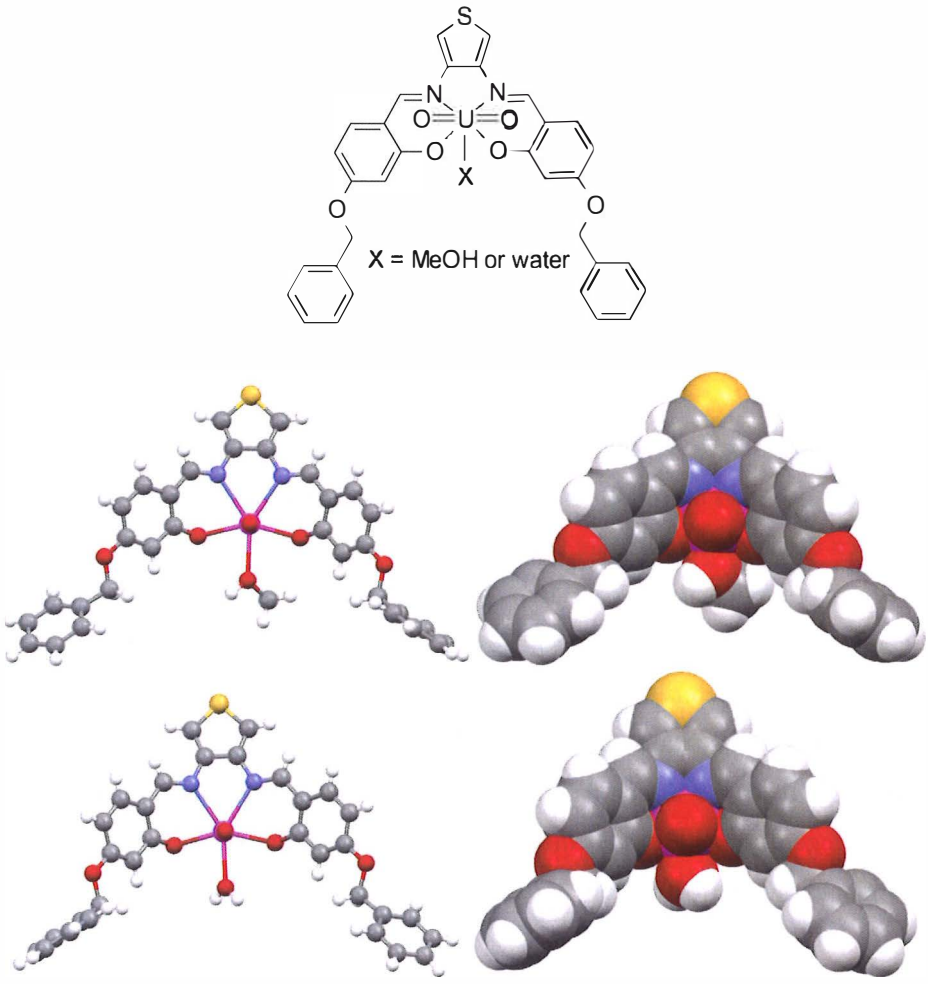

Figure 59 Chemical structure, ball and stick and CPK plots of **106**•MeOH (top) and **106**•H_2O (bottom).

4.2.2.2 Solid state complexation studies of 105 and 106

In order to compare the complexation behavior of thiosalophen with the corresponding salophen analogs, a similar study with the tetraalkyl ammonium salts in both solid state and solution was executed. Surprisingly, the uranyl salothiophen-R_4NX complexes turned out to be much more insoluble to $CDCl_3$, causing precipitation with all R_4NXs used, thus rendering the determination of binding constants impossible. The focus was directed to solid state complexation experiments with tetraalkyl ammonium chlorides (DMDEACl **98a**, DMDPACl **98b**, DMDBACl **98c**, TMACl **99a**, TEACl **99b**, TPACl **99c** and TBACl **99d**). These experiments resulted in four R_4NCl complex structures, two for the 3-phenylmethoxy uranyl salothiophen (**105**) and two for the 4-phenylmethoxy uranyl salothiophen (**106**). Figure 60 (Appendix 14) shows the TMACl complex of 3-phenylmethoxy salothiophen **105•99a**. The crystals were obtained by adding an excess amount of the salt to the chloroform solution of the receptor and then slowly evaporating the solvent. The interactions and their distances in **105•99a** are shown in Table 10.

In the structure of **105•99a** the chloride anion is bound to the uranium with a distance of 2.71 Å, which is a bit shorter than the distances in normal salophen structures. The bond lengths from the uranium to the salothiophen O- and N-atoms are 2.26-2.65 Å. The TMA cation is bound to one sidearm via C-H···π interactions from one methyl hydrogen of the TMA to the aromatic carbon in the arm (2.88 Å). The TMA cation is connected to the chloride via three hydrogen atoms from three different carbons (C-H···Cl: 2.90 Å, 2.79 Å, and 2.81 Å). One of these methyl hydrogen atoms is also simultaneously connected to the phenolic oxygen of the salothiophen ligand (2.46 Å). The distance between the chloride

and the nitrogen is 3.97 Å. Like in the **9•99a**[67-68], also **105•99a** exists in the crystal as a 4:4 assembly,

Table 10 Interactions and their distances in **105•99a**.

Interaction	Distance [A]
C-H···π (C)	2.88
C-H···π (centroid)	2.91
C-H···Cl$^-$	2.79 – 2.90
C-H···O=U	2.96
C-H···O$^-$-Ph	2.46
N$^+$··· π (centroid)	4.64
N$^+$··· Cl$^-$	3.97
U··· Cl$^-$	2.71
U-O/N	2.26 – 2.65

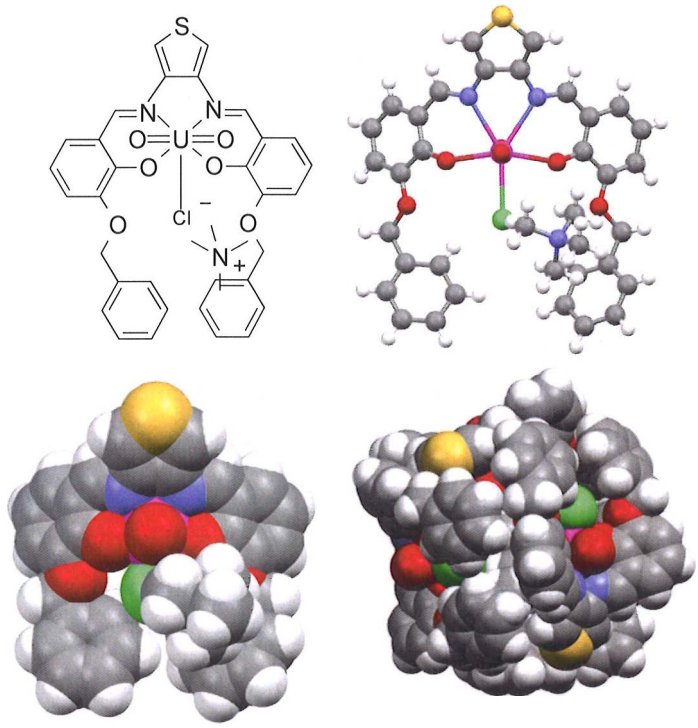

Figure 60 The chemical structure, ball and stick and CPK plot of **105•99a**. On the right bottom a structure of the spherical 4:4 assembly is shown.

where four uranyl salothiophen chloride molecules create a football-like structure and the four TMA cations are located inside the ball (Figure 60, bottom, right).

Using the same technique as with **105•99a**, crystals of dimethyldibutyl ammonium chloride (**98c**) complex with **105** were obtained. Figure 61 (Appendix 15) shows the X-ray structure of **105•98c**. Interactions and their distances in **105•98c** are shown in Table 11.

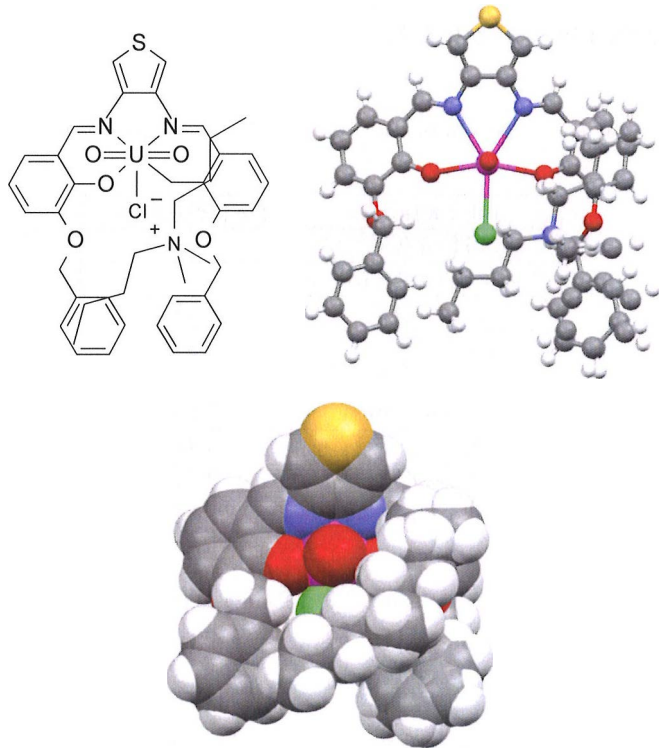

Figure 61 The chemical structure, ball and stick and CPK plot of **105•98c**.

In the X-ray structure of **105•98c** the chloride anion is bound to the uranium with a distance of 2.74 Å, which is about the same as in **105•99a**. The bond lengths from the uranium to the salothiophen O- and N-atoms are 2.26 - 2.61 Å. There are no obvious C-H···π interactions as in the case of the corresponding salophen complex **9•98c**. Instead ion-pairing and hydrogen bonding play an important role. One of the methyl hydrogen atoms is weakly hydrogen bonded (2.62 Å) to the ether oxygen of the sidearm. Two methylene hydrogens close to the N-atom are weakly hydrogen bonded to the chloride (2.65 Å) and to the uranyl oxygen (2.50 Å). The distance for N···π (centroid) is 5.08 Å and the distance between the chloride and the nitrogen is 4.24 Å.

Table 11 Interactions and their distances in **105•98c**.

Interaction	Distance [A]
C-H···π (C)	-
C-H···π (centroid)	-
C-H···Cl^-	2.65
C-H···O=U	2.50
C-H···O^--Ph	2.65
N^+··· π (centroid)	5.08
N^+··· Cl^-	4.24
U··· Cl^-	2.74
U-O/N	2.26 – 2.61

The 4-phenylmethoxy uranyl salothiophen **106** cocrystallizes with TMACl **99a** by a slow evaporation of chloroform with an excess amount of the salt. The crystal structure of the complex is shown in Figure 62 (Appendix 16). Interactions and their distances between the receptor **106** and TMACl **99** are shown in Table 12.

Table 12 Interactions and their distances in **106•99a**.

Interaction	Distance [A]
C-H···π (C)	2.80
C-H···π (centroid)	2.80
C-H···Cl⁻	2.77
C-H···O=U	-
C-H···O⁻-Ph	-
N⁺··· π (centroid)	4.44
N⁺··· Cl⁻	4.00
U··· Cl⁻	2.77
U-O/N	2.24 - 2.60

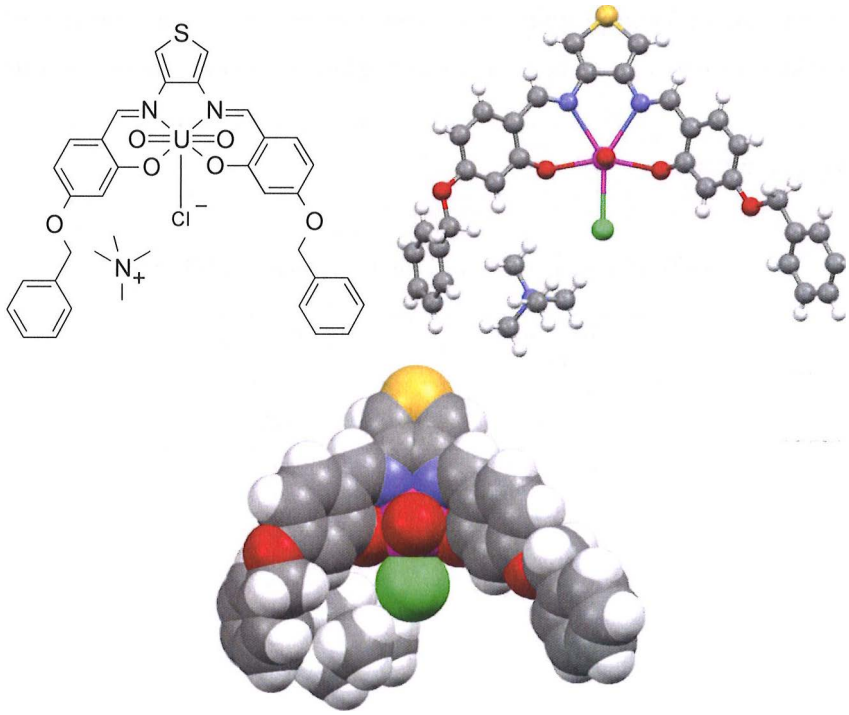

Figure 62 The chemical structure, ball and stick and CPK plots of **106•99a**.

In the structure of **106•99a** the chloride anion is bound to the uranium with a distance of 2.77 Å, which is again about the same as the distance in a normal

salophen structure. The bond lengths from the uranium to the salothiophen ligand vary from 2.24 to 2.60 Å. The cation is bound to the sidearm via C-H···π interactions exactly as in **95•99a** by a connection from a hydrogen atom of one methyl group to one aromatic carbon of the arm (2.80 Å). One hydrogen atom of the other methyl group is also connected to chloride (2.77 Å). The closest distance for CH···π (centroid) is 2.80 Å and the closest distance for N···π (centroid) is 4.44 Å. The distance between the chloride and the nitrogen is 4.00 Å.

In Figure 63 (Appendix 17) the complex of 4-phenylmethoxy uranyl salothiophen **106** with dimethyldiethyl ammonium chloride **98a** is shown. Interactions and their distances between receptor **106** and DMDEACl **98a** are shown in Table 13. This structure was obtained by a slow evaporation of acetone with an excess amount of the salt.

Table 13 Interactions and their distances in **106•98a**.

Interaction	Distance [A]
C-H···π (C)	-
C-H···π (centroid)	-
C-H···Cl^-	2.76/2.94
C-H···O=U	2.64
C-H···O^--Ph	2.64
N^+··· π (centroid)	7.66
N^+··· Cl^-	4.06
U··· Cl^-	2.76
U-O/N	2.25 – 2.61

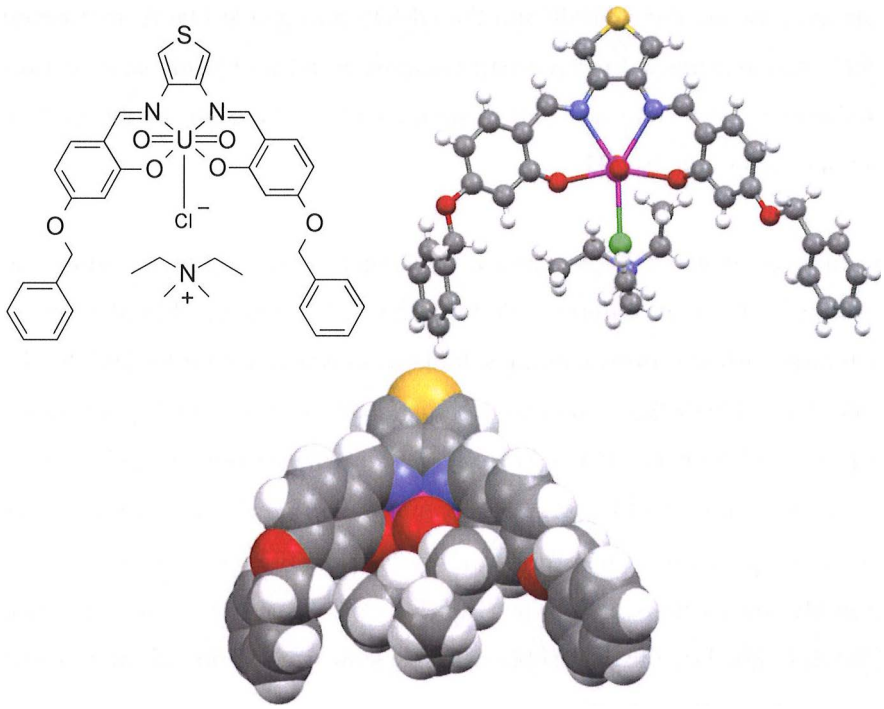

Figure 63 The chemical structure, ball and stick and CPK plots of **106•98a**.

In the X-ray structure of **106•98a** the chloride anion is bound to the uranyl cation with a distance of 2.76 Å, the same as in salophen structures. The bond lengths from the uranyl to the salothiophen ligand are 2.25 - 2.61 Å. No cation-π interaction is observed in this structure. The methylene hydrogen atoms from the same ethyl chain and one methyl hydrogen atom are weakly hydrogen bonded to chloride (2.76 Å and 2.94 Å) and one hydrogen atom at the end of the other ethyl chain is interacting with the phenolic oxygen of the salothiophen ligand (2.64 Å).

When compared with receptor **95** the location of the DMDE cation is very different in receptor **106**. The distance for N···π (centroid) is 7.66 Å while the

distance between the chloride and the DMDE nitrogen is 4.06 Å. In **106•98a** the DMDE cation forms a direct ion-pair complex with the chloride anion containing salothiophen; there are no C-H···π interactions as there are in the case of the corresponding salophen **95**.

In order to see if the TMA cation with a much more strongly binding fluoride anion would show different binding modes in uranyl thiosalophen when compared with the corresponding salophens as was observed for DMDE binding in **95•98a** and **106•98a**, a solid state crystallization study with 3-phenylmethoxy uranyl salothiophene **105** and tetramethyl ammonium fluoride **101a** was conducted. Unlike **95•101a** which is 2:1 complex (page 89), the resulting **105•101a** is a 1:1 complex (Figure 64, Appendix 18) that, like **105•99a**, forms a spherical 4:4 assembly. Interactions and their distances in **105•101a** are shown in Table 14. Crystals of good quality were obtained by a slow evaporation of chloroform with an excess amount of the salt.

Table 14 Interactions and their distances in **105•101a**.

Interaction	Distance [Å]
C-H···π (C)	2.86
C-H···π (centroid)	2.67
C-H···F^-	2.40/2.60
C-H···O=U	2.68
C-H···O^--Ph	2.27
N^+··· π (centroid)	4.54
N^+··· F^-	3.70
U··· F^-	2.17
U-O/N	2.20 – 2.67

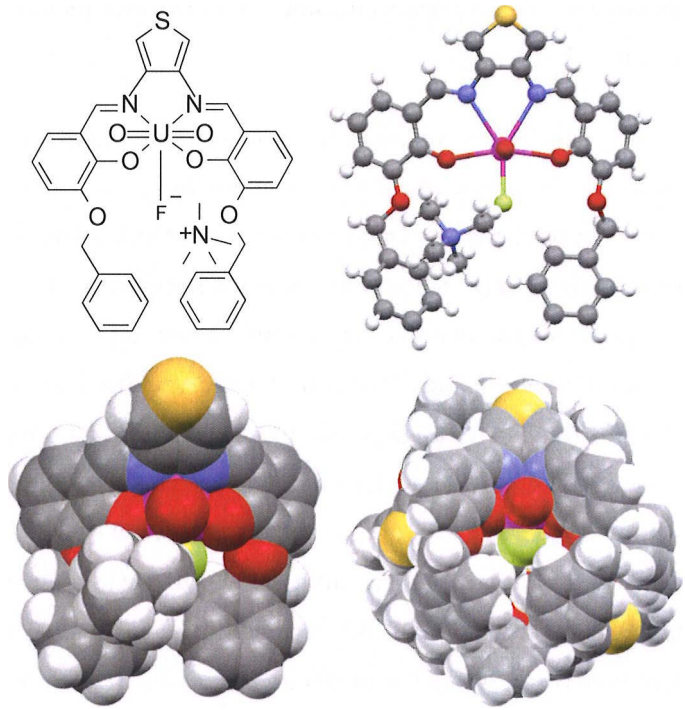

Figure 64 The chemical structure, ball and stick and CPK plots for **105•101a**. On the right bottom a structure of the spherical 4:4 assembly is shown.

In the X-ray structure of **105•101**, the fluoride anion is bound to the uranium at a distance of 2.17 Å, which is clearly shorter than the distance to the chloride, yet very similar to that in **(95)$_2$•101** (page 89). The bond lengths from the uranium to the salothiophen ligand are 2.20 - 2.67 Å. The TMA cation is bound to one sidearm via C-H···π interactions from one methyl hydrogen of the TMA to two aromatic carbons in the arm (2.86 Å and 2.86 Å) with a short CH···π (centroid) distance of 2.67 Å. In addition the TMA cation is bonded via two hydrogen atoms in different carbons to the fluoride anion (2.40 Å and 2.60 Å). One of these hydrogen atoms is also weakly hydrogen bonded to uranyl oxygen (2.68 Å). One of the methyl groups is hydrogen bonded (2.27 Å) to the phenolic oxygen of the

salophen ligand. The N···π (centroid) distance is 4.54 Å and that of fluoride and TMA nitrogen is 3.70 Å.

As a conclusion for the R_4NX complexation studies of the phenylmethoxy uranyl salophens and salothiophens, all the 3-phenylmethoxy and 4-phenylmethoxy salophens and salothiophens form complexes with TMACl in the solid state. The complex **9•99a** has been reported before.[67] **9•99a** is formally a 1:1 complex, but it exists in the crystal as a football-like 4:4 assembly where all four cations are fully enclosed by the salophen ligands. The complexes crystallized in this study, viz. **105•99a and 105•101a**, behave analogously forming spherical 4:4 assemblies. The 4-phenylmethoxy receptors **95** and **106** co-crystallize as 1:1 complexes with very similar structures with TMACl. Contrary to this, the two DMDEACl complexes **95•98a** and **106•98a** are surprisingly different. DMDPACl co-crystallizes only with receptor **9**. The larger DMDBACl cocrystallizes with **9**, **100 and 105**. The complex structures of receptors **9** and **105** are very similar. The bond distances are nearly identical and the cation lies similarly between the aromatic arms of the receptor molecule. However, the structure of the complex of receptor **100** with DMDBACl is very different due to the position of the sidearms, as expected. The strongly binding TMAF **101a** cocrystallizes with receptors **95** and **105** (see above). With receptor **95** the structure is a 2:1 complex where the two uranium atoms of salophen complexes share the fluoride anion, while the TMA cation is trapped between two benzene rings via cation···π interactions. This kind of fluoride-bridged dimer has not previously been observed with any uranyl salo- or salothiophens.

4.3. Bipyridyl uranyl salophens

In order to extend the selection of the guest molecules from tetraalkyl ammonium salts to poorly soluble copper and silver halides, bipyridyl[141-142] uranyl salophens were prepared. The ability of the 2,2'-bipyridine moiety to complex metal cations is well known[143-147]. According to simple molecular modeling both bipyridyl salophens **107-108** should be able to complex metal cations (Figure 65). 3-(2,2'-bipyridine)-5-methoxy uranyl salophen **107** forms an 1:1 complex and 4-(2,2'-bipyridine)-5-methoxy uranyl salophen **108** a 2:2 complex with a tetrahedral Cu^{+} or Ag^{+} cation. As the salophens are ditopic receptors, the anion of the metal salts should be bound to the seventh coordination site of the uranium cation.

Despite several crystallization experiments performed, no single crystals of the complexes with silver or copper salts were obtained. Instead the structures of the interesting water complex, creating a hydrogen bonded chain of water molecules inside the bipyridyl cavity of **107**, was determined in the solid state.

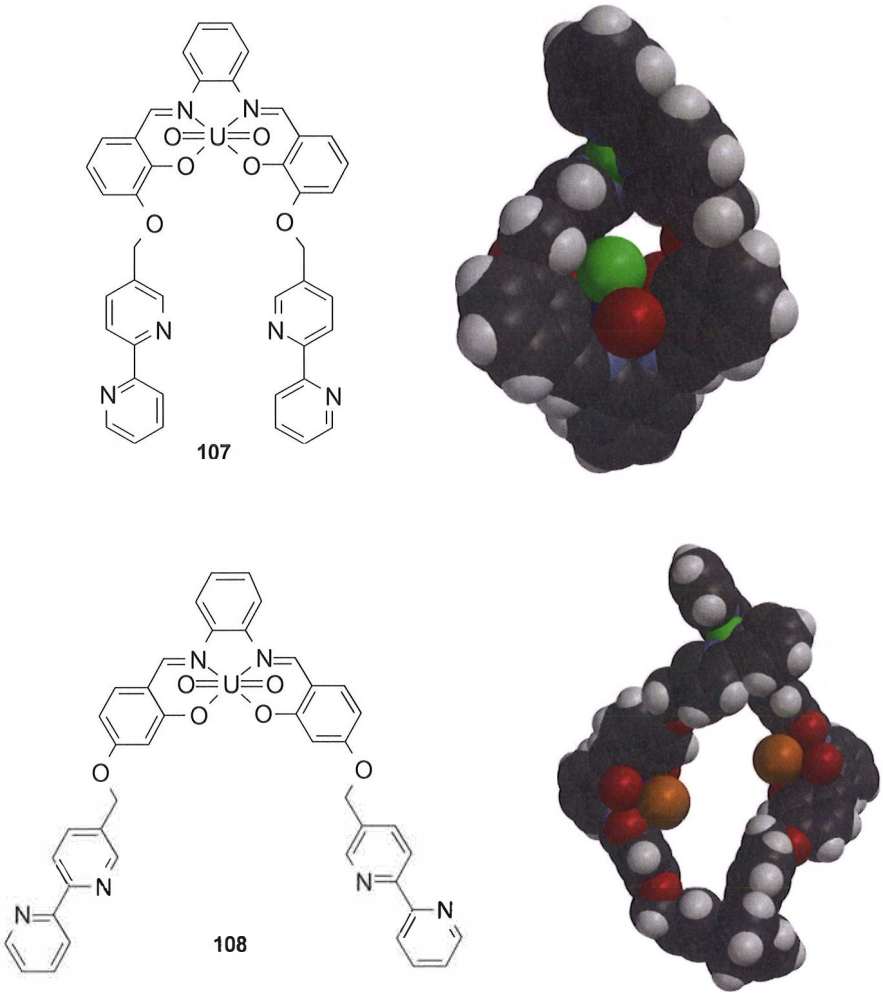

Figure 65 The chemical structures of receptors **107** and **108** and molecular models of their Cu^{+}-complexes.

4.3.1 Synthesis and characterization of 107 and 108

The synthesis of **107** and **108** starts with the synthesis of the 2,2'-bipyridine-5-methoxy derivated aldehydes **109** and **110**, which were prepared and

characterized (^{1}H NMR, ^{13}C NMR, MS and EA) according to the literature.[44,148-151] The exact synthetic procedures and characterization data of ^{1}H NMR, ^{13}C NMR, MS, and EA for all the products are descriped in the experimental section (page 150).

In the synthesis of the bipyridine moiety (Scheme 14)[149-151] 2-acetylpyridine **111** was first treated with iodine in pyridine at 80 °C to get (2-pyridacyl)pyridium iodide **112** in 33 % yield, whereupon **112** was used in the Krohnke pyridine synthesis with methacrolein **113** and ammonium acetate in formamide at 75 °C to get 5-methyl-2,2'-bipyridine **114** in a quantitative yield. The bipyridine derivative **114** underwent AIBN-catalyzed bromination with NBS in CCl_4, giving 5-bromomethyl-2,2'bipyridine **115** in a 65 % yield, which was used in the Williamson ether synthesis with the corresponding benzaldehyde.

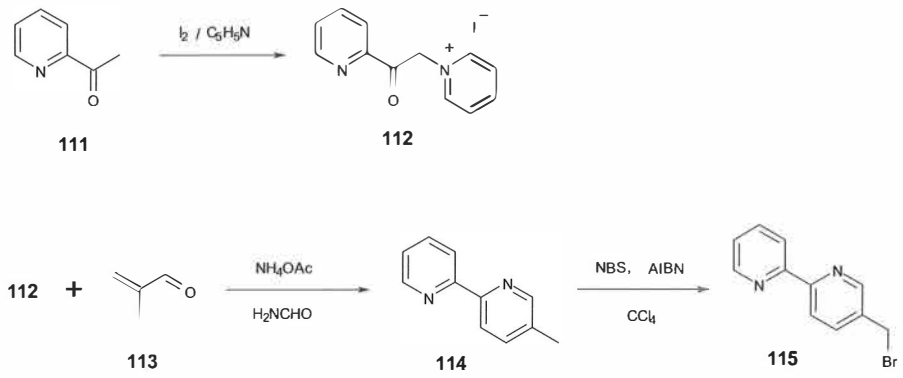

Scheme 14 Synthesis of 5-bromomethyl-2,2'bipyridine **115**.[149-151]

The acidity of the hydroxyl group differs on whether it is located in the 3- or 4-position in dihydroxybenzaldehydes. Hence, while 2-hydroxyl-4-(2,2'-bipyridine-5-methoxy)benzaldehyde **110** can be synthesized in a 28 % yield by a

one-pot synthesis, where 2,4-dihydroxybenzaldehyde **91** is treated with 5-bromomethyl-2,2′bipyridine **115**, $NaHCO_3$ and KI in acetonitrile at room temperature under nitrogen (Scheme 15), the synthesis of 2-hydroxyl-3-(2,2′-bipyridine-5-methoxy)benzaldehyde **109** needs extra synthetic steps because the hydroxyl group in position 3 in 2,3-dihydroxybenzaldehyde **116** needs to be protected before the ether synthesis. The hydroxyl group in position 2 is selectively protected by 3-bromo-1-propene **117** in a reaction with NaH in DMSO at room temperature to give 2-allyloxy-3-hydroxybenzaldehyde **118** in a 38 % yield, which was then used in the ether synthesis with 5-bromomethyl-2,2′bipyridine **115** and K_2CO_3 in acetonitrile at room temperature under nitrogen to give 2-allyloxy-3-(2,2′bipyridine-5-methoxy)-benzaldehyde **119** in a 27 % yield. The protecting allyl group was removed by a reaction with SeO_2, acetic acid, and 1,4-dioxane to give 2-hydroxyl-3-(2,2′bipyridine-5-methoxy)-benzaldehyde **109** in a 31 % yield. The deprotection reaction was made under reflux.

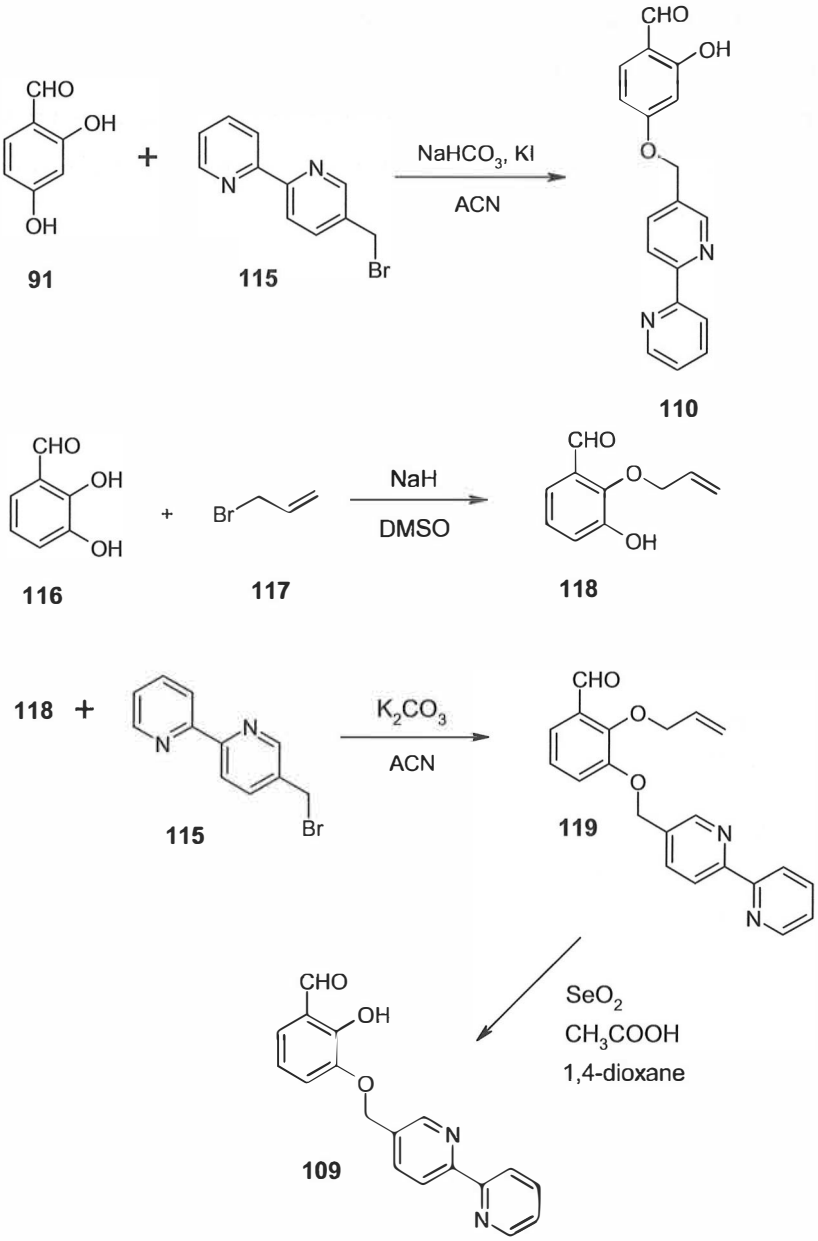

Scheme 15 Synthesis of 2-hydroxyl-4-(2,2′-bipyridine-5-methoxy)benzaldehyde **110** and 2-hydroxyl-3-(2,2′bipyridine-5-methoxy)-benzaldehyde **109**. [44,148-151]

3-(2,2'-bipyridine)-5-methoxy uranyl salophen **107** and 4-(2,2'-bipyridine)-5-methoxy uranyl salophen **108** were prepared by adding 1,2-diaminobenzene **94** with the corresponding benzaldehyde (**109** or **110**) to uranyl acetate in methanol under reflux (Scheme 16). The uranyl salophens **107 - 108** were isolated in 67 % (**107**) and 45 % (**108**) yields.

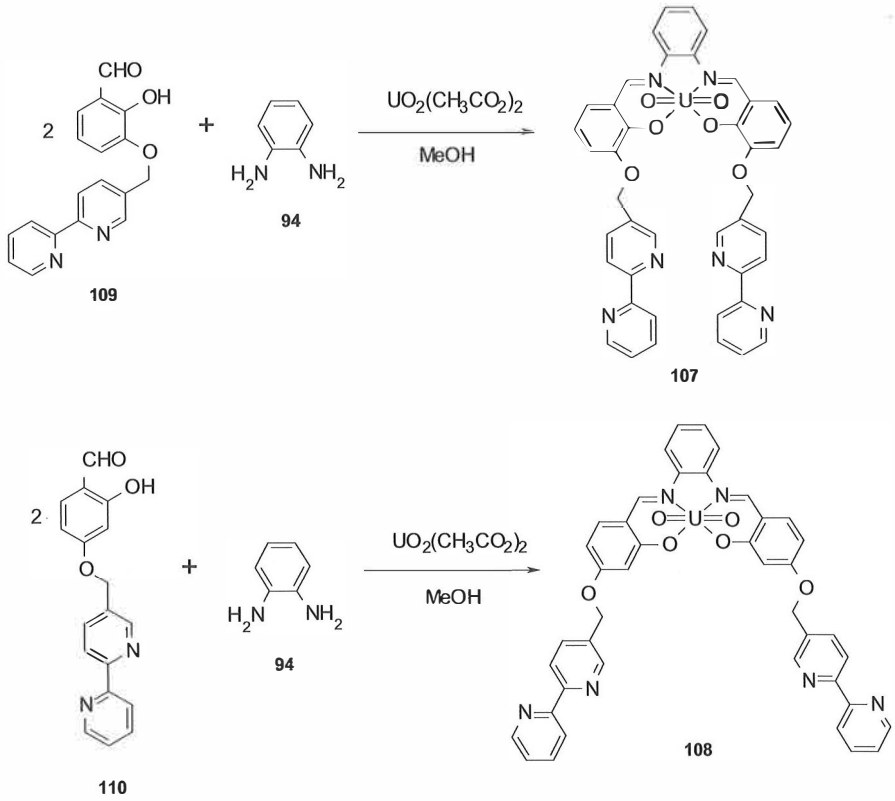

Scheme 16 Synthesis of 3-(2,2'-bipyridine)-5-methoxy uranyl salophen **107** and 4-(2,2'-bipyridine)-5-methoxy uranyl salophen **108**.

The uranyl salophens were characterized by ^{1}H NMR, ^{13}C NMR, mass spectrometry and elemental analysis. The ^{1}H NMR spectrum of **107** shows a singlet at 9.60 ppm due to the imine protons. In the ^{1}H NMR of **108** a singlet due

to imine protons is at 9.51 ppm. The peak pattern due to the bipyridine moiety is almost the same in both the spectra, the chemical shifts being only slightly different. The detailed analysis of the ^{1}H NMR spectrum of **107** is shown in Figure 66. In the MS-spectrum of **107**, the $M+CH_3O^-$ peak is observed at m/z = 983.6, and in case of **108**, the $M+CH_3O^-$ peak is observed at m/z = 983.4. The exact synthetic procedure and characterization data of ^{1}H NMR, ^{13}C NMR, MS, and EA for both products is in the experimental section (page 151).

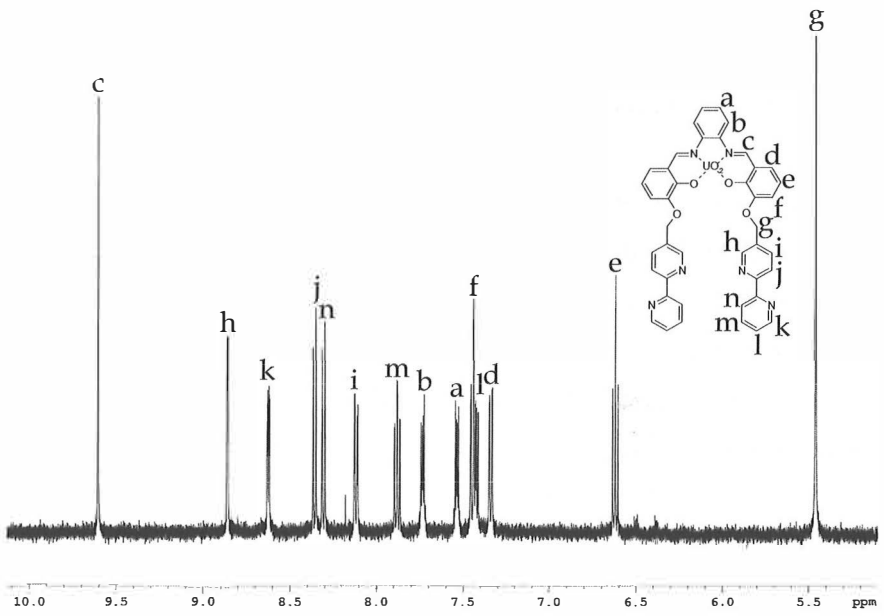

Figure 66 The ^{1}H NMR spectrum of **107** in D_6-DMSO.

4.3.2 Crystallization experiments

3-(2,2′-bipyridine)-5-methoxy uranyl salophen **107** was crystallized by a slow evaporation of acetonitrile and acetone to give three different solvent complex

structures. The first X-ray structure includes two different salophen-water complexes, one with two and the other one with three water molecules (from a slow evaporation of acetonitrile) (Figure 67, Appendix 19). A slow evaporation of acetone gave the acetone solvate complex (Figure 68, Appendix 20). All crystallization experiments of 4-(2,2′-bipyridine)-5-methoxy derivative **108** with metal salts or from pure solvent were unfortunately unsuccessful.

Figure 67 shows the two independent water complexes, one having three water molecules, **107**•3H_2O, and the other with two water molecules, **107**•2H_2O. In **107**•3H_2O there are three water molecules forming a chain between the uranium and the bipyridine at the 3′ position. The water chain starts from the uranium atom where the water is bound with a U-O distance of 2.45 Å; the second water is hydrogen bonded to the uranyl water (O-H···O, 1.82 Å) and to the third water (O-H···O, 1.89 Å). The third water molecule is hydrogen bonded to the nitrogen atom (O-H···N, 1.99 Å) of the bipyridine at the 3′ position forming a U-H_2O-H_2O-H_2O-N(bipyr) chain. In **107**•2H_2O a very similar, yet one water molecule shorter chain is observed. The first water is bound to uranium (2.47 Å) and forms a hydrogen bond (O-H···O, 1.96 Å) to the second water, which is then hydrogen bonded (2.06 Å) to the nitrogen atom of the bipyridine at the 3-position. The remarkable feature of these structures is the orientation of the bipyridine arm into which the water chain is formed. In both cases the bipyridine nitrogens are in an *E*-configuration, but in **107**•3H_2O the nitrogen at the 3-position points out from the cleft, while the 3′ nitrogen points into the cleft; this order is reversed in **107**•2H_2O resulting in two differently sized clefts for the water molecules to bind, just suitable for three waters in the first case and two waters in the latter one.

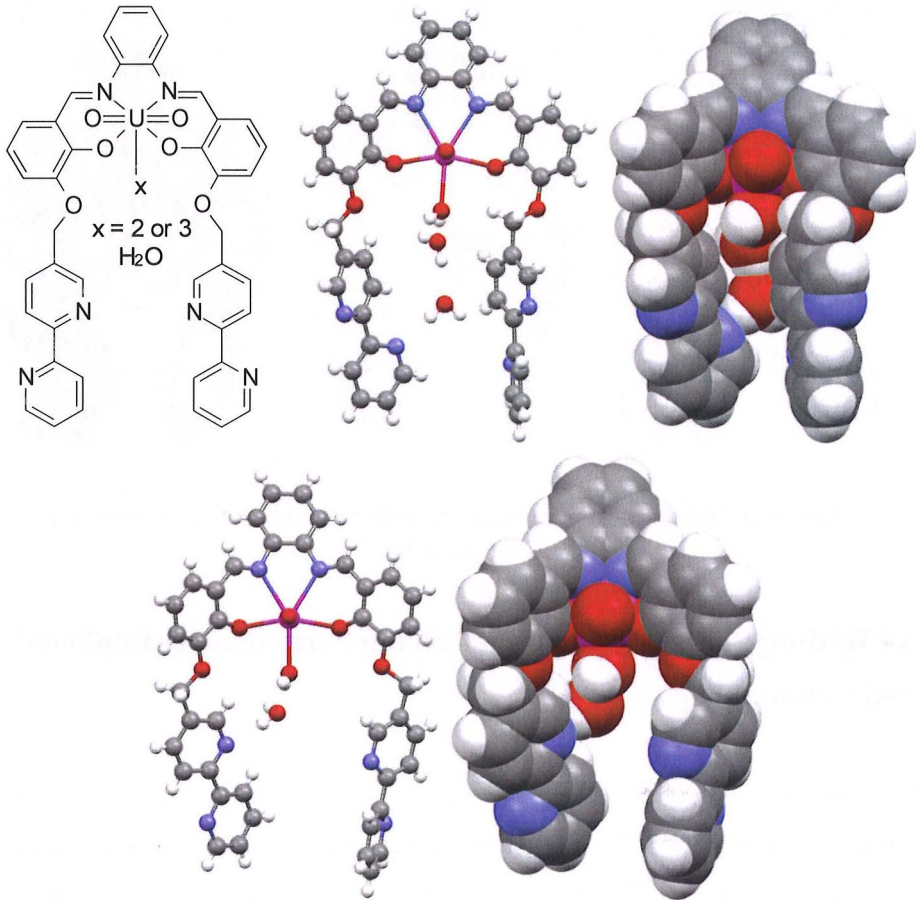

Figure 67 The chemical structure, ball and stick and CPK plots of **107**•3H_2O (top) and **107**•2H_2O (bottom) found in the same crystal structure.

In the structure of **107**•acetone (Figure 68, Appendix 20), the distance from uranium to the oxygen and nitrogen atoms is 2.26 and 2.55 Å. The oxygen atom of the acetone is bound to uranium with a distance of 2.50 Å, a typical U-O distance for neutral oxygen donors. The bipyridine sidearms form a tight cleft similar to other 3-position substituted salo- and salothiophens.

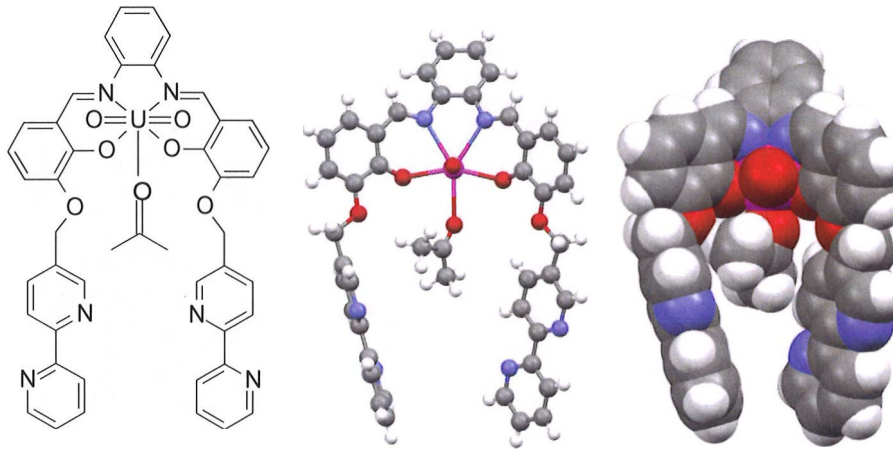

Figure 68 The chemical structure, the ball and stick and CPK plots for **107**•acetone.

4.4 Hydroxy, methoxy and cyclohexylmethoxy uranyl salophens and salothiophens

In order to have some additional information of the structures and binding abilities of the different salophen complexes without the aromatic sidearms, hydroxy, methoxy and cyclohexylmethoxy uranyl salophens and hydroxy salothiophens were prepared. Unlike phenylmethoxy and bipyridyl uranyl salophens, the hydroxy and methoxy uranyl salophens are not well soluble in non-polar solvents such as chloroform, and hence complexation experiments via similar NMR titrations performed as for **9**, **95** and **100** were not possible. Even though **129** is soluble in $CHCl_3$, complexation examination of it in solution was not part of this work. Thus the focus was directed to the solid state complexation experiments; unfortunately cocrystallization with neither tetraalkyl ammonium nor alkali metal salts did produce any complexes.

4.4.1 Synthesis and characterization

Hydroxy uranyl salophens and salothiophens from 2,3-dihydroxylbenzaldehyde **116** and 2,4-dihydroxylbenzaldehyde **91** were prepared, both with 1,2-diaminobenzene **94** and 3,4-diaminotiophene **104** (Scheme 17). The synthesis of **120** and **121** was performed in methanol at room temperature with yields of 75 % for both. For the synthesis of **122** and **123** reflux was needed because of the poor solubility of 3,4-diamino thiophene **104** in methanol. Yields were 91 % for **122** and 79 % for **123**.

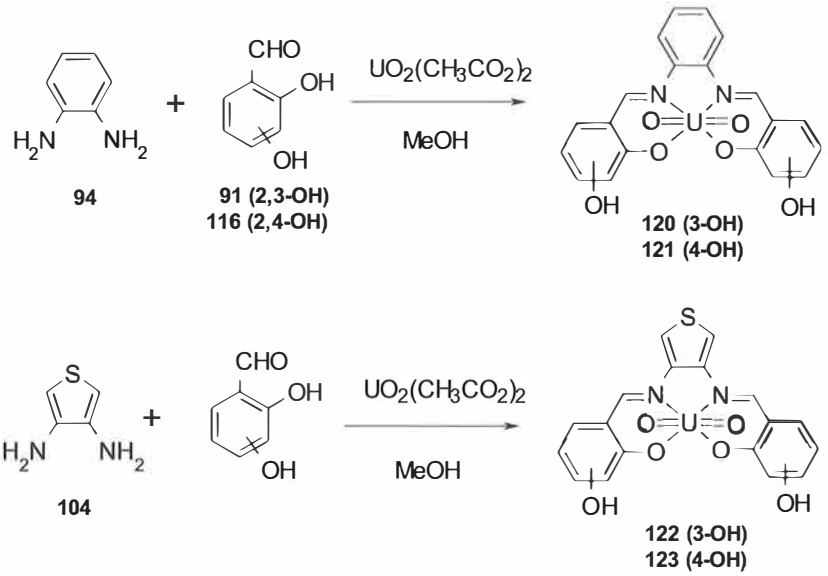

Scheme 17 Synthesis of hydroxy uranyl salophens **120** and **121** and hydroxyl salothiophens **122** and **123**.

The products were characterized by ^{1}H NMR, ^{13}C NMR, mass spectrometry and elemental analysis. The ^{1}H NMR spectra of 3-hydroxy uranyl salo- and salothiophens show a singlet due to imine protons at 9.58 ppm for **120** and at 9.68

ppm for **122**, and a singlet due to hydroxyl protons at 8.48 ppm for **120** and at 8.46 ppm for **122**. For the 4-hydroxyl analogs singlets due to imine protons are at 9.41 ppm for **121** and at 9.50 ppm for **123**. Singlets due to hydroxyl protons are at 10.16 ppm for **121** and at 10.20 ppm for **123**. Peak patterns due to aromatic protons are the same as in phenyl methoxy uranyl salo(thio)phens. In the MS-spectrum of **120** M-1 peak is observed at m/z = 615.3; for the **122** $M+CH_3O^-$ peak is observed at m / z = 653.3. For the **121**, M+Na peak is observed at m/z = 639.1, and for the **123** M-1 is observed at m/z = 624.2. Exact synthetic procedures and characterization data of ^1H NMR, ^{13}C NMR, MS, and EA for all products are in the experimental section (Page 157).

Methoxy uranyl salophens **126** and **127** from 2-hydroxyl-3-methoxy benzaldehyde **124** and 2-hydroxyl-4-methoxy benzaldehyde **125,** and 3-cyclohexylmethoxy uranyl salophen **129** from 2-hydroxyl-3-cyclohexyl benzaldehyde **128**, were also synthesized in methanol at room temperature (Scheme 18). Yields were quantitative for **126** and **127** and 65 % for **129**.

The products were characterized by ^1H NMR, ^{13}C NMR, mass spectrometry and elemental analysis. The ^1H NMR spectra show a singlet due to imine protons at 9.59 ppm for **126**, at 9.49 ppm for **127** and at 9.59 ppm for **129**, and a singlet due to methoxy protons at 3.98 ppm for **126** and at 3.87 ppm for **127**. The singlet for the methylene protons of **129** is at 4.99 ppm. In the mass spectra of **126** the $M+CH_3O^-$ peak is observed at m/z = 675.4; for the **127** the $M+CH_3O^-$ peak is observed at m/z = 675.3, and for the **129** the M+CH3O- peak is observed at m/z = 839.5. The exact synthetic procedures and characterization data of ^1H NMR, ^{13}C NMR, MS, and EA for all products are in the experimental section (Page 159).

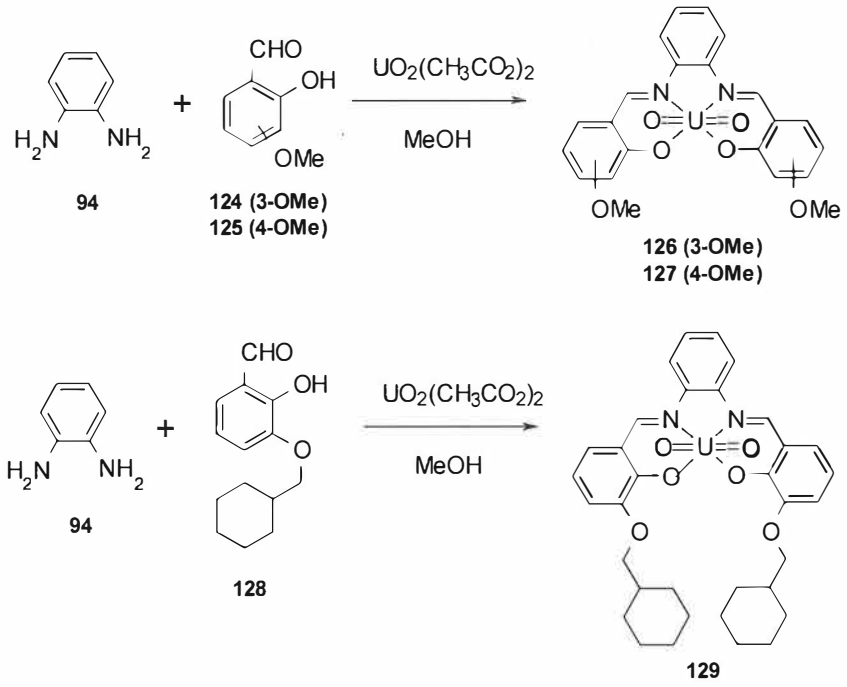

Scheme 18 Synthesis of methoxy uranyl salophens **126** and **127** and cyclohexylmethoxy uranyl salophen **129**.

4.4.2 Crystallization experiments

4.4.2.1 Crystal structures of solvent complexes of 121, 127 and 129

Despite several crystallization experiments, only salophens **121**, **127** and **129** formed good quality crystals as solvent complexes. Crystals were produced by a slow evaporation of the solvent or, in the case of water complex, from moist acetone. Solvent complex structures of salophen **121** with water can be seen in Figure 69 (Appendix 21).

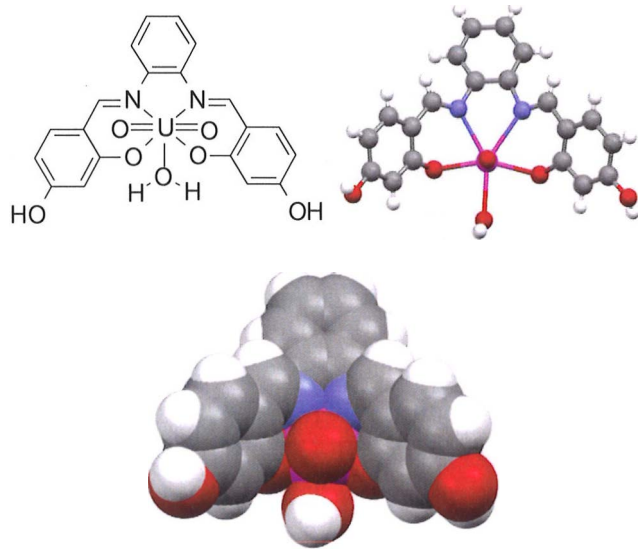

Figure 69 Chemical structure, the ball and stick and CPK plots for **121**•H_2O.

In the structure of salophen **121** complexed with water the distances between uranium and oxygen atoms of salophen are both 2.27 Å. The distances between uranium and nitrogen atoms of salophen are 2.48 Å and 2.57 Å. The oxygen of the water molecule is connected to the uranium at a distance of 2.44 Å, which is about the same as the distances between the uranium and the salophen oxygens and nitrogens.

The acetone complex of uranyl salophen **127** is shown in Figure 70 (Appendix 22).

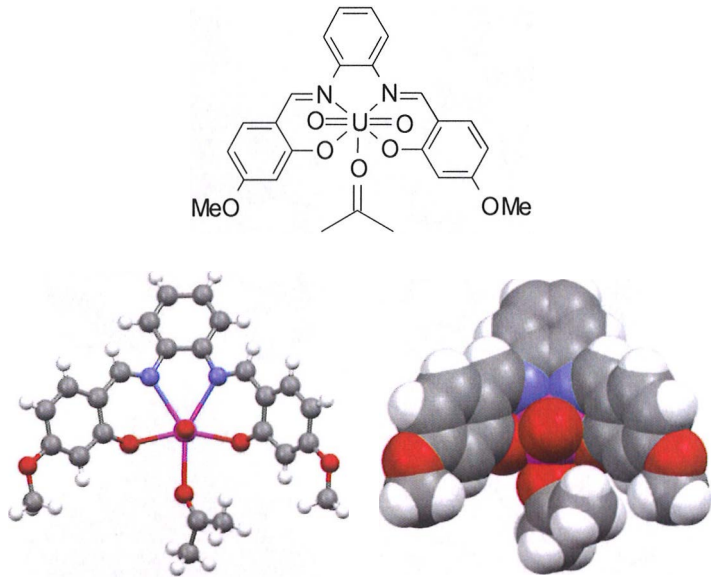

Figure 70 Chemical structure, ball and stick and CPK plots for **127**•acetone.

In **127**•acetone the structure is analogous to that of **107**•acetone with similar bond distances around uranium atom (C=O-U, 2.50 Å, U-O/N being 2.25 and 2.26 Å and 2.55 and 2.51 Å, respectively.

Receptor **129** crystallizes as a solvent complex with methanol, water, and dimethyl sulfoxide (Figure 71, Appendices 23–25). The methanol complex was obtained by a slow evaporation of methanol, the water complex from a slow evaporation of moist acetonitrile and the DMSO complex from a 1:1 mixture of DMSO and acetone.

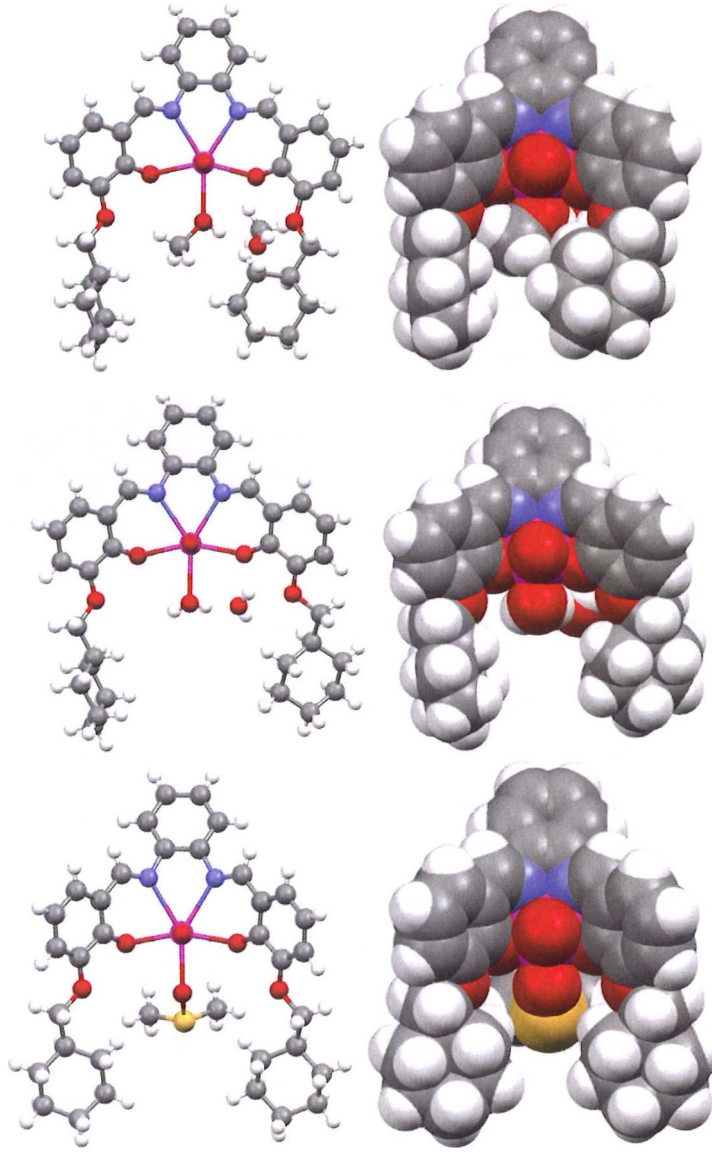

Figure 71 Ball and stick and CPK plots for **129**•MeOH (top), **129**•2H_2O (middle) and **129**•DMSO (bottom).

The two large cyclohexyl sidechains at the 3-position create a cleft which is slightly smaller in **129** than in the corresponding 3-methoxyphenyl uranyl salophen (**9**) and 3-methoxyphenyl uranyl salothiophen (105). In **129**•MeOH the bond lengths from the uranium to the oxygen and nitrogen atoms in the salophen ligand are 2.26, 2.26 Å and 2.54, 2.57 Å, respectively. The bond length from the uranyl to the methanol oxygen is 2.46 Å, the same as in many other studied methanol solvates. The **129**•H_2O structure shows nearly identical bond distances, as expected. Both **129**•MeOH and **129**•H_2O form hydrogen bonded (via O-H···O) dimers in the crystal. In **129**•DMSO such a hydrogen bonded dimer does not exist and the U-O/N distances are very similar to those in the methanol and water complexes. Only the sulphoxide oxygen to uranium distance in **129**•DMSO, 2.39 Å, is somewhat shorter than the usual oxygen-uranium distance.

4.4.2.2 Dimer formation of the 3-OH and 4-OH uranyl salophens

To quite a surprise, the 4-hydroxy uranyl salophen **121** crystallizes like the 4-methoxyphenyl uranyl salophen **95** as a dimer where the uranyl cation of one salophen binds the oxygen atom of the other uranyl salophen and vice versa. The crystals were grown by a slow evaporation of acetone and the crystal structure is shown in Figure 72 (Appendix 26).

In the dimer structure a phenolic oxygen atom of the salophen ligand is bound to the uranyl cation of the other salophen and vice versa. These U-O bonds are both 2.45 Å long. The distances between uranium and phenol oxygen atoms of the salophen ligands are 2.29 Å and 2.38 Å and the distances between the uranium and nitrogen atoms of the salophen ligands are 2.48 Å and 2.51 Å. Due to the

formation of the $U(O)_2$-$[O(Ph)]_2$-$U(O)_2$ moiety the dimer is neutral and it has an overall structure like two intertwining U-letters (Figure 72).

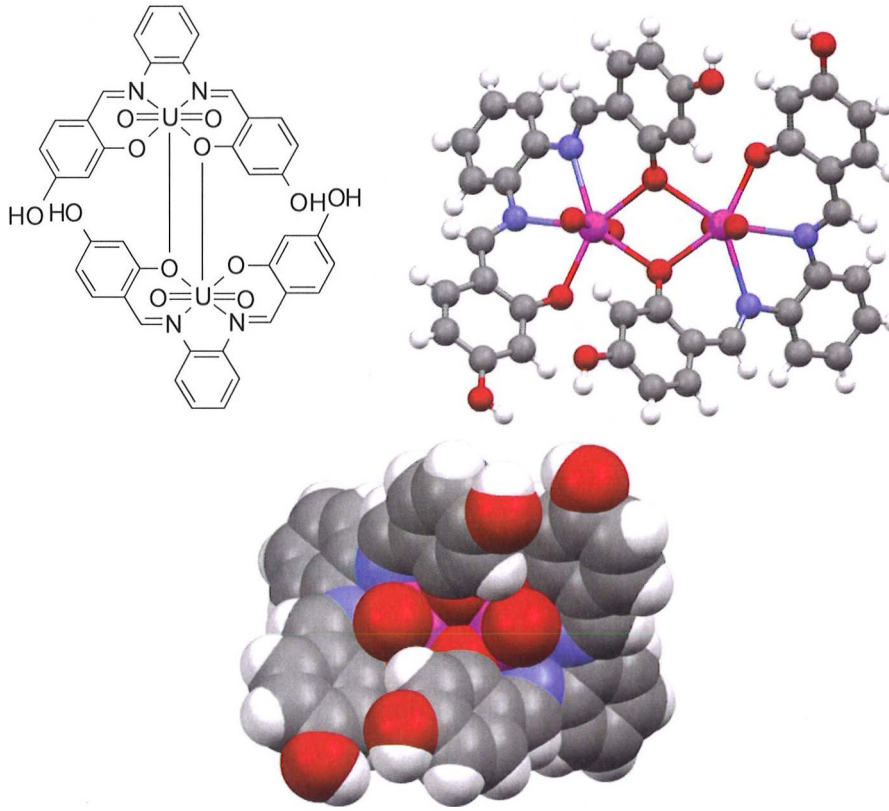

Figure 72 Chemical structure, ball and stick and CPK plots for (**121**)$_2$.

During the solid state complexation studies it turned out that the hydroxyl protons in the hydroxyl groups of the salophens are acidic regardless of their position in the phenyl ring and hence these hydroxyl groups can be deprotonated by treating them with a mild base. The product of this reaction is a water soluble uranyl salophen phenoxide. Despite the quite polar nature of the uranyl salo- and salopthiophen structures, where the uranyl cation is bound to

two deprotonated hydroxyl group and two iminic nitrogen atoms, the core uranyl salophen **1** and its derivatives are quite insoluble to protic and aprotic solvents and are completely insoluble in water. The attachment of large (aromatic) sidearms will improve the solubility to common organic solvents such as chloroform. When 3-hydroxy uranyl salophen **126** was treated with an organic base such as triethylamine **130** or DABCO **102**, one of the hydroxyl groups of **126** deprotonates, forms the phenoxide and coordinates with a second phenoxide, into a macrocyclic structure where two uranyl salophen units are joined together. The uranium binds to the deprotonated negatively charged phenolic oxygen of the other salophen molecule and vice versa (Scheme 19) creating a doubly charged metallacycle. The crystal structure of the metallacycle with triethylammonium as a counter cation is shown in Figure 73 (Appendix 27). Crystallization was accomplished by adding an excess amount of the base to the acetone solution of the receptor and slowly evaporating the solvent.

In the dimer structure shown in Figure 73 the distances between the uranium and the salophen ligand are normal (2.30-2.65 Å). The distances between the uranium and the phenolic oxygen of the other salophen ligand are both 2.23 Å. Because the metallacycle is formed via the phenolic oxygens in the 3-position of the salophen instead of the 2-position as in the neutral dimer structures (**95**)$_2$ and (**121**)$_2$, a small cavity is formed inside the metallacycle. Based on the X-ray structure the possibility of small cations being bound into the cavity of the negatively charged metallacycle was studied. Mass spectrometry studies indicated that (**121**)$_2$ showed a marked selectivity to lithium cations over larger alkali metal cations (Na^+ and K^+). This selectivity was determined by electrospray ionization mass spectrometry and ^1H NMR techniques in collaboration with Dr. Massimo Cametti.[152] Despite several crystallization experiments no diffraction quality crystals with Li^+ inside the macrocyclic cavity

were obtained. The salophen phenoxide based (**121**)$_2$ is the first dimeric metallacycle obtained from a large family of uranyl salophens. Dimer structures of neutral salophens and salens without an uranyl cation have been reported in the literature.[153-155]

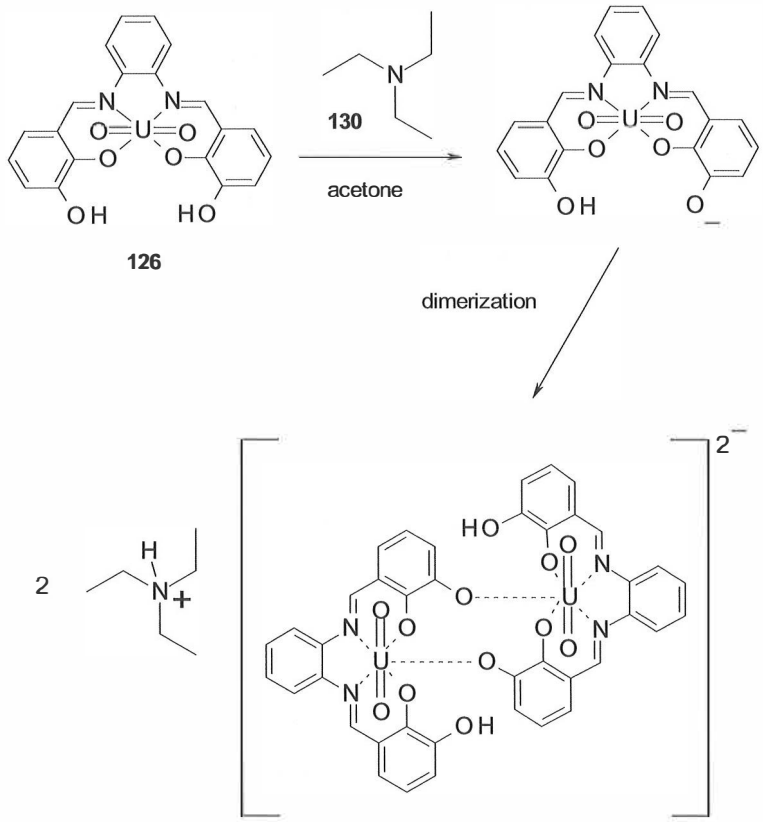

Scheme 19 Receptor **126** deprotonates and forms a self-complementary dimer when treated with a base.

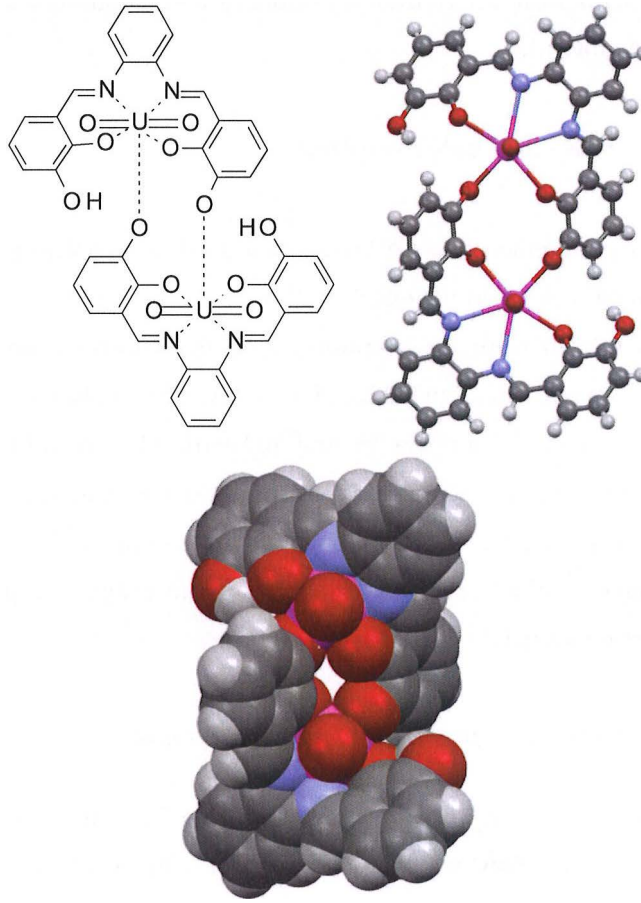

Figure 73 Chemical structure, ball and stick and CPK plots for **126**$^{2-}$. The two triethylammonium cations and solvent acetone molecules were removed for clarity.

As discussed above, the uncomplexed hydroxyl group of the salophen structure can be easily deprotonated regardless of its position in the benzene ring. These phenoxide salts of uranyl salo- and salothiophens (from both 1,2-diamino benzene and 3,4-diamino thiophene) are very soluble in water. Unfortunately, no other good quality crystals were obtained despite several crystallization

experiments with all hydroxy uranyl salophens and salothiophens and several different base molecules.

4.5 The core salo- and salothiophens

The core uranyl salophen **1** (page 13) is often used as a control molecule[67-68] in complexation studies when the effect of different "arms" on the complexation is in focus. As known from the literature, 3-phenylmethoxy uranyl-salophen **9** forms complexes with alkali metal halides[73] while similar studies with 4- and 5-phenylmethoxy uranyl salophens **95** and **100** with alkali metal halides in this Ph.D. thesis revealed no such solid state complexation. Contrary to the claims about alkali metal complexation of core salophen **1** with alkali metal halides [73], we did manage to obtain single crystals from core uranyl salophen **1** with a cesium cation, not as halide, but as carbonate salt.

4.5.1 Synthesis and characterization of core salothiophen

The core uranyl salophen **1** with no "arms" with a 1,2-diaminobenzene moiety was reported by Bandoli in 1971[16]. The isomer with a 3,4-diaminothiophene moiety **132** was prepared for the purposes of comparison for the complexation studies. The synthesis of **132** (Scheme 20) was done in methanol under reflux and the product was isolated in a 65 % yield.

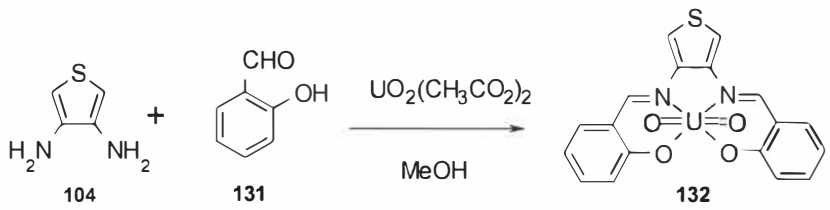

Scheme 20 Synthesis of the core salothiophen **132.**

Core salothiophen **132** was characterized by ^{1}H NMR, ^{13}C NMR, mass spectrometry and elemental analysis. Its ^{1}H NMR spectrum shows a singlet due to imine protons at 9.71 ppm and a singlet due to aromatic protons in the thiophene moiety at 7.96 ppm. In the mass spectrum the $M+CH_3O^-$ peak is observed at m/z = 621.2. The exact synthetic procedure and characterization data of ^{1}H NMR, ^{13}C NMR, MS, and EA are in the experimental section (Page 161).

4.5.2 Crystallization experiments of 1 and 132 with Cs_2CO_3

In the previous study done in collaboration with universities in Jyväskylä and Rome complexation of alkali metal halides with core uranyl salophen **1** failed. When the halide part of the salt is changed to carbonate and complexation is done at the same time with salophen synthesis, a complex of the core uranyl salophen **1** with cesium is gained. The same phenomenon is unfortunately not seen with core uranyl salothiophen **132** prepared for the comparison. Unlike phenylmethoxy uranyl salophen-alkali metal halide complexes this complex is not a dimeric capsule. There are instead four uranyl salophen complexes around two cesium cations bridged by two oxygen atoms (Figure 74, Appendix 28). Crystals were obtained by a slow evaporation of methanol from the reaction mixture.

In the crystal there are two pairs of uranyl salophens connected to each other by acetate ions with the two oxygen atoms bound to different uranyls (2.38 and 2.41 Å). Both these acetate oxygens are also bound by one cesium cation (3.14 and 3.43 Å). The same cesium cation binds also uranyl oxygen atoms of the same salophen ligands (3.50 and 3.55 Å). The two cesium atoms are bound by four oxygen atoms, two from methanol molecules (3.16 and 3.20 Å) (methanol was used as a solvent) and two from the uranyl oxygen atom of the salophen ligands

across from each other. These four salophen ligands are not directly connected to each other, but only through these acetate and cesium ions. The distances between the uranium and the salophen ligand are 2.23-2.57 Å.

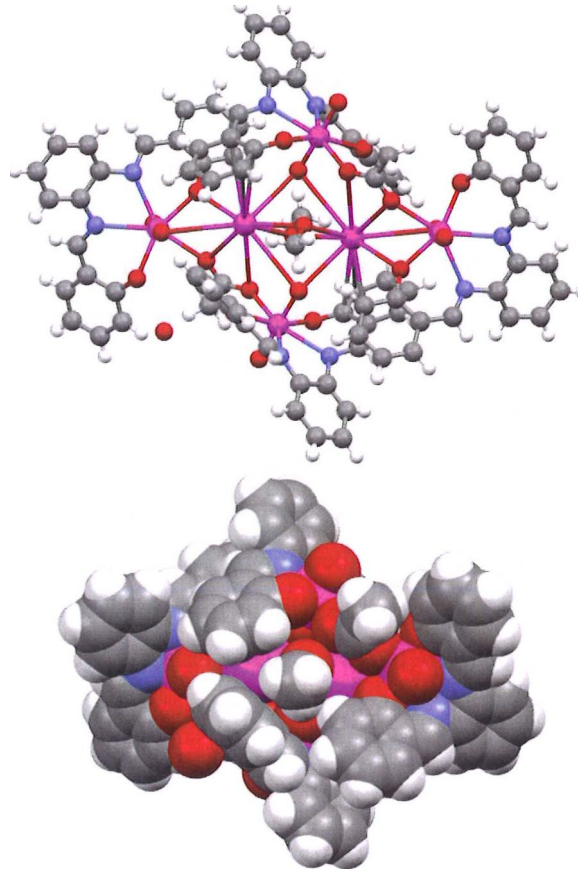

Figure 74 Crystal structure (ball and stick and CPK) of the cesium acetate complex of receptor **1**.

5 CONCLUSIONS

The 12 novel uranyl salo- and salothiophens prepared and characterized in this Ph. D. thesis, supplemented by four other uranyl salophens (two were available from earlier studies and two were prepared during the preparation of this Ph. D. thesis by Dr. Massimo Cametti at the same laboratory) form a uniform family of structurally varied uranyl complexes. All the 16 uranyl salo- and salothiophen complexes were used in the complexation studies with a group of differently sized tetraalkyl ammonium halides and few other smaller guest molecules, where uranyl salophens acted as ditopic receptors. The complexation studies were performed in solution by the NMR titration technique for the isomeric 3-, 4- and 5-phenylmethoxy uranyl salophens. Hundreds of crystallization experiments to obtain solid state complexes of the salo- and salothiophens resulted in altogether 28 new single-crystal X-ray structures. In many cases the uranyl complexes formed good quality crystals from various solvents resulting 12 new solvent complex X-ray structures reported in this thesis. R_4NX, X = Cl or F, complexation and a subsequent evaporation of the solvent led to 11 new salo- or

salothiophen•R_4NX complex X-ray structures and in addition one Cs_2CO_3 complex and one DABCO-complex were determined. Three novel and unreported dimeric uranyl salophen structures were also determined by single crystal X-ray crystallography.

A most remarkable and totally unexpected result was the inability of the 4-phenylmethoxy uranyl salophen **95** to complex any of the R_4NCl salts in non-coordinative solvents. Very careful NMR experiments and subsequent crystallization experiments revealed that **95** forms in chloroform a very stable dimeric structure that blocks the anion binding site of the uranium atom and thus renders complexation impossible. The dimer formation and structure were also proven by a single crystal X-ray study of the dimeric complex $(\mathbf{95})_2$ obtained from acetone. The binding constants of 3-phenylmethoxy uranyl salophen **9** with TMACl (K = 13 600 M^{-1}) and TBACl (K = 22 000 M^{-1}) had been determined earlier; they served as reference points for the other, structurally different tetraalkyl ammonium chlorides. The binding constants for **9** and intermediate sized, yet unsymmetrical, TEACl and TPACl are respectively 11 600 and 11 300 M^{-1}, while with the less symmetrical $R_2R'_2NCl$ only DMDEACl binds equally, K = 13 800 M^{-1}. The larger and less symmetrical DMDPACl and DMDBACl have clearly smaller binding constants, K = 8390 and 6920 M^{-1}. These binding studies revealed that 3-phenylmethoxy uranyl salophen **9** is an excellent receptor for tetraalkyl ammonium chlorides, favouring the binding of larger symmetrical ammonium cations. The 5-phenylmethoxy isomer **100** is a markedly weaker receptor for all tetraalkyl ammonium chlorides studied and the binding does not show any selectivity. All R_4NCl is bound more or less equally (K = 640 - 960 M^{-1}), being very similar to the core uranyl salophen **1** (K = 1000 M^{-1}).

The binding behavior of the isomeric phenylmethoxy uranyl salophens in chloroform towards differently sized tetraalkyl ammonium chlorides is a function of the solubility of the uranyl salo- or salothiophen's R_4NCl complexes, the spatial position of the aromatic side arms and the ability of the uranium to bind the chloride anion. The seventh coordination site of the uranium atom has to be free to bind the chloride anion; if not, like in 4-phenylmethoxy uranyl salophen **95**, the complexation is completely inhibited due to the dimer formation of the salophen itself. When the aromatic arms are placed close to the anion binding site, the cation-π interactions are fully functional and a marked increase in the binding affinity is observed. The binding is maximized with large symmetrical tetraalkyl ammonium cations with a better fit to the binding cleft. Placing the aromatic arms further apart from the anion binding site, as in 5-phenylmethoxy uranyl salophen **100**, disfavors the cation-π interactions and reduces the binding affinity to the level of unsubstituted core uranyl salophen **1**.

The solid state X-ray structures of the crystalline solvate and R_4NX complexes of the uranyl salophens and analogous uranyl salothiophens revealed marked structural similarities in the uranyl moiety despite the structural differences of the 1,2-diaminobenzene and 3,4-diaminothiophene skeletons. Nearly analogous R_4NX complex structures of the uranyl salo- and salothiophens manifest the importance of the overall similarity of the receptors. The observed multitude of structural modulations, solvent complexes, dimers or larger assemblies highlight the versatile nature of the uranyl salo- and salothiophens as efficient receptors and structural components for more complex structures.

6 EXPERIMENTAL

General

The NMR spectra were measured with a Bruker Avance DRX 500 spectrometer. The NMR solvents were used as standards. The mass spectrometric measurements were performed using a Micromass LCT time-of-flight (TOF) mass spectrometer with ionization (ESI). Elemental analyses were performed using a VarioEL III elemental analyzer. Novel compounds were analyzed by ^{1}H and ^{13}C NMR, MS and EA, earlier published intermediate products only by ^{1}H and ^{13}C NMR. All reagents and solvents (purity ≥ 96 % or better) were purchased from Sigma-Aldrich or Fluka and were used without further purification.

6.1 Phenylmethoxy uranyl salophens

2-hydroxy-4-(phenylmethoxy)benzaldehyde **93**

2,4-dihydroxybenzaldehyde (1.00 g, 7.24 mmol), K_2CO_3 (1.45 g, 10.5 mmol) and a catalytic amount of 18-crown-6 were stirred in acetone (30 mL) at 45 °C for 1 h. The benzyl bromide was added in acetone (10 mL) in 10 min. Stirring was continued at 45 °C for 2 h, whereupon the mixture was allowed to cool to room temperature and filtered. The solvent was evaporated. The residue was purified by column chromatography (silica gel, CH_2Cl_2) and recrystallized from ethanol. Yield: 26 %.

^{1}H NMR (500 MHz, CD_2Cl_2-d_6, 30 °C): δ = 11.48 (s, 1H), 9.76 (s, 1H), 7.51 (d, 1H, J = 8.7 Hz), 7.37-7.48 (m, 5H), 6.67 (dd, 1H, J_1 = 2.4 Hz, J_2 = 8.7 Hz, e), 6.55 (d, 1H, J = 2.4 Hz), and 5.16 ppm (s, 2H,); ^{13}C NMR (126 MHz, CD_2Cl_2, 30 °C): δ = 195.2, 166.5, 165.0, 136.6, 136.0, 129.3, 129.0, 128.2, 116.0, 109.3, 102.2, and 71.1 ppm; MS(ES): m/z calcd. for $C_{14}H_{11}O_3$ 227.2 $[M-H]^-$; found: 227.1.

Dioxo{[2,2'-[1,2-phenylenebis(nitrilomethylidyne)]bis-[5-(phenylmethoxy)-phenolato]](2-)-N,N',O,O'}uranium **95**

To a refluxing solution of $UO_2(OAc)_2 \bullet 2H_2O$ (0.26 g, 0.60 mmol) in methanol (200 mL) were added a solution of 2-hydroxy-4-(phenylmethoxy)benzaldehyde (0.255 g, 1.20 mmol) in CH_2Cl_2 (40 mL) and a solution of 1,2-benzenediamine (0.065g, 0.60 mmol) in methanol (40 mL) in 3 h. Reflux was maintained for 15 min whereupon the mixture was allowed to cool to room temperature overnight. Most of the solvent was evaporated. The reaction mixture was dissolved in

$CHCl_3$ (50 mL) and washed with water (20 mL) 3 times to yield a red solid. Yield: 93 %.

^{1}H NMR (500 MHz, DMSO-d_6, 30 °C): δ = 9.49 (s, 1H), 7.70 (d, 2H, J = 8.8 Hz), 7.68-7.69 (m, 2H), 7.50-7.52 (m, 4H), 7.47-7.49 (m, 2 H), 7.41-7.44 (m, 4H), 7.34-7.38 (m, 2H), 6.58 (d, 2H, J = 2.4 Hz), 6.44 (dd, 2H, J_1 = 2.5 Hz, J_2 = 8.7 Hz), and 5.24 ppm (s, 4H); ^{13}C NMR (126 MHz , DMSO, 30 °C): δ = 171.9, 165.6, 165.0, 146.9, 137.2, 136.8, 128.4, 128.0, 127.9, 127.7, 119.9, 118.7, 106.3, 104.4, and 69.4 ppm; MS(ES): m/z calcd. for $C_{35}H_{29}O_7N_2U$ 827.6 $[M+CH_3O]^-$; found: 827.5. Anal. Calcd. for $C_{34}H_{26}O_6N_2U$+1.5 H_2O (M_r 823.676): C, 49.58; H, 3.55; N, 3.40. Found: C, 49.34; H, 3,57; N, 3.44.

6.2 Tetraalkyl ammonium salts

Dimethyl dibutyl ammonium bromide **98c**

Butyl bromide (3.50 g, 25.5 mmol) and K_2CO_3 (3.50 g, 25.3 mmol) was diluted to DMF (10.00g, 136.8 mmol). The mixture was stirred at 70 °C for 6 days. The white precipitate was filtered and the filtrate was evaporated. The residue was precipitated with diethyl ether and filtered. The precipitate was diluted to CH_2Cl_2 and non-soluble KBr was filtered. The filtrate was evaporated and the product dried in vacuo. An ion-exchange (Dowex, 6 mol/l HCl) was done for the product. Yield: 31 %.

^{1}H NMR (500 MHz, $CDCl_3$-d_6, 30 °C): δ = 3.45-3.52 (m, 8H), 3.31 (s, 6H), 1.60-1.68 (m, 8H), 1.36 (m, 8H), and 0.97 ppm (t, 12H, J = 7.3 Hz); ^{13}C NMR (126 MHz , $CDCl_3$, 30 °C): δ = 63.5, 51.0, 24.5, 19.5 and 13.5 ppm; MS(ES): m/z calcd. for $C_{10}H_{24}N$ 158.3 $[M-Cl]^+$; found: 158.2.

Tetraethyl ammonium bromide

A mixture of triethylamine (1.40 g, 14.0 mmol) and ethyl bromide (3.02 g, 28.0 mmol) was strirred overnight. The pure product was filtered and an ion-exchange (Dowex, 6 mol/l HCl) was done. Yield: 23 %.

^{1}H NMR (500 MHz, $CDCl_3$-d_6, 30 °C): δ = 3.45 (q, 8H, J = 7.3 Hz), and 1.35 ppm (tt, 12H, J_1 = 1.7 Hz, J_2 = 7.3 Hz); ^{13}C NMR (126 MHz, $CDCl_3$, 30 °C): δ = 52.8, and 7.9 ppm; MS(ES): m/z calcd. for $C_8H_{20}N$ 130.2 $[M\text{-}Cl]^+$; found: 130.1.

6.3 Phenylmethoxy uranyl salothiophens

Dioxo{[2,2'-[3,4-thiophenebis(nitrilomethylidyne)]bis-[6-(phenylmethoxy)-phenolato]](2-)-N,N',O,O'}uranium **105**
Dioxo{[2,2'-[3,4-thiophenebis(nitrilomethylidyne)]-bis-[5-(phenylmethoxy)-phenolato]](2-) N,N',O,O'}uranium **106**

To a refluxing solution of $UO_2(OAc)_2 \bullet 2H_2O$ (0.40 g, 0.88 mmol) in methanol (50 mL) were added a solution of 2-hydroxy-3/4-(phenylmethoxy)benzaldehyde (0.40 g, 1.80 mmol) in CH_2Cl_2 (10 mL) and in methanol (30 mL) and a solution of 3,4-diaminothiophene (0.10 g, 0.88 mmol) in methanol (40 mL) in 1 h. Reflux was maintained for 30 min whereupon the mixture was allowed to cool to room temperature overnight. Most of the solvents were evaporated and the red product precipitated was filtered and dried in vacuo. Yields: 60 % (**105**), 88 % (**106**).

105

^{1}H NMR (500 MHz, DMSO-d_6, 30 °C): δ = 9.71 (s, 2H), 7.96 (s, 2H), 7.60 (d, 4H, J = 7.5 Hz), 7.43 (tt, 4H, J_1 = 1.5 Hz, J_2 = 7.6 Hz), 7.40 (dd, 2H, J_1 = 1.6 Hz, J_2 = 8.2 Hz), 7.36 (tt, 2H, J_1 = 1.3 Hz, J_2 = 2.2 Hz, J_3 = 7.4 Hz); 7.33 (dd, 2H, J_1 = 1.6 Hz, J_2 = 7.8 Hz) and 6.63 ppm (t, 2H, J = 7.8 Hz); ^{13}C NMR (126 MHz, DMSO, 30 °C): δ = 166.3, 161.3, 150.0, 147.9, 137.7, 128.5, 128.2, 127.9, 124.3, 122.9, 119.8, 116.1, 111.4, and 70.5 ppm; MS(ES): m/z calcd for $C_{33}H_{27}O_7N_2SU$ 833.7 $[M+CH_3O]^-$; found: 833.4; Anal. Calcd. for $C_{18}H_{12}O_6N_2SU$+1.5 H_2O (M_r 649.454): C, 33.29; H, 2.33; N, 4.31. Found: C, 33.59; H, 2.34; N, 4.42.

106

^{1}H NMR (500 MHz, DMSO-d_6, 30 °C): δ = 9.59 (s, 2H), 7.82 (s, 2H), 7.67 (d, 2H, J = 9.0 Hz), 7.52 (d, 4H, J = 7.0 Hz), 7.43 (td, 4H, J_1 = 1.5 Hz, J_2 = 7.5 Hz), 7.36 (tt, 2H, J_1 = 1.5 Hz, J_2 = 7.5 Hz) 6.59 (d, 2H, J = 2.5 Hz), and 6.46 ppm (dd, 2H, J_1 = 2.5 Hz, J_2 = 9.0 Hz); ^{13}C NMR (126 MHz, DMSO, 30 °C): δ = 171.9, 165.6, 164.9, 148.1, 136.9, 136.8, 128.5, 127.9, 127.8, 118.4, 110.0, 106.5, 104.6, and 69.4 ppm; MS(ES): m/z calcd for $C_{33}H_{27}O_7N_2SU$ 833.7 $[M+CH_3O]^-$; found: 833.5; Anal. Calcd. for $C_{32}H_{24}O_6N_2SU$+2 C_3H_6O (M_r 918.842): C, 49.67; H, 3.95; N, 3.05. Found: C, 49.36; H, 3.57; N, 3.41.

6.4 Bipyridyl uranyl salophens

Dioxo{[2,2′-[1,2-phenylenebis(nitrilomethylidyne)]bis-[6-(2,2′-bipyridine-5-methoxy)phenolato]](2-)-N,N′,O,O′}uranium **107**

To a refluxing solution of $UO_2(OAc)_2$•$2H_2O$ (0.155 g, 0.367 mmol) in methanol (50 mL) were added a solution of 2-hydroxy-3-(2,2′-bipyridine-5-methoxy)benzaldehyde (0.150 g, 0.490 mmol) in CH_2Cl_2 (10 mL) and methanol

(25 mL), and a solution of 1,2-benzenediamine (0.027g, 0.245 mmol) in methanol (40 mL) in 45 min. Reflux was maintained for 45 min whereupon the mixture was allowed to cool to room temperature overnight. Most of the solvents were evaporated and the precipitated red solid was filtered. Yield: 67 %.

^{1}H NMR (500 MHz, DMSO-d_6, 30 °C): δ = 9.60 (s, 2H), 8.86 (s, 2H), 8.63 (dq, 2H, J_1 = 0.9 Hz, J_2 = 4.8 Hz), 8.36 (dd, 2H, J_1 = 0.5 Hz, J_2 = 8.2 Hz), 8.31 (dt, 2H, J_1 = 0.8 Hz, J_2 = 7.0 Hz), 8.12 (dd, 2H, J_1 = 2.3 Hz, J_2 = 8.2 Hz), 7.88 (td, 2H, J_1 = 1.8 Hz, J_2 = 7.8 Hz), 7.728-7.746 (m, 2H), 7.529-7.548 (m, 2H), 7.45 (dd, 2H, J_1 = 1.5 Hz, J_2 = 8.1 Hz), 7.42-7.43 (m, 2H), 7.34 (dd, 2H, J_1 = 1.5 Hz, J_2 = 7.8 Hz), 6.63 (t, 2H, J = 7.8 Hz) and 5.47 ppm (s, 4H); ^{13}C NMR (126 MHz, DMSO, 30 °C): δ = 166.9, 161.4, 155.3, 155.2, 149.7, 149.4, 147.0, 137.8, 137.6, 134.0, 129.4, 128.8, 125.0, 124.7, 121.0, 120.9, 120.7, 120.6, 116.7, and 68.4 ppm; MS(ES): m/z calcd for $C_{43}H_{33}O_7N_6U$ 983.8 $[M+CH_3O]^-$; found: 983.6; Anal. Calcd. for $C_{42}H_{30}O_6N_6U$+2 H_2O + $CHCl_3$ (M_r 1108.242): C, 46.38; H, 3.46; N, 7.19. Found: C, 46.60; H, 3.18; N, 7.58.

Dioxo{[2,2′-[1,2-phenylenebis(nitrilomethylidyne)]bis-[5-(2,2′-bipyridine-5-methoxy)phenolato]](2-)-N,N′,O,O′}uranium **108**

To a refluxing solution of $UO_2(OAc)_2 \cdot 2H_2O$ (0.139 g, 0.327 mmol) in methanol (30 mL) were added a solution of 2-hydroxy-4-(2,2′-bipyridine-5-methoxy)benzaldehyde (0.20 g, 0.65 mmol) in CH_2Cl_2 (10 mL) and methanol (20 mL) and a solution of 1,2-benzenediamine (0.035g, 0.327 mmol) in methanol (30 mL) in 45 min. Reflux was maintained for 45 min whereupon the mixture was allowed to cool to room temperature overnight. Most of the solvent was evaporated and the precipitated red solid was filtered. Yield: 45 %.

^{1}H NMR (500 MHz, DMSO-d_6, 30 °C): δ = 9.51 (s, 2H), 8.84 (s, 2H), 8.70 (d, 2H, J = 4.8 Hz), 8.44 (d, 2H, J = 8.2 Hz), 8.41 (d, 2H, J = 7.6 Hz), 8.09 (d, 2H, J = 8.1 Hz), 7.96 (t, 2H, J = 7.8 Hz) 7.74 (d, 2H, J = 8.8 Hz), 7.69-7.71 (m, 2H), 7.45-7.49 (m, 4H), 6.65 (d, 1H, J = 2.1 Hz), 6.49 (dd, 1H, J_1 = 2.0 Hz, J_2 = 8.5 Hz), and 5.67 ppm (s, 4H); ^{13}C NMR (126 MHz, DMSO, 30 °C): δ = 171.9, 165.3, 165.1, 155.0, 154.9, 149.3, 148.8, 146.9, 137.3, 136.8, 132.7, 128.0, 124.2, 120.5, 120.2, 120.0, 118.9, 106.2, 104.5, and 66.9 ppm; MS(ES): m/z calcd for $C_{43}H_{33}O_7N_6U$ 983.8 $[M+CH_3O]^-$; found: 983.4. Anal. Calcd. for $C_{42}H_{30}O_6N_6U$+ H_2O + $CHCl_3$ (M_r 1090.226): C, 47.37; H, 3.14; N, 7.71. Found: C, 47.05; H, 3.39; N, 7.77.

2-hydroxyl-3-(2,2′-bipyridine-5-methoxy)-benzaldehyde **109**

A mixture of 2-allyloxy-3-(2,2′-bipyridine-5-methoxy)-benzaldehyde (0.59 g, 1.70 mmol), SeO_2 (0.19 g, 1.70 mmol), acetic acid (0.102 g, 1.70 mmol), and 1,4-dioxane (25 mL) was refluxed under nitrogen overnight. To the cooled mixture water (20 mL) and $CHCl_3$ (25 mL) was added. Layers were extracted and organic phase was washed with water (4x10 ml), dried with Na_2SO_4 and evaporated. The product was purified by column chromatography (silica gel, acetone). Yield: 31 %.

^{1}H NMR (500 MHz, $CDCl_3$-d_6, 30 °C): δ = 11.17 (s, 1H), 9.92 (s, 1H), 8.74 (s, 1H), 8.68 (dq, 1H, J_1 = 0.9 Hz, J_2 = 4.8 Hz), 8.42 (dd, 1H, J_1 = 0.6 Hz, J_2 = 8.1 Hz), 8.40 (dt, 1H, J_1 = 1.0 Hz, J_2 = 8.0 Hz), 7.94 (dd, 1H, J_1 = 2.3 Hz, J_2 = 8.2 Hz) 7.82 (td, 1H, J_1 = 1.8 Hz, J_2 = 7.5 Hz), 7.30-7.35 (m, 1H), 7.23 (dd, 1H, J_1 = 1.5 Hz, J_2 = 7.8 Hz), 7.17 (dd, 1H, J_1 = 1.0 Hz, J_2 = 8.0 Hz), 6.92 (t, 1H, J = 7.9 Hz), and 5.27 ppm (s, 2H); ^{13}C NMR (126 MHz, $CDCl_3$, 30 °C): δ = 196.5, 156.2, 155.8, 152.6, 149.2, 148.5, 146.7, 136.9, 136.4, 132.1, 126.2, 123.8, 122.0, 121.3, 121.1, 121.0, 119.5, and 69.3 ppm; MS(ES): m/z calcd for $C_{18}H_{15}O_3N_2$ 307.3 $[M+H]^+$; found: 307.1.

2-hydroxyl-4-(2,2′-bipyridine-5-methoxy)-benzaldehyde **110**

$NaHCO_3$ (0.52 g, 6.23 mmol), and KI (0.10 g, 0.62 mmol) were added to a solution of 2,4-dihydroxybenzaldehyde (0.86 g, 6.23 mmol) in dry acetonitrile (30 ml) at room temperature under nitrogen. The mixture was warmed to 60 °C during 2 h, followed by addition of 5-bromomethyl-2,2′-bipyridine (1.550 g, 6.230 mmol). The mixture was warmed to 90 °C and stirred overnight. The cooled mixture was filtered and the filtrate was evaporated. The residue was recrystallized from acetone/$CHCl_3$ 1:2. Yield: 28 %.

^{1}H NMR (500 MHz, $CDCl_3$-d_6, 30 °C): δ = 11.46 (s, 1H), 9.75 (s, 1H), 8.74 (dd, 1H, J_1 = 0.9 Hz, J_2 = 2.3 Hz), 8.69 (dq, 1H, J_1 = 0.9 Hz, J_2 = 4.8 Hz), 8.46 (dd, 1H, J_1 = 0.7 Hz, J_2 = 8.2 Hz), 8.42 (dt, 1H, J_1 = 1.1 Hz, J_2 = 8.0 Hz), 7.89 (dd, 1H, J_1 = 2.3 Hz, J_2 = 5.9 Hz) 7.89 (td, 1H, J_1 = 1.8 Hz, J_2 = 7.5 Hz), 7.47 (d, 1H, J = 8.6 Hz), 7.33 (ddd, 1H, J_1 = 1.2 Hz, J_2 = 4.8 Hz, J_3 = 7.5 Hz), 6.64 (dd, 1H, J_1 = 2.4 Hz, J_2 = 8.7 Hz), 6.54 (d, 1H, J = 2.4 Hz), and 5.19 ppm (s, 2H); ^{13}C NMR (126 MHz, $CDCl_3$, 30 °C): δ = 194.4, 165.4, 164.5, 156.4, 155.7, 149.2, 148.4, 137.0, 136.3, 135.4, 131.3, 123.9, 121.2, 121.0, 115.6, 108.8, 101.8, and 67.9 ppm; MS(ES): m/z calcd for $C_{18}H_{13}O_3N_2$ 305.3 $[M+H]^+$; found: 305.1.

(2-Pyridacyl)pyridium Iodide **112**

Iodine (13.6 g, 160 mmol) in warm pyridine (50 mL) was added under nitrogen to a solution of 2-acetylpyridine (20 mL). The reaction mixture was stirred at 80 °C overnight whereupon it was allowed to cool to the room temperature and the pure yellow-green product was filtered. The filtrate was evaporated, dissolved in ethanol and treated with decolorizing coal to obtain more of product. Yield: 33 %.

^{1}H NMR (500 MHz, $CDCl_3$-d_6, 30 °C): δ = 9.02 (dd, 1H, J_1 = 1.1 Hz, J_2 = 6.6 Hz), 8.87 (dt, 1H, J_1 = 1.0 Hz, J_2 = 8.1 Hz), 8.28 (td, 1H, J_1 = 1.0 Hz, J_2 = 7.2 Hz), 8.14 (td, 1H, J_1 = 1.7 Hz, J_2 = 7.7 Hz), 8.08 (dd, 1H, J_1 = 0.9 Hz, J_2 = 6.9 Hz), 7.34 (ddd, 1H, J_1 = 1.3 Hz, J_2 = 4.8 Hz, J_3 = 7.5 Hz), and 6.52 ppm (s, 2H); ^{13}C NMR (126 MHz, $CDCl_3$, 30 °C): δ = 191.4, 150.4, 149.5, 146.3, 146.2, 138.1, 129.0, 127.6, 122.0, and 66.6 ppm; MS(ES): m/z): calcd for $C_{12}H_{11}O_1N_2$ 199.2 $[M\text{-}I]^+$; found: 199.0.

5-Methyl 2,2′-bipyridine **114**

(2-Pyridacyl)pyridium iodide (6.5 g, 20 mmol), and ammonium acetate (3.54g, 46.0 mmol) were dissolved in formamide (63 mL). The reaction mixture was stirred at 75 °C for 3.5 h. After addition of water (20 mL), the reaction mixture was extracted with CH_2Cl_2 (3x20 mL). CH_2Cl_2 was evaporated and the residue was dissolved in CCl_4. CCl_4 –layer was extracted and evaporated to give the pure product. Yield: 99 %.

^{1}H NMR (500 MHz, $CDCl_3$-d_6, 30 °C): δ = 8.62 (dq, 1H, J_1 = 1.0 Hz, J_2 = 5.0 Hz), 8.46 (s, 1H), 8.31 (dt, 1H, J_1 = 1.0 Hz, J_2 = 8.0 Hz), 7.84 (dd, 1H, J_1 = 0.2 Hz, J_2 = 8.2 Hz), 7.75 (td, 1H, J_1 = 1.8 Hz, J_2 = 7.5 Hz), 7.56 (dd, 1H, J_1 = 2.2 Hz, J_2 = 8.0 Hz), 7.23 (ddd, 1H, J_1 = 1.3 Hz, J_2 = 4.9 Hz, J_3 = 7.5 Hz), and 2.33 ppm (s, 3H); ^{13}C NMR (126 MHz, $CDCl_3$, 30 °C): δ = 156.1, 153.4, 149.4, 148.9, 137.3, 136.7, 133.3, 123.2, 120.8, 120.5, and 18.2 ppm.

5-Bromomethyl-2,2′-bipyridine **115**

5-Methyl 2,2′-bipyridine (1.67 g, 9.90 mmol), and N-bromosuccinimide (1.76 g, 9.90 mmol) were dissolved in CCl_4 (150 mL). The reaction mixture was stirred and warmed using lamps to 30 °C whereupon AIBN (0.41 g, 2.50 mmol) was

added and the reaction mixture was left to stir with lamps overnight. CCl_4 was evaporated. The product was purified by column chromatography (silica gel, acetone/$CHCl_3$, 2:3). The yellow precipitate was washed with hexane to give the pure product. Yield: 65 %.

^{1}H NMR (500 MHz, $CDCl_3$-d_6, 30 °C): δ = 8.69 (s, 2H), 8.40 (d, 2H, J = 8.5 Hz), 7.85 (dd, 1H, J_1 = 2.4 Hz, J_2 = 8.2 Hz), 7.82 (td, 1H, J_1 = 1.8 Hz, J_2 = 7.8 Hz), 7.30-7.33 (m, 1H), and 4.53 ppm (s, 2H); ^{13}C NMR (126 MHz, $CDCl_3$, 30 °C): δ = 156.1, 155.5, 149.3, 149.2, 137.5, 137.1, 133.6, 124.2, 121.2, 121.0, and 29.6 ppm.

2-allyloxy-3-hydroxybenzaldehyde **118**

To a suspension of NaH (0.5 g, 60 % in oil), pre-washed with light petroleum, in DMSO (23 mL) was added a solution of 2,3-dihydoxybenzaldehyde (1.5 g, 11.0 mmol) in DMSO (10 mL). After 40 min of stirring 3-bromo-1-propene was added whereupon the mixture was left to stir overnight. The mixture was poured into water (50 mL) and extracted with $CHCl_3$ (3x50 mL) whereupon combined $CHCl_3$ layers were washed with water (3x30 mL). $CHCl_3$ was evaporated. The product was purified by column chromatography (silica gel, $CHCl_3$) and recrystallized from light petroleum to give light yellow needles. Yield: 38 %.

^{1}H NMR (500 MHz, $CDCl_3$-d_6, 30 °C): δ = 10.26 (s, 1H), 7.37 (dd, 1H, J_1 = 1.7 Hz, J_2 = 7.5 Hz), 7.22 (dd, 1H, J_1 = 2.0 Hz, J_2 = 8.0 Hz), 7.15 (td, 1H, J_1 = 0.5 Hz, J_2 = 7.7 Hz), 6.07-6.15 (m, 1H), 5.83 (s, 1H), 5.34-5.45 (m, 1H), and 4.58 ppm (dt, 1H, J_1 = 1.0 Hz, J_2 = 6.0 Hz); ^{13}C NMR (126 MHz, $CDCl_3$, 30 °C): δ = 189.6, 149.7, 147.8, 132.4, 129.4, 125.1, 121.7, 121.6, 120.1, and 25.1 ppm.

2-allyloxy-3-(2,2′-bipyridine-5-methoxy)-benzaldehyde **119**

2-allyloxy-3-hydroxybenzaldehyde (1.12 g, 6.30 mmol), and K_2CO_3 (13.13 g, 95.00 mmol) were stirred under nitrogen in acetonitrile (30 mL) for 45 min. 5-bromomethyl-2,2′-bipyridine was added in acetonitrile (20 mL) whereupon the mixture was stirred overnight. The solvent was evaporated and the residue was purified by column chromatography (silica gel, acetone/CH_2Cl_2, 1:6). Yield: 27 %.

^{1}H NMR (500 MHz, $CDCl_3$-d_6, 30 °C): δ = 10.44 (s, 1H), 8.77 (s, 1H), 8.71 (dq, 1H, J_1 = 1.0 Hz, J_2 = 5.0 Hz), 8.49 (d, 1H, J = 8.1 Hz), 8.43 (d, 1H, J = 8.0 Hz), 7.94 (dd, 1H, J_1 = 2.1 Hz, J_2 = 8.1 Hz), 7.86 (td, 1H, J_1 = 1.7 Hz, J_2 = 7.7 Hz) 7.48 (dd, 1H, J_1 = 1.5 Hz, J_2 = 7.8 Hz), 7.35 (ddd, 1H, J_1 = 1.0 Hz, J_2 = 4.5 Hz, J_3 = 7.5 Hz), 7.23 (dd, 1H, J_1 = 1.5 Hz, J_2 = 8.1 Hz), 7.27 (t, 1H, J = 7.9 Hz), 6.02-6.07 (m, 1H), 5.35 (t, 0.5 H, J = 1.4 Hz), 5.31 (t, 0.5 H J = 1.4 Hz), 5.25 (dd, 1H, J_1 = 1.0 Hz, J_2 = 10.6 Hz), 5.22 (s, 2 H), and 4.69 ppm (dt, 2H, J1 = 1.0 Hz, J2 = 6.0 Hz); ^{13}C NMR (126 MHz, $CDCl_3$, 30 °C): δ = 190.1, 155.7, 155.3, 151.8, 151.7, 148.9, 148.3, 137.4, 136.4, 132.9, 132.1, 130.6, 124.2, 124.0, 121.4, 121.3, 120.4, 120.3, 119.1, 75.4, and 68.9 ppm; MS(ES): m/z calcd for $C_{21}H_{18}O_3N_2Na$ 369.4 $[M+Na]^+$; found: 369.1.

6.5 Hydroxy, methoxy and cyclohexylmethoxy uranyl salophens and hydroxyl salothiophens

Dioxo{[2,2′-[1,2-phenylenebis(nitrilomethylidyne)]bis-[6-(hydroxyl)-phenolato]](2-)-N,N′,O,O′}uranium **120**

Dioxo{[2,2′-[1,2-phenylenebis(nitrilomethylidyne)]bis-[5-(hydroxyl)-phenolato]]-(2-)-N,N′,O,O′}uranium **121**

To a solution of of 2-3/4-dihydroxybenzaldehyde (2.0 g, 14.5 mmol) in methanol (100 mL) a solution of 1,2-benzenediamine (0.78 g, 7.2 mmol) in methanol (60 mL) was added during 1.5 h whereupon $UO_2(OAc)_2 \bullet 2H_2O$ (3.06 g, 7.2 mmol) was added at once in methanol (5 mL). The mixture was stirred overnight. Most of solvents were evaporated and the red product precipitated was filtered and washed with a small amount of CH_2Cl_2. The product was dried in vacuo. Yield: 75 %.

120

^{1}H NMR (500 MHz, DMSO-d_6, 30 °C): δ = 9.58 (s, 2H, c), 8.48 (s, 2H, g), 7.75-7.78 (m, 2H, b), 7.52-7.56 (m, 2H, a), 7.28 (dd, 2H, J_1 = 1.6 Hz, J_2 = 8.1 Hz, f), 7.16 (dd, 2H, J_1= 1.6 Hz, J_2 = 7.5 Hz, d), and 6.57 ppm (t, 2H, J_1 = 7.7 Hz, J_2 = 7.8 Hz, e); ^{13}C NMR (126 MHz, DMSO, 30 °C): δ = 166.8 (d), 158.9 (f), 148.1 (g), 146.7 (c), 128.7 (e), 125.7 (h), 123.4 (i), 120.2 (a), 118.9 (b), and 116.4 ppm (j); MS(ES): m/z calcd for $C_{20}H_{13}O_6N_2U$ 615.4 [M-H]; found: 615.3; Anal. Calcd. for $C_{20}H_{14}O_6N_2U$ + H_2O (M_r 634.418): C, 37.86; H, 2.54; N, 4.42. Found: C, 38.24; H, 2.70; N, 4.50.

121

^{1}H NMR (500 MHz, DMSO-d_6, 30 °C): δ = 10.16 (s, 2H, f), 9.41 (s, 2H, c), 7.62-7.66 (m, 2H, b), 7.60 (d, 2H, J = 8.7 Hz, d), 7.42-7.46 (m, 2H, a), 6.35 (d, 2H, J= 2.3 Hz, g), and 6.23 ppm (dd, 2H, J_1 = 2.3 Hz, J_2 = 8.5 Hz, e); ^{13}C NMR (126 MHz, DMSO, 30 °C): δ = 172.1 (d), 165.5 (f), 164.7 (h), 147.0 (c), 137.6 (g), 127.7 (e), 119.7 (a), 117.8 (b), 106.9 (i), and 105.2 ppm (j); MS(ES): m/z calcd for $C_{20}H_{14}O_6N_2UNa$ 639.4 $[M+Na]^+$; found: 639.1; Anal. Calcd. for $C_{20}H_{14}O_6N_2U$+1.5 H_2O (M_r 666.417): C, 37.33; H, 2.66; N, 4.36. Found: C, 37.53; H, 3.14; N, 4.27.

Dioxo{[2,2′-[3,4-thiophenebis(nitrilomethylidyne)]bis-[6-(hydroxyl)phenolato]] (2-)-N,N′,O,O′}uranium **122**
Dioxo{[2,2′-[3,4-thiophenebis(nitrilo-methylidyne)]bis-[5-(hydroxyl)phenolato]] (2-)-N,N′,O,O′}uranium **123**

To a refluxing solution of 3,4-diaminothiophene (0.10 g, 0.88 mmol) in methanol (30 mL) a solution of 2-3/4-dihydroxybenzaldehyde (0.24 g, 1.45 mmol) in methanol (20 mL) was added during 1 h whereupon $UO_2(OAc)_2 \bullet 2H_2O$ (0.37 g, 0.87 mmol) was added at once in methanol (5 mL). Reflux was maintained for 0.5 h whereupon the mixture was allowed to cool to room temperature overnight. Most of the solvents were evaporated and the red product precipitated was filtered and dried in vacuo. Yields: 91 % (**122**), 79 % (**123**).

122

^{1}H NMR (500 MHz, DMSO-d_6, 30 °C): δ = 9.68 (s, 2H), 8.46 (s, 2H), 7.95 (s, 2H), 7.26 (dd, 2H, J_1 = 1.5 Hz, J_2 = 8.0 Hz), 7.18 dd, 2H, J_1 = 1.5 Hz, J_2 = 7.5 Hz), and 6.59 ppm (t, 2H, J= 7.8 Hz); ^{13}C NMR (126 MHz, DMSO, 30 °C): δ = 166.5 (CH), 158.9 (C), 148.3 (C), 147.8 (C), 125.5 (C), 123.2 (CH), 118.8 (CH), 116.5 (CH), and 111.3 ppm (CH); MS(ES): m/z calcd for $C_{19}H_{15}O_7N_2SU$ 653.5 $[M+CH_3O]^-$; found: 653.3; Anal. Calcd. for $C_{18}H_{12}O_6N_2SU$+1.5 H_2O (M_r 649.454): C, 33.29; H, 2.33; N, 4.31. Found: C, 33.29; H, 2.55; N, 4.24.

123

^{1}H NMR (500 MHz, DMSO-d_6, 30 °C): δ = 10.20 (s, 2H), 9.50 (s, 2H), 7.74 (s, 2H), 7.56 (d, 2H, J= 8.5 Hz), 6.34 (d, 2H, J = 2.5 Hz), and 6.25 ppm (dd, 2H, J_1 = 2.5 Hz, J_2 = 8.5 Hz); ^{13}C NMR (126 MHz, DMSO, 30 °C): δ = 172.1 (CH), 165.5 (C), 164.6 (C), 148.3 (C), 137.3 (C), 117.5 (CH), 109.4 (CH), 107.0 (CH), and 105.4 ppm (CH); MS(ES): m/z calcd for $C_{18}H_{11}O_6N_2SU$ 621.4 $[M-H]^-$; found: 621.2; Anal. Calcd. for

$C_{18}H_{12}O_6N_2SU+1.5\ H_2O$ (M_r 649.454): C, 33.29; H, 2.33; N, 4.31. Found: C, 33.59; H, 2.34; N, 4.42.

Dioxo{[2,2′-[1,2-phenylenebis(nitrilomethylidyne)]bis-[6-(methoxy)phenolato]] (2-)-N,N′,O,O′}uranium **126**
Dioxo{[2,2′-[1,2-phenylenebis(nitrilomethylidyne)]bis-[5-(methoxy)phenolato]] (2-)-N,N′,O,O′}uranium **127**

A mixture of 2-hydroxy-(3/4)-methoxybenzaldehyde (0.15 g, 0.99 mmol) and 1,2-benzenediamine (0.053 g, 0.49 mmol) in methanol (30 mL) was stirred for an hour. $UO_2(OAc)_2 \bullet 2H_2O$ (0.21 g, 0.49 mmol) was added at once in methanol (5 mL). The mixture was stirred overnight. The red product precipitated in a quantitative yield was filtered and dried in vacuo.

126

^{1}H NMR (500 MHz, DMSO-d_6, 30 °C): δ = 9.59 (s, 2H), 7.75-7.77 (m, 2H), 7.52-7.54 (m, 2H), 7.40 (dd, 2H J_1 = 1.5 Hz, J_2 = 8.2 Hz), 7.26 (dd, 2H, J_1 = 1.6 Hz, J_2 = 7.8 Hz), 6.63 (t, 2H, J_1= 7.8 Hz, J_2 = 7.7 Hz), and 3.98 ppm (s, 6H); ^{13}C NMR (126 MHz, DMSO, 30 °C): δ = 166.4 (CH), 161.0 (C), 151.1 (C), 146.8 (C), 128.6 (C), 127.3 (CH), 124.1 (CH), 120.2 (CH), 117.5 (CH), 115.9 (CH), and 56.1 ppm (CH_3); MS(ES): m/z calcd for $C_{35}H_{29}O_7N_2U$ 675.5 $[M+CH_3O]^-$; found: 675.4; Anal. Calcd. for $C_{22}H_{18}O_6N_2U+2\ H_2O$ (M_r 680.418): C, 38.78; H, 3.25; N, 4.11. Found: C, 38.40; H, 3,20; N, 4.15.

127

^{1}H NMR (500 MHz, DMSO-d_6, 30 °C): δ = 9.49 (s, 1H), 7.70 (d, 2H, J = 8.7 Hz), 7.67-7.68 (m, 2H), 7.47-7.48 (m, 2H), 6.51 (d, 2H, J = 2.4 Hz), 6.37 (dd, 2H, J_1 = 2.5 Hz, J_2 = 8.7 Hz), and 3.87 ppm (s, 3H); ^{13}C NMR (126 MHz, DMSO, 30 °C): δ =

172.0 (C), 166.6 (C), 165.0 (C), 146.9 (C), 137.2 (CH), 128.0 (C), 119.9 (CH), 118.6 (CH), 105.8 (CH), 103.4 (CH), and 55.4 ppm (CH_3); MS(ES): m/z calcd for $C_{35}H_{29}O_7N_2U$ 675.5 $[M+CH_3O]^-$; found: 675.3; Anal. Calcd. for $C_{22}H_{18}O_6N_2U$+1.5 H_2O (M_r 671.480): C, 39.36; H, 3.15; N, 4.17. Found: C, 39.73; H, 3,20; N, 4.15.

Dioxo{[2,2′-[1,2-phenylenebis(nitrilomethylidyne)]bis-[6-(cyclohexylmethoxy)-phenolato]](2-)-N,N′,O,O′}uranium **129**

A mixture of 2-hydroxy-3-(cyclohexylmethoxy)benzaldehyde (0.10 g, 0.43 mmol) and 1,2-benzenediamine (0.023 g, 0.21 mmol) in methanol (30 mL) was stirred for an hour. $UO_2(OAc)_2 \bullet 2H_2O$ (0.09 g, 0.023 mmol) was added at once in methanol (5 mL). The mixture was stirred overnight. Most of solvents were evaporated and the reaction mixture was dissolved in $CHCl_3$ (30 mL) and washed with water (10 mL) 3 times to yield a red solid. The residue was purified by column chromatography (silica gel, acetone/$CHCl_3$, 1:9) and recrystallized from methanol. Yield 65 %.

^{1}H NMR (500 MHz, DMSO-d_6, 30 °C): δ = 9.59 (s, 2H), 7.74-7.76 (m, 2H), 7.52-7.54 (m, 2H), 7.39 (dd, 2H, J_1 =1.5 Hz, J_2 = 8.1 Hz), 7.24 (dd, 2H, J_1 = 1.5 Hz, J_2 = 7.7 Hz), 6.59 (t, 2H, J_1=7.8 Hz, J_2=7.8 Hz), 4.99 (d, 4H, J = 7.0 Hz), 1.78-1.81 (m, 4H), 1.70-1.73 (m, 2H), 1.24-1.39 (m, 8H), and 1.12-1.19 ppm (m, 4H); ^{13}C NMR (126 MHz , DMSO, 30 °C): δ = 166.4 (CH), 161.1 (C), 150.4 (C), 146.8 (C), 128.6 (C), 127.2 (CH), 124.2 (CH), 120.1 (CH), 118.7 (CH), 115.9 (CH), 74.0 (CH_2), 37.3 (CH_2), 29.5 (CH_2), 26.1 (CH_2), and 25.3 ppm (CH_2); MS(ES): m/z calcd. for $C_{35}H_{39}O_7N_2U$ 839.8 $[M+CH_3O]^-$; found: 839.5; Anal. Calcd. for $C_{34}H_{38}O_6N_2U$+3 H_2O (M_r 862.796): C, 47.44; H, 4.92; N, 3.25. Found: C, 47.47; H, 4,79; N, 3.27.

6.6 Core uranyl salothiophen

Dioxo{[2,2′-[3,4-thiophenebis(nitrilomethylidyne)]bisphenolato]
(2-)-N,N′,O,O′}uranium **132**

To a refluxing solution of 3,4-diaminothiophene (0.1 g, 0.88 mmol) in methanol (30 mL) a solution of 2-3/4-dihydroxybenzaldehyde (0.24 g, 1.4 mmol) in methanol (20 mL) was added during 1 h whereupon $UO_2(OAc)_2 \bullet 2H_2O$ (0.37 g, 0.87 mmol) was added at once in methanol (5 mL). Reflux was maintained for 0.5 h whereupon the mixture was allowed to cool to room temperature overnight. Most of solvents were evaporated and the red product precipitated was filtered and dried in vacuo. Yield 65 %.

^{1}H NMR (500 MHz, DMSO-d_6, 30 °C): δ = 9.71 (s, 2H), 7.96 (s, 2H), 7.78 (dd, 2H J_1 = 1.8 Hz, J_2 = 8 Hz), 7.64 (td, 2H, J_1 = 1.5 Hz, J_2 = 5 Hz), 7.0 (d, 2H, J = 8.0 Hz), and 6.75 ppm (td, 2H, J_1 = 1.0 Hz, J_2 = 8.0 Hz); ^{13}C NMR (126 MHz, DMSO, 30 °C): δ = 169.9 (CH), 166.3 (C), 147.8 (C), 136.0 (C), 135.7 (C), 124.0 (CH), 120.8 (CH), 116.8 (CH), 106.9 (CH), and 111.4 ppm (CH); MS(ES): m/z calcd for $C_{19}H_{15}O_5N_2SU$ 621.5 $[M+CH_3O]^-$; found: 621.2; Anal. Calcd. for $C_{18}H_{12}O_4N_2SU$+1.5 H_2O (M_r 617.489): C, 35.01; H, 2.45; N, 4.53. Found: C, 34.65; H, 2.66; N, 4.35.

6.7 NMR-titration procedure:

Uranyl salophen water complex was weighed (from 1 mg to 4 mg) directly to the NMR-tube and dissolved to a certain concentration (from 0.40 mM to 0.80 mM) of salt in $CDCl_3$. The ratio between the concentrations of salophen and salt in the beginning of measurements was about 14. The same concentration of the salt, in a $CDCl_3$ –solution was added between measurements so that the concentration of

salophen decreased during the titration. At the end of the titration the concentration of the salt was more than double the concentration of the salophen. All peaks from salts were monitored, but because of overlap with the water peak, only methyl singlets from unsymmetrical salts and NCH_2-peaks from symmetrical salts were taken into account. SigmaPlot 10.0 was used to determine binding constants. User-defined 1:1 isotherm was used.

Used isotherm:

f=((D*K*L)/(1+K*L)+z
L=col(1)-g
g=(-b-sqrt((b^2)-4*c)))/2
c=5.0e-1*col(1)
b=-(5.0e-1+col(1)+1/K)

fit f to y

Where c = concentration of the salt, here 5.0e-1
col(1) = concentration of the host
col(2) = ppm-value of the monitored salt peak

REFERENCES

1. Stupp, S. I. *Chemical Reviews*, **2005**, 105, Editorial.

2. Steed, J. W.; Atwood, J. L. *Supramolecular Chemistry, Wiley*, **2000**, 2.

3. Muller-Dethlefs, K.; Hobza, P. *Chem. Rev.*, **2000**, 100, 143.

4. Ma, J. C.; Dougherty, D. A. *Chem. Rev.*, **1997**, 97, 1303.

5. Gellman, S. H. *Chemical Reviews*, **1997**, 97, Editorial.

6. Braga, D.; Grepioni, F.; Desiraju, G. R. *Chem. Rev.*, **1998**, 98, 1375.

7. Atwood, D. *Coordination Chemistry Reviews*, **1997**, 165, 267.

8. Atwood, D.; Harvey, M. *Chem. Rev.*, **2001**, 101, 37.

9. van Veggel, F. C. J. M.; Verboom, W.; Reinhoudt, D. N. *Chemical Reviews*, **1994**, 94, 279.

10. Lewinski, J.; Zachara, J.; Justyniak, I.; Dranka, M. *Coordination Chemistry Reviews*, **2005**, 249, 1185.

11. Sessler, J. L.; Melfi, P. J.; Dan Pantos, G. *Coordination Chemistry Reviews*, **2006**, 250, 816.

12. Arnold, P. L.; Love, J. B.; Patel, D. *Coordination Chemistry Reviews*, **2009**, doi:10.1016/j.ccr.2009.03.014.

13. Dalla Cort, A.; Mandolini, L.; Palmieri, G.; Pasquini, C.; Schiffiano, L. *Chem. Commun.*, **2003**, 2178.

14. van Doorn, A. R.; Bos, M.; Harkema, S.; van Eerden, J.; Verboom, W.; Reinhoudt, D. N. *J. Org. Chem.*, **1991**, 56, 2371.

15. Jones, L. H.; Penneman, R. A. *The Journal of Chemical Physics*, **1953**, 21, 542.

16. Bandoli, G.; Cattalini, L.; Clemente, D. A.; Croatto, U.; Vidali, M.; Vigato, P. A. *J. Chem. Soc., Chem. Commun.*, **1971**, 1330.

17. Bandoli, G.; Cattalini, L.; Clemente, D. A.; Vidali, M.; Vigato, P. A. *J. Chem. Soc., Chem. Comm.*, **1972**, 344.

18. Bandoli, G.; Clemente, D. A. *J. Chem. Soc., Dalton Trans.*, **1975**, 7, 612.

19. Fenton, D. E.; Casellato, U.; Vigato, P. A.; Vidali, M. *Inorganica Chimica Acta,* **1984**, 94, 6.

20. Rudkevich, D. M.; Verboom, W.; Brozozka, Z.;Palys, M. J.; Stauthamer, W. P. R. V.; van Hummel, G. J.; Franken, S. M.; Harkema, S.; Engbersen, J. F. J.; Reinhoudt, D. N. *J. Am. Chem. Soc.,* **1994**, 116, 4341.

21. Takao, K.; Ikeda, Y. *Inorg. Chem.,* **2007**, 46, 1550.

22. Layer, R. W. *Chem. Rev.,* **1963**, 63,489.

23. Eisch, J. J.; Sanchez, R. *J. Org. Chem.,* **1986**, 51, 1848.

24. Schiff, H. *Ann. Chem. Pharm.,* **1864**, 131, 118.

25. Comyns, A. E.; Gatehouse, B. M.; Wait, E. *J. Chem. Soc.,* **1958**, 4655.

26. Wintner, E. A.; Tsao, B.; Rebek Jr, J. *J. Org. Chem.,* **1995**, 60, 7997.

27. Reinhoudt, D. N.; Rudkevich, D. M.; de Jong, F. *J. Am. Chem. Soc.,* **1996**, 118, 6880.

28. Robertson, A.; Sinclair, A. J.; Philp, D. *Chem. Soc. Rev.,* **2000**, 29, 141.

29. Quayle, J. M.; Slawin, A. M. Z.; Philp, D. *Tetrahedron Letters,* **2002**, 43, 7229.

30. Silverman, A. P.; Kool, E. T. *Chem. Rev.,* **2006**, 106, 3775.

31. Vidonne, A.; Philp, D. *Tetrahedron,* **2008**, 64, 8464.

32. Mizuguchi, K.; Park, Y.; Tomiyasu, H. *Journal of Nuclear Science and Technology,* **1993**, 30, 542.

33. Lee, S.; Mizuguchi, K.; Tomiyasu, H. *Journal of Nuclear Science and Technology,* **1996**, 33, 190.

34. Mizuguchi, K.; Lee, S.; Ikeda, Y.; Tomiyasu, H. *Journal of Alloys and Compounds,* **1998**, 271-273, 163.

35. Kim, S.; Tomiasy, H.; Ikeda, Y. *Journal of Nuclear Science and Technology,* **2002**, 39, 160.

36. Mizuoka, K.; Ikeda, Y. *Inorg. Chem.,* **2003**, 42, 3396.

37. Mizuoka, K.; Tsushima, S.; Hasegava, M.; Hoshi, T.; Ikeda, Y. *Inorg. Chem.,* **2005**, 44, 6211.

38. Mizuoka, K.; Kim, S.; Hasegava, M.; Hoshi, T.; Uchiyama, G.; Ikeda, Y. *Inorg. Chem.*, **2003**, 42, 1031.

39. Van Staveren, C. J.; Fenton, D. E.; Reinhoudt, D. N.; van Eerden, J.; Harkema, S. *J. Am. Chem. Soc.*, **1987**, 109, 3456.

40. Zollinger, D. PH.; Bos, M.; Van Veen-Blaauw, A. M. W.; Ven Der Linden, W. E. *Analytica Chimica Acta*, **1984**, 161, 83.

41. Benini, S.; Rypniewski, W. R.; Wilson, K. S.; Miletti, S.; Ciurli, S.; Mangani, S. *Structure*, **1999**, 7, 205.

42. Vial, S.; Prevot, V.; Forano, C. *Journal of Physics and Chemistry of Solids*, **2006**, 67, 1048.

43. Deyhimi, F.; Bajalan, M. *Bioelectrochemistry*, **2008**, 74, 176.

44. Van Staveren, C. J.; van Eerden, J.; van Veggel, F. C. J. M.; Harkema, S.; Reinhoudt, D. N. *J. Am. Chem. Soc.*, **1988**, 110, 4994.

45. Van Doorn, A. R.; Schaafstra, R.; Bos, M.; Harkema, S.; van Eerden, J.; Verboom, W.; Reinhoudt, D. N. *J. Org. Chem.*, **1991**, 56, 6083.

46. Nijenhuis, W. F.; Van Doorn, A. R.; Reichwein, A. M.; De Jong, F.; Reinhoudt, D. N. *J. Am. Chem. Soc.*, **1991**, 113, 3607.

47. Reichwein, A. M.; Verboom, W.; Harkema, S.; Spek, A. L.; Reinhoudt, D. N. *J. Chem. Soc., Perkin Trans 2*, **1994**, 1167.

48. Schmidtchen, F. P. *J. Org. Chem.*, **1986**, 51, 5161.

49. Katz, H. E. *J. Org. Chem.*, **1989**, 54, 2179.

50. Jung, M. E.; Xia, H. *Tetrahedron Letters*, **1988**, 29, 297.

51. Blanda, M. T.; Horner, J. H.; Newcomb, M. *J. Org. Chem.*, **1989**, 54, 4626.

52. Wuest, J.; Zacharie, B. *J. Am. Chem. Soc.*, **1987**, 109, 4714.

53. Kanyo, Z. F.; Christianson, D. W. *The Journal of Biological Chemistry*, **1991**, 266, 4264.

54. Rudkevich, D. M.; Stauthamer, W. P. R. V.; Verboom, W.; Engbersen, J. F. J.; Harkema, S.; Reinhoudt, D. N. *J. Am. Chem. Soc.*, **1992**, 114, 9671.

55. Antonisse, M. M. G.; Snellink-Rul, B. H. M.; Engbersen, J. F. J.; Reinhoudt, D. N. *J. Org. Chem.,* **1998**, 63, 9776.

56. Antonisse, M. M. G.; Reinhoudt, D. N. *Chem. Commun.,* **1998**, 443.

57. Gale, P. A. *Coordination Chemistry Reviews,* **2003**, 240, 191.

58. Mateos-Timoneda, M. A.; Kerckhoffs, J. M. C. A.; Crego-Calama, M.; Reinhoudt, D. N. *Angew. Chem. Int. Ed.,* **2005**, 44, 3248.

59. Quici, S.; Manfredi, A.; Pozzi, G.; Cavazzini, M.; Rozzoni, A. *Tetrahedron,* **1999**, 55. 10487.

60. Lacy, S. M.; Rudkevich, D. M.; Verboom, W.; Reinhoudt, D. N. *Tetrahedron Letters,* **1994**, 35, 5953.

61. Schmidtchen, F. P. *Tetrahedron Letters,* **1984**, 25, 4361.

62. Chae, M. K.; Lee, J-I.; Kim, N-K.; Jeong, K-S. *Tetrahedron Letters,* **2007**, 48, 6624.

63. Kubic, S.; Goddard, R. *J. Org. Chem.,* **1999**, 64, 9475.

64. Mansikkamäki, H.; Nissinen, M.; Rissanen, K. *Chem. Commun.,* **2002**, 1902.

65. Mansikkamäki, H.; Schalley, C. A.; Nissinen, M.; Rissanen, K. *New J. Chem.,* **2005**, 29, 116.

66. Busi, S.; Saxell, H.; Fröhlich, R.; Rissanen, K. *CrystEngComm.,* **2008**, 10, 1803.

67. Cametti, M.; Nissinen, M.; Dalla Cort, A.; Mandolini, L.; Rissanen, K. *Chem. Commun.,* **2003**, 2420.

68. Cametti, M.; Nissinen, M.; Dalla Cort, A.; Mandolini, L.; Rissanen, K. *J. Am. Chem. Soc.,* **2007**, 129, 3641.

69. Reetz, M. T.; Johnson, B. M.; Harms, K. *Tetrahedron Letters,* **1994**, 35, 2525.

70. Scheerder, J.; Duynhoven, J. P. M.; Engbersen, F. j.; Reinhoudt, D. N. *Angew. Chem. Int. Ed. Engl.,* **1996**, 35, 1090.

71. Mahoney, J. M.; Beatty, A. M.; Smith, B. *J. Am. Chem. Soc.,* **2001**, 123, 5847.

72. Chae, M. K.; Lee, J.; Kim, N.; Jeong, K. *Tetrahedron Letters,* **2007**, 48, 6624.

73. Cametti, M.; Nissinen, M.; Dalla Cort, A.; Mandolini, L.; Rissanen, K. *J. Am. Chem. Soc.,* **2005**, 127, 3831.

74. Cametti, M.; Nissinen, M.; Dalla Cort, A.; Mandolini, L.; Rissanen, K. *Inorg. Chem.,* **2006,** 45, 6099.

75. Böhmer, V.; Kraft, D.; Tabatabai, M. *J. Inclusion Phenom. Mol. Recognit. Chem.,* **1994,** 19, 17.

76. Dalla Cort, A.; Mandolini, L.; Pasquini, C.; Schiffiano, L. *New J. Chem.,* **2004,** 28, 1198.

77. Knof, U.; von Zelewsky, A. *Angew, Chem. Int. Ed.,* **1999,** 38, 302.

78. Dalla Cort, A.; Mandolini, L.; Pasquini, C.; Schiffiano, L. *Org. Lett.,* **2004,** 6, 1697.

79. Dalla Cort, A.; Gasparrini, F.; Lunazzi, L.; Mandolini, L.; Mazzanti, A.; Pasquini, C.; Pierini, M.; Rompietti, R.; Schiffiano, L. *J. Org. Chem.,* **2005,** 70, 8877.

80. Dalla Cort, A.; Murua, J. I. M.; Pasquini, C.; Pons, M.; Schiffiano, L. *Chem. Eur. J.,* **2004,** 10, 3301.

81. Dalla Cort, A.; Mandolini, L.; Pasquini, C.; Schiffiano, L. *J. Org. Chem.,* **2005,** 70, 9814.

82. Ciogli, A.; Dalla Cort, A.; Gasparrini, F.; Lunazzi, L.; Mandolini, L.; Mazzanti, A.; Pasquini, C.; Pierini, M.; Schiffiano, L.; Mihan, F. Y. *J. Org. Chem.,* **2008,** 73, 6108.

83. Jeffrey, J. C.; Rauchfuss, T. B. *Inorganic Chemistry,* **1979,** 18, 2658.

84. Braunstein, P.; Naud, F. *Angew. Chem. Int. Ed.,* **2001,** 40, 680.

85. Bassetti, M. *Eur. J. Inorg. Chem.,* **2006,** 4473.

86. Jacobsen, E. N.; Zhang, W.; Muci, A. R.; Ecker, J. R.; Deng, L. *J. Am. Chem. Soc.,* **1991,** 113, 7063.

87. van Axel Castelli, V.; Dalla Cort, A.; Mandolini, L.; Reinhoudt, D. N. *J. Am. Chem. Soc.,* **1998,** 120, 12688.

88. Dalla Cort, A.; Mandolini, L.; Schiffiano, L. *J. Org. Chem.,* **2008,** 73, 9439.

89. Dalla Cort, A.; Mandolini, L.; Schiffiano, L. *Chem. Commun.,* **2005,** 3867.

90. van Axel Castelli, V.; Dalla Cort, A.; Mandolini, L.; Pinto, V.; Schiffiano, L. *J. Org. Chem.,* **2007**, 72, 5383.

91. van Axel Castelli, V.; Dalla Cort, A.; Mandolini, L.; Reinhoudt, D. N.; Schiffiano, L. *Chem. Eur. J.,* **2000**, 6, 1193.

92. van Axel Castelli, V.; Dalla Cort, A.; Mandolini, L.; Reinhoudt, D. N.; Schiffiano, L. *Eur. J. Org. Chem.,* **2003**, 627.

93. van Axel Castelli, V.; Cacciapaglia, R.; Chiosis, G.; van Veggel, F. C. J. M.; Mandolini, L.; Reinhoudt, D. N. *Inorganica Chimica Acta,* **1996**, 246, 181.

94. Campbell, N. A.; Reese, J. B.; Mitchell, L. G. *Biology, Fift Edition, Benjamin Cummings*, **1999**, 130.

95. Stolwijk, T. B.; Sudhoelter, E. J. R.; Reinhoudt, D. N. *J. Am. Chem. Soc.,* **1987**, 109, 7042.

96. Ensafi, A. A.; Far, A. K.; Meghdadi, S. *Sensors and Actuators B,* **2008**, 133, 84.

97. Brynda, M.; Wesolowski, T. A.; Wojciechowski, K. *J. Phys. Chem. A.,* **2004**, 108, 5091.

98. Kim, D. W.; Park, K-Y.; Yang, M-H.; Kim, T. H.; Mahajan, R. K.; Kim, J. S. *Talanta,* **2007**, 74, 223.

99. Wroblewski, W.; Brzozka, Z.; Rudkevich, D. M.; Reinhoudt, D. N. *Sensors and Actuators B,* **1996**, 37, 151.

100. Hassan, S. S. M.; Marzouk, S. A. M.; Sayour, H. E. M. *Talanta,* **2003**, 59, 1237.

101. Buck, R. P.; Lindner, E. *Pure & Appl. Chem.,* **1994**, 66, 2527.

102. Bakker, E.; Qin, Y. *Anal. Chem.* **2006**, 78, 3965.

103. Steed, J. W.; Atwood, J. L. *Supramolecular Chemistry, Wiley,* **2000**, 603.

104. Jain, A. K.; Gupta, V. K.; Raisoni, J. R. *Talanta,* **2006**, 69, 1007.

105. Kim, J.; Kang, D. M.; Shin, S. c.; choi, M. Y.; Kim, J.; Lee, S. S.; Kim, J. S. *Analytica Chimica Acta,* **2008**, 614, 85.

106. Ganjali, M. R.; Norouzi, P.; Ghomi, M.; Salavati-Niazari, M. *Analytica Chimica Acta,* **2006**, 567, 196.

107. Pietrzak, M.; Meyerhoff, M. E.; Malinowska, E. *Analytica Chimica Acta,* **2007**, 596, 201.

108. Wang, L.; Meyerhoff, M. E. *Analytica Chimica Acta,* **2008**, 611, 97.

109. Gorski, L.; Mroczkiewicz, M.; Pietrzak, M.; Malinowska, E. *Analytica Chimica Acta,* **2009**, 633, 181.

110. Antonisse, M. M. G.; Snellink-Ruel, B. H. M.; Yigit, I.; Engbersen, J. F. J.; Reinhoudt, D. N. *J. Org. Chem.,* **1997**, 62, 9034.

111. Antonisse, M. M. G.; Snellink-Ruel, B. H. M.; Engbersen, J. F. J.; Reinhoudt, D. N. *Sensors and Actuators B*, **1998**, 47, 9.

112. Wroblewski, W.; Wojciechowski, K.; Dybco, A.; Brzozka, Z.; Engberink, R. J. M.; Snellink-Ruel, B. H. M.; Reinhoudt, D. N. *Sensors and Actuators B,* **2000**, 68, 313.

113. Antonisse, M. M. G.; Snellink-Ruel, B. H. M.; Ion, A. C.; Engbersen, J. F. J.; Reinhoudt, D. N. *J. Chem. Soc., Perkin Trans. 2,* **1999**, 1211.

114. Ion, A. C.; Ion I.; Antonisse, M. M. G.; Snellink-Ruel, B. H. M.; Reinhoudt, D. N. *Russian Journal of General Chemistry*, **2001**, 71, 181.

115. Wroblewski, W.; Wojciechowski, K.; Dybco, A.; Brzozka, Z.; Engberink, R. J. M.; Snellink-Ruel, B. H. M.; Reinhoudt, D. N. *Analytica Chimica Acta,* **2001**, 432, 79.

116. Wroblewski, W.; Wojciechowski, K.; Dybco, A.; Brzozka, Z.; Engberink, R. J. M.; Snellink-Ruel, B. H. M.; Reinhoudt, D. N. *Sensors and Actuators B,* **2001**, 78, 315.

117. Wojciechowski, K.; Wroblewski, W.; Brzzka, Z. *Anal. Chem.,* **2003**, 75, 3270.

118. Araki, T.; Tsukube, H. *CRC, Liquid Membranes: Chemical Applications, CRC-PRESS,* **1990**, chapters 3-5.

119. Straaten-Nijenhuis, W. F.; Van Doorn, A. R.; Reichwein, A. M.; De Jong, F.; Reinhoudt, D. N. *J. Org. Chem.*, **1993**, 58, 2265.

120. Chrisstoffels, L. A. J.; de Jong, F.; Reinhoudt, D. N. *Chem. Eur. J.*, **2000**, 6, 1376.

121. Park, K. K.; Seo, H.; Kim, J-G.; Suh, I-H. *Tetrahedron Letters*, **2000**, 41, 1393.

122. Park, K. K.; Han, I. H.; Park, J. W. *J. Org. Chem.,* **2001**, 66, 6800.

123. Ropponen, J.; Lahtinen, M.; Busi, S.; Nissinen, M.; Kolehmainen, E.; Rissanen, K. *New J. Chem.,* **2004**, 28, 1426.

124. Busi, S.; Lahtinen, M.; Ropponen, J.; Valkonen, J.; Rissanen, K. *Journal of Solid State Chemistry,* **2004**, 177, 3757.

125. Busi, S.; Lahtinen, M.; Mansikkamäki, H.; Valkonen, J.; Rissanen, K. *Journal of Solid State Chemistry,* **2005**, 178, 1722.

126. Kovacheva, P.; Djingova, R. *Analytica Chimica Acta,* **2002**, 464, 7.

127. Cametti, M.; Dalla Cort, A.; Mandolini, L.; Nissinen, M.; Rissanen K. *New Journal of Chemistry,* **2008**, 32, 1113.

128. Cametti, M.; Dalla Cort, A.; Bartik, K. *ChemPhyschem.,* **2008**, 9, 2168.

129. Steed, J. W.; Atwood, J. L. *Supramolecular Chemistry, Wiley,* **2000**, 15.

130. Benesi, H. A.; Hildebrand, J. H. *J. Am Chem. Soc.,* **1949**, 71, 2703.

131. Horman, I.; Dreux, B. *Anal. Chem.,* **1983**, 55, 1219.

132. Hirose, K. *Journal of Inclusion Phenomena and Macrocyclic Chemistry,* **2001**, 39, 193.

133. Popov, K.; Rönkkömäki, H.; Lajunen, L. H. J. *Pure Appl. Chem.,* **2006**, 78, 663.

134. Schneider, H-J.; Kramer, R.; Simova, S.; Schneider, U. *J. Am. Chem. Soc.,* **1988**, 110, 6442.

135. Fielding, L. *Tetrahedron,* **2000**, 56, 6151.

136. Bohra, R.; Sharma, S.; Dhammani, A. *Acta Cryst.,* **1994**, C50, 1449.

137. Boghaei, D. M.; Mohebi, S. *Tetrahedron,* **2002**, 58, 5357.

138. Frank, E. R.; Chen, X. X.; Hamers, R. J. *Surface Science,* **1995**, 334, L709.

139. Grobosch, M.; Knupher, M. *Organic Electronics,* **2007**, 8, 625.

140. Tang, M. L.; Oh, J. H.; Reichardt, A. D.; Bao, Z. *J. Am. Chem. Soc.,* **2009**, 131, 3733.

141. Kaes, C.; Katz, A.; Hosseini, M. W. *Chem. Rev.,* **2000**, 100, 3553.

142. Chelucci, G.; Thummel, R. P. *Chem. Rev.,* **2002**, 102, 3129.

143. Haino, T.; Araki, H.; Yamanaka, Y.; Fukazawa, Y. *Tetrahedron Letters,* **2001**, 42, 3203.

144. Packheiser, R.; Ecorchard, P.; Walfort, B.; Lang, H. *Journal of Organometal Chemistry,* **2008**, 693, 933.

145. Psychogios, N.; Regnouf-de-Vains, J-B. *Tetrahedron Letters,* **2002**, 43, 7691.

146. Psychogios, N.; Regnouf-de-Vains, J-B. *Tetrahedron Letters,* **2002**, 43, 77.

147. Xie, Y.; Jiang, H.; Yu, M.; Du, C.; Liu, Q.; Xu, X.; Zhu, Y. *Journal of Molecular Structure*, **2002**, 608, 139.

148. Maslak, V.; Yan, Z.; Xia, S.; Gallucci, J.; Hadad, C. M.; Badjic, J. D. *J. Am. Chem. Soc.,* **2006**, 128, 5887.

149. Huang, T. L. J.; Brewer, D. G. *Can. J. Chem.,* **1981**, 59, 1689.

150. Ballardini, R.; Balzani, V.; Clemente-Leon, M.; Credi, A.; Gandolfi, M. T.; Ishow, E.; Perkins, J.; Stoddard, J. F.; Tseng, H-R.; Wenger, S. *J. Am. Chem. Soc.,* **2002**, 124, 12786.

151. Chung, C. W. Y.; Toy, P. H. *J. Comb. Chem.,* **2007**, 9, 115.

152. Cametti, M.; Ilander, L.; Rissanen, K. *Inorg, Chem.,* **2009**, 48, 8632.

153. De Angelis, S.; Solari, E.; Gallo, E.; Floriani, C.; Chiesi-Villa, A.; Rizzoli, C. *Inorg. Chem.,* **1996**, 35, 5995.

154. Gallo, E.; Solari, E.; Re, N.; Floriani, C.; Chiesi-Villa, A.; Rizzoli, C. *J. Am. Chem. Soc.,* **1997**, 119, 5144.

155. Cametti, M.; Dalla-Cort, A.; Colapietro, M.; Portalone, G.; Russo, L.; Rissanen, K. *Inorg. Chem.,* **2007**, 46, 9057.

APPENDICES

APPENDIX 1

Crystal data and structure refinement for	**95** • H_2O	
Identification code	4-bz-teacl	
Empirical formula	$C_{38.65} H_{36.92} N_2 O_{8.95} U$	
Formula weight	910.66	
Temperature	123(2) K	
Wavelength	0.71073 Å	
Crystal system	Triclinic	
Space group	P-1	
Unit cell dimensions	a = 10.7863(2) Å	α = 95.2710(10)°.
	b = 15.8191(3) Å	β = 94.8880(10)°.
	c = 22.1267(4) Å	γ = 103.0720(10)°.
Volume	3640.15(12) $Å^3$	
Z	4	
Density (calculated)	1.662 Mg/m^3	
Absorption coefficient	4.516 mm^{-1}	
F(000)	1786	
Crystal size	0.12 x 0.10 x 0.06 mm^3	
Theta range for data collection	2.07 to 25.00°.	
Index ranges	-12<=h<=11, -18<=k<=18, -26<=l<=26	
Reflections collected	47787	
Independent reflections	12724 [R(int) = 0.0936]	
Completeness to theta = 25.00°	99.4 %	
Absorption correction	Semi-empirical from equivalents	
Max. and min. transmission	0.7733 and 0.6133	
Refinement method	Full-matrix least-squares on F^2	
Data / restraints / parameters	12724 / 6 / 907	
Goodness-of-fit on F^2	1.032	
Final R indices [I>2sigma(I)]	R1 = 0.0500, wR2 = 0.0957	
R indices (all data)	R1 = 0.0802, wR2 = 0.1054	
Largest diff. peak and hole	1.764 and -1.649 e.$Å^{-3}$	

APPENDIX 2

Crystal data and structure refinement		
for	**95**•MeOH	
Identification code	val011	
Empirical formula	$C_{17.50}H_{14.50}NO_{5.50}U_{0.50}$	
Formula weight	445.82	
Temperature	123(2) K	
Wavelength	0.71073 Å	
Crystal system	Orthorhombic	
Space group	P n a m	
Unit cell dimensions	a = 9.2059(3) Å	α= 90°.
	b = 17.0711(5) Å	β= 90°.
	c = 22.9541(5) Å	γ= 90°.
Volume	3607.35(18) $Å^3$	
Z	8	
Density (calculated)	1.642 Mg/m^3	
Absorption coefficient	4.559 mm^{-1}	
F(000)	1732	
Crystal size	0.27 x 0.15 x 0.15 mm^3	
Theta range for data collection	2.67 to 24.99°.	
Index ranges	-10<=h<=10, -20<=k<=20, -27<=l<=27	
Reflections collected	5994	
Independent reflections	3252 [R(int) = 0.0325]	
Completeness to theta = 24.99°	99.9 %	
Max. and min. transmission	0.5479 and 0.3724	
Refinement method	Full-matrix least-squares on F^2	
Data / restraints / parameters	3252 / 0 / 245	
Goodness-of-fit on F^2	1.123	
Final R indices [I>2sigma(I)]	R1 = 0.0408, wR2 = 0.0839	
R indices (all data)	R1 = 0.0522, wR2 = 0.0880	
Largest diff. peak and hole	1.110 and -0.746 e.$Å^{-3}$	

APPENDIX 3

Crystal data and structure refinement		
for	**9**•MeOH	
Identification code	oda-3salof-dmdeacl	
Empirical formula	C_{35} H_{30} N_2 O_7 U	
Formula weight	828.64	
Temperature	123(2) K	
Wavelength	0.71073 Å	
Crystal system	Orthorhombic	
Space group	Pnma	
Unit cell dimensions	a = 9.56390(10) Å	α = 90°.
	b = 22.4144(2) Å	β = 90°.
	c = 13.69490(10) Å	γ = 90°.
Volume	2935.76(5) $Å^3$	
Z	4	
Density (calculated)	1.875 Mg/m^3	
Absorption coefficient	5.585 mm^{-1}	
F(000)	1608	
Crystal size	0.20 x 0.12 x 0.12 mm^3	
Theta range for data collection	2.60 to 25.00°.	
Index ranges	-11<=h<=10, -26<=k<=26, -16<=l<=16	
Reflections collected	35825	
Independent reflections	2650 [R(int) = 0.0428]	
Completeness to theta = 25.00°	99.9 %	
Absorption correction	Semi-empirical from equivalents	
Max. and min. transmission	0.5100 and 0.4328	
Refinement method	Full-matrix least-squares on F^2	
Data / restraints / parameters	2650 / 6 / 218	
Goodness-of-fit on F^2	1.093	
Final R indices [I>2sigma(I)]	R1 = 0.0160, wR2 = 0.0337	
R indices (all data)	R1 = 0.0180, wR2 = 0.0344	
Largest diff. peak and hole	0.459 and -0.423 e.$Å^{-3}$	

APPENDIX 4

Crystal data and structure refinement for	**9**•DMDPACl
Identification code	oda-3salof
Empirical formula	$C_{177}\ H_{202}\ Cl_4\ N_{12}\ O_{30}\ U_4$
Formula weight	4071.43
Temperature	123(2) K
Wavelength	0.71073 Å
Crystal system	Monoclinic
Space group	P21/c
Unit cell dimensions	a = 14.1252(3) Å α = 90°. b = 20.4511(4) Å β = 104.3950(10)°. c = 15.7079(3) Å γ = 90°.
Volume	4395.17(15) $Å^3$
Z	1
Density (calculated)	1.538 Mg/m^3
Absorption coefficient	3.806 mm^{-1}
F(000)	2024
Crystal size	0.35 x 0.17 x 0.15 mm^3
Theta range for data collection	2.40 to 25.00°.
Index ranges	-16<=h<=16, -22<=k<=24, -18<=l<=18
Reflections collected	56838
Independent reflections	7728 [R(int) = 0.0989]
Completeness to theta = 25.00°	99.9 %
Absorption correction	Semi-empirical from equivalents
Max. and min. transmission	0.5612 and 0.4625
Refinement method	Full-matrix least-squares on F^2
Data / restraints / parameters	7728 / 45 / 560
Goodness-of-fit on F^2	1.023
Final R indices [I>2sigma(I)]	R1 = 0.0394, wR2 = 0.0731
R indices (all data)	R1 = 0.0606, wR2 = 0.0797
Largest diff. peak and hole	0.814 and -0.499 $e.Å^{-3}$

APPENDIX 5

Crystal data and structure refinement for	**9**•DMDBACl	
Identification code	3der-salof-dmdbacl	
Empirical formula	$C_{46.55}H_{55.10}ClN_3O_{7.75}U$	
Formula weight	1054.12	
Temperature	123(2) K	
Wavelength	0.71073 Å	
Crystal system	Monoclinic	
Space group	P21/c	
Unit cell dimensions	a = 14.8243(2) Å	α= 90°.
	b = 20.7799(3) Å	β= 106.2520(10)°.
	c = 15.5557(2) Å	γ = 90°.
Volume	4600.41(11) $Å^3$	
Z	4	
Density (calculated)	1.522 Mg/m^3	
Absorption coefficient	3.640 mm^{-1}	
F(000)	2106	
Crystal size	0.20 x 0.16 x 0.10 mm^3	
Theta range for data collection	1.94 to 25.00°.	
Index ranges	-17<=h<=17, -23<=k<=24, -18<=l<=18	
Reflections collected	60956	
Independent reflections	8104 [R(int) = 0.0939]	
Completeness to theta = 25.00°	99.9 %	
Absorption correction	Semi-empirical from equivalents	
Max. and min. transmission	0.7123 and 0.5297	
Refinement method	Full-matrix least-squares on F^2	
Data / restraints / parameters	8104 / 10 / 544	
Goodness-of-fit on F^2	1.033	
Final R indices [I>2sigma(I)]	R1 = 0.0356, wR2 = 0.0656	
R indices (all data)	R1 = 0.0525, wR2 = 0.0704	
Largest diff. peak and hole	0.890 and -0.494 $e.Å^{-3}$	

APPENDIX 6

Crystal data and structure refinement for	**95** •TMACl	
Identification code	val008	
Empirical formula	C_{41} H_{44} Cl N_3 O_7 U	
Formula weight	964.27	
Temperature	123(2) K	
Wavelength	0.71073 Å	
Crystal system	monoclinic	
Space group	P21/a	
Unit cell dimensions	a = 10.0613(3) Å	α= 90°.
	b = 16.2562(4) Å	β= 97.0250(10)°.
	c = 24.3881(6) Å	γ = 90°.
Volume	3958.94(18) $Å^3$	
Z	4	
Density (calculated)	1.618 Mg/m^3	
Absorption coefficient	4.220 mm^{-1}	
F(000)	1904	
Crystal size	0.30 x 0.20 x 0.15 mm^3	
Theta range for data collection	3.76 to 21.47°.	
Index ranges	-10<=h<=10, -16<=k<=16, -25<=l<=25	
Reflections collected	8312	
Independent reflections	4429 [R(int) = 0.0492]	
Completeness to theta = 21.47°	97.6 %	
Max. and min. transmission	0.5702 and 0.3642	
Refinement method	Full-matrix least-squares on F^2	
Data / restraints / parameters	4429 / 0 / 478	
Goodness-of-fit on F^2	1.078	
Final R indices [I>2sigma(I)]	R1 = 0.0362, wR2 = 0.0712	
R indices (all data)	R1 = 0.0531, wR2 = 0.0783	
Largest diff. peak and hole	0.654 and -0.720 e.$Å^{-3}$	

APPENDIX 7

Crystal data and structure refinement		
for	**95**•DMDEACl	
Identification code	val012	
Empirical formula	C_{43} H_{48} Cl N_3 O_7 U	
Formula weight	992.32	
Temperature	123.0(1) K	
Wavelength	0.71073 A	
Crystal system, space group	Monoclinic	
Space group	P 21/a	
Unit cell dimensions	a = 10.0526(1) Å	α = 90°.
	b = 16.2162(2) Å	β = 96.099(1)°.
	c = 24.8321(3) Å	γ = 90°.
Volume	4025.09(8) Å^3	
Z	4	
Density (calculated)	1.638 Mg/m^3	
Absorption coefficient	4.153 mm^{-1}	
F(000)	1968	
Crystal size	0.2 x 0.15 x 0.15 mm	
Theta range for data collection	2.07 to 25.00 deg.	
Limiting indices	-11<=h<=10, -19<=k<=18, -29<=l<=28	
Reflections collected / unique	31293 / 7042 [R(int) = 0.0768]	
Completeness to theta = 25.00	99.5 %	
Absorption correction	Semi-empirical from equivalents	
Max. and min. transmission	0.537 and 0.459	
Refinement method	Full-matrix least-squares on F^2	
Data / restraints / parameters	7042 / 0 / 490	
Goodness-of-fit on F^2	1.025	
Final R indices [I>2sigma(I)]	R1 = 0.0356, wR2 = 0.0660	
R indices (all data)	R1 = 0.0551, wR2 = 0.0718	
Largest diff. peak and hole	0.934 and -0.903 e/Å^3	

APPENDIX 8

Crystal data and structure refinement for	**100**•DMDBACl
Identification code	val023
Empirical formula	$C_{94}\ H_{110}\ Cl_2\ N_6\ O_{14}\ U_2$
Formula weight	2094.84
Temperature	123(2) K
Wavelength	0.71073 Å
Crystal system	Monoclinic
Space group	P21/n
Unit cell dimensions	a = 9.7675(4) Å α= 90°. b = 29.8763(13) Å β= 92.7360(10)°. c = 30.4195(13) Å γ = 90°.
Volume	8866.8(7) $Å^3$
Z	4
Density (calculated)	1.569 Mg/m^3
Absorption coefficient	3.775 mm^{-1}
F(000)	4184
Crystal size	0.20 x 0.20 x 0.10 mm^3
Theta range for data collection	0.96 to 25.00°.
Index ranges	-11<=h<=11, -35<=k<=35, -21<=l<=36
Reflections collected	53865
Independent reflections	14983 [R(int) = 0.0851]
Completeness to theta = 25.00°	95.8 %
Max. and min. transmission	0.7040 and 0.5190
Refinement method	Full-matrix least-squares on F^2
Data / restraints / parameters	14983 / 0 / 1063
Goodness-of-fit on F^2	1.050
Final R indices [I>2sigma(I)]	R1 = 0.0547, wR2 = 0.1084
R indices (all data)	R1 = 0.0935, wR2 = 0.1279
Largest diff. peak and hole	1.097 and -1.928 e.$Å^{-3}$

APPENDIX 9

Crystal data and structure refinement		
for	**(95)$_2$** • TMAF	
Identification code	val009	
Empirical formula	C_{72} H_{64} F N_5 O_{12} U_2	
Formula weight	1686.34	
Temperature	123(2) K	
Wavelength	0.71073 Å	
Crystal system	Monoclinic	
Space group	C2/c	
Unit cell dimensions	a = 11.2400(2) Å	α= 90°.
	b = 26.9834(9) Å	β= 91.749(2)°.
	c = 24.5219(9) Å	γ = 90°.
Volume	7433.9(4) Å^3	
Z	4	
Density (calculated)	1.507 Mg/m^3	
Absorption coefficient	4.413 mm^{-1}	
F(000)	3280	
Crystal size	0.28 x 0.22 x 0.17 mm^3	
Theta range for data collection	2.61 to 25.00°.	
Index ranges	-13<=h<=13, -32<=k<=24, -28<=l<=29	
Reflections collected	16848	
Independent reflections	6533 [R(int) = 0.0757]	
Completeness to theta = 25.00°	99.5 %	
Max. and min. transmission	0.5209 and 0.3713	
Refinement method	Full-matrix least-squares on F^2	
Data / restraints / parameters	6533 / 0 / 416	
Goodness-of-fit on F^2	1.347	
Final R indices [I>2sigma(I)]	R1 = 0.0645, wR2 = 0.1566	
R indices (all data)	R1 = 0.0932, wR2 = 0.1685	
Largest diff. peak and hole	2.905 and -1.001 e.Å^{-3}	

APPENDIX 10

Crystal data and structure refinement for	**95**•DABCO
Identification code	val003
Empirical formula	$C_{35.50}H_{31}N_3O_7U$
Formula weight	849.66
Temperature	123(2) K
Wavelength	0.71073 Å
Crystal system	Monoclinic
Space group	P21/a
Unit cell dimensions	a = 10.3686(3) Å α= 90°. b = 16.6099(3) Å β= 100.2390(10)°. c = 25.1053(7) Å γ = 90°.
Volume	4254.81(19) $Å^3$
Z	4
Density (calculated)	1.326 Mg/m^3
Absorption coefficient	3.856 mm^{-1}
F(000)	1652
Crystal size	0.30 x 0.20 x 0.20 mm^3
Theta range for data collection	2.96 to 25.00°.
Index ranges	-12<=h<=12, -19<=k<=17, -24<=l<=29
Reflections collected	20678
Independent reflections	7496 [R(int) = 0.0895]
Completeness to theta = 25.00°	99.8 %
Max. and min. transmission	0.5127 and 0.3909
Refinement method	Full-matrix least-squares on F^2
Data / restraints / parameters	7496 / 16 / 433
Goodness-of-fit on F^2	1.117
Final R indices [I>2sigma(I)]	R1 = 0.0792, wR2 = 0.1971
R indices (all data)	R1 = 0.1101, wR2 = 0.2150
Largest diff. peak and hole	3.162 and -1.206 $e.Å^{-3}$

APPENDIX 11

Crystal data and structure refinement for	**(95)$_2$**	
Identification code	4-bz-teacl-2	
Empirical formula	C_{151} H_{134} N_8 O_{29} U_4	
Formula weight	3476.78	
Temperature	123(2) K	
Wavelength	0.71073 Å	
Crystal system	Triclinic	
Space group	P-1	
Unit cell dimensions	a = 13.9377(2) Å	α= 80.4680(10)°.
	b = 15.5825(3) Å	β = 80.8980(10)°.
	c = 15.8426(3) Å	γ = 85.5140(10)°.
Volume	3345.75(10) Å^3	
Z	1	
Density (calculated)	1.726 Mg/m^3	
Absorption coefficient	4.905 mm^{-1}	
F(000)	1696	
Crystal size	0.18 x 0.10 x 0.08 mm^3	
Theta range for data collection	2.57 to 25.00°.	
Index ranges	-16<=h<=15, -18<=k<=18, -18<=l<=18	
Reflections collected	43537	
Independent reflections	11754 [R(int) = 0.0682]	
Completeness to theta = 25.00°	99.8 %	
Absorption correction	Semi-empirical from equivalents	
Max. and min. transmission	0.6950 and 0.4722	
Refinement method	Full-matrix least-squares on F^2	
Data / restraints / parameters	11754 / 142 / 937	
Goodness-of-fit on F^2	1.073	
Final R indices [I>2sigma(I)]	R1 = 0.0436, wR2 = 0.0843	
R indices (all data)	R1 = 0.0653, wR2 = 0.0924	
Largest diff. peak and hole	1.691 and -0.804 e.Å^{-3}	

APPENDIX 12

Crystal data and structure refinement for	**106**•MeOH	
Identification code	oda-105+tbacl	
Empirical formula	$C_{65}\ H_{56}\ N_4\ O_{15}\ S_2\ U_2$	
Formula weight	1673.32	
Temperature	123(2) K	
Wavelength	0.71073 Å	
Crystal system	Monoclinic	
Space group	P21/c	
Unit cell dimensions	a = 13.8399(3) Å	α = 90°.
	b = 16.9209(4) Å	β = 107.018(2)°.
	c = 28.2371(8) Å	γ = 90°.
Volume	6323.1(3) $Å^3$	
Z	4	
Density (calculated)	1.758 Mg/m^3	
Absorption coefficient	5.251 mm^{-1}	
F(000)	3240	
Crystal size	0.15 x 0.12 x 0.08 mm^3	
Theta range for data collection	2.41 to 25.00°.	
Index ranges	-16<=h<=16, -20<=k<=20, -33<=l<=33	
Reflections collected	72131	
Independent reflections	11127 [R(int) = 0.1121]	
Completeness to theta = 25.00°	99.9 %	
Absorption correction	Semi-empirical from equivalents	
Max. and min. transmission	0.6583 and 0.4912	
Refinement method	Full-matrix least-squares on F^2	
Data / restraints / parameters	11127 / 101 / 808	
Goodness-of-fit on F^2	1.102	
Final R indices [I>2sigma(I)]	R1 = 0.0737, wR2 = 0.1362	
R indices (all data)	R1 = 0.1107, wR2 = 0.1490	
Largest diff. peak and hole	1.991 and -0.909 $e.Å^{-3}$	

APPENDIX 13

Crystal data and structure refinement		
for	**106** • H_2O	
Identification code	val017	
Empirical formula	C_{69} H_{67} N_5 O_{16} S_2 U_2	
Formula weight	1762.46	
Temperature	123(2) K	
Wavelength	0.71073 Å	
Crystal system	Monoclinic	
Space group	P21/n	
Unit cell dimensions	a = 13.8504(2) Å	α= 90°.
	b = 17.5937(2) Å	β= 102.5050(10)°.
	c = 27.9422(4) Å	γ = 90°.
Volume	6647.42(15) $Å^3$	
Z	4	
Density (calculated)	1.761 Mg/m^3	
Absorption coefficient	5.001 mm^{-1}	
F(000)	3440	
Crystal size	0.20 x 0.15 x 0.15 mm^3	
Theta range for data collection	1.38 to 25.00°.	
Index ranges	0<=h<=16, 0<=k<=20, -33<=l<=32	
Reflections collected	11597	
Independent reflections	11597 [R(int) = 0.0000]	
Completeness to theta = 25.00°	99.1 %	
Max. and min. transmission	0.5208 and 0.4345	
Refinement method	Full-matrix least-squares on F^2	
Data / restraints / parameters	11597 / 4 / 861	
Goodness-of-fit on F^2	1.081	
Final R indices [I>2sigma(I)]	R1 = 0.0426, wR2 = 0.0875	
R indices (all data)	R1 = 0.0582, wR2 = 0.0989	
Largest diff. peak and hole	0.874 and -0.813 e.$Å^{-3}$	

APPENDIX 14

Crystal data and structure refinement for	**105**•TMACl
Identification code	val015
Empirical formula	C_{72} H_{72} Cl_2 N_6 O_{12} S_2 U_2
Formula weight	1824.44
Temperature	173.0(1) K
Wavelength	0.71073 Å
Crystal system	Tetragonal
Space group	I -4
Unit cell dimensions	a = 18.9226(2) Å α= 90°. b = 18.9226(2) Å β= 90°. c = 19.5451(4) Å γ = 90°.
Volume	6998.41(18) $Å^3$
Z	4
Density (calculated)	1.732 Mg/m^3
Absorption coefficient	4.824 mm^{-1}
F(000)	3568
Crystal size	0.30 x 0.20 x 0.15 mm^3
Theta range for data collection	2.58 to 24.99°.
Index ranges	-20<=h<=22, -22<=k<=18, -21<=l<=22
Reflections collected	19105
Independent reflections	6060 [R(int) = 0.0466]
Completeness to theta = 24.99°	99.7 %
Absorption correction	None
Max. and min. transmission	0.5315 and 0.3255
Refinement method	Full-matrix least-squares on F^2
Data / restraints / parameters	6060 / 0 / 433
Goodness-of-fit on F^2	0.989
Final R indices [I>2sigma(I)]	R1 = 0.0301, wR2 = 0.0590
R indices (all data)	R1 = 0.0368, wR2 = 0.0610
Absolute structure parameter	0.037(6)
Largest diff. peak and hole	0.587 and -0.420 e.$Å^{-3}$

APPENDIX 15

Crystal data and structure refinement for	**105**•DMDBACl	
Identification code	3-bz-tio-dmdbacl	
Empirical formula	C_{43} H_{49} Cl_4 N_3 O_7 S U	
Formula weight	1131.74	
Temperature	123(2) K	
Wavelength	0.71073 Å	
Crystal system	Monoclinic	
Space group	P21/c	
Unit cell dimensions	a = 15.4076(4) Å	α = 90°.
	b = 20.6993(5) Å	β = 108.764(2)°.
	c = 15.4903(4) Å	γ = 90°.
Volume	4677.7(2) $Å^3$	
Z	4	
Density (calculated)	1.607 Mg/m^3	
Absorption coefficient	3.793 mm^{-1}	
F(000)	2240	
Crystal size	0.11 x 0.06 x 0.05 mm^3	
Theta range for data collection	2.41 to 25.02°.	
Index ranges	-17<=h<=18, -24<=k<=24, -17<=l<=18	
Reflections collected	62751	
Independent reflections	8268 [R(int) = 0.1850]	
Completeness to theta = 25.02°	99.9 %	
Absorption correction	Semi-empirical from equivalents	
Max. and min. transmission	0.8330 and 0.6804	
Refinement method	Full-matrix least-squares on F^2	
Data / restraints / parameters	8268 / 205 / 588	
Goodness-of-fit on F^2	1.020	
Final R indices [I>2sigma(I)]	R1 = 0.0645, wR2 = 0.1328	
R indices (all data)	R1 = 0.1143, wR2 = 0.1530	
Largest diff. peak and hole	2.865 and -2.182 e.$Å^{-3}$	

APPENDIX 16

Crystal data and structure refinement for	**106**•TMACl	
Identification code	oda-105+tmacl	
Empirical formula	C_{37} H_{37} Cl_4 N_3 O_6 S U	
Formula weight	1031.59	
Temperature	123(2) K	
Wavelength	0.71073 Å	
Crystal system	Monoclinic	
Space group	P21/c	
Unit cell dimensions	a = 24.8568(4) Å	α = 90°.
	b = 16.0807(3) Å	β = 97.3760(10)°.
	c = 9.7663(2) Å	γ = 90°.
Volume	3871.43(12) $Å^3$	
Z	4	
Density (calculated)	1.770 Mg/m^3	
Absorption coefficient	4.572 mm^{-1}	
F(000)	2016	
Crystal size	0.15 x 0.10 x 0.04 mm^3	
Theta range for data collection	2.08 to 25.00°.	
Index ranges	-29<=h<=27, -19<=k<=15, -11<=l<=11	
Reflections collected	39453	
Independent reflections	6790 [R(int) = 0.0887]	
Completeness to theta = 25.00°	99.5 %	
Absorption correction	Semi-empirical from equivalents	
Max. and min. transmission	0.8327 and 0.5863	
Refinement method	Full-matrix least-squares on F^2	
Data / restraints / parameters	6790 / 0 / 469	
Goodness-of-fit on F^2	1.054	
Final R indices [I>2sigma(I)]	R1 = 0.0443, wR2 = 0.0750	
R indices (all data)	R1 = 0.0667, wR2 = 0.0815	
Largest diff. peak and hole	0.812 and -0.667 $e.Å^{-3}$	

APPENDIX 17

Crystal data and structure refinement		
for	**106**•DMDEACl	
Identification code	oda-105-dmdeacl	
Empirical formula	C_{41} H_{46} Cl N_3 O_7 S U	
Formula weight	998.35	
Temperature	123(2) K	
Wavelength	0.71073 Å	
Crystal system	Monoclinic	
Space group	P21/c	
Unit cell dimensions	a = 25.0362(4) Å	α = 90°.
	b = 16.1045(3) Å	β = 95.7720(10)°.
	c = 9.8842(2) Å	γ = 90°.
Volume	3965.06(13) $Å^3$	
Z	4	
Density (calculated)	1.672 Mg/m^3	
Absorption coefficient	4.267 mm^{-1}	
F(000)	1976	
Crystal size	0.10 x 0.06 x 0.04 mm^3	
Theta range for data collection	2.07 to 25.00°.	
Index ranges	-29<=h<=29, -19<=k<=18, -11<=l<=11	
Reflections collected	23270	
Independent reflections	6977 [R(int) = 0.1003]	
Completeness to theta = 25.00°	99.9 %	
Absorption correction	Empirical	
Max. and min. transmission	0.8479 and 0.6749	
Refinement method	Full-matrix least-squares on F^2	
Data / restraints / parameters	6977 / 49 / 493	
Goodness-of-fit on F^2	1.076	
Final R indices [I>2sigma(I)]	R1 = 0.0625, wR2 = 0.1373	
R indices (all data)	R1 = 0.0874, wR2 = 0.1497	
Largest diff. peak and hole	7.127 and -1.059 e.$Å^{-3}$	

APPENDIX 18

Crystal data and structure refinement for	**105**•TMAF	
Identification code	oda-108-tmaf	
Empirical formula	C_{36} H_{36} F N_3 O_6 S U	
Formula weight	895.77	
Temperature	123(2) K	
Wavelength	0.71073 Å	
Crystal system	Tetragonal	
Space group	I-4	
Unit cell dimensions	a = 18.9641(4) Å	α = 90°.
	b = 18.9641(4) Å	β = 90°.
	c = 19.0964(3) Å	γ = 90°.
Volume	6867.8(2) $Å^3$	
Z	8	
Density (calculated)	1.733 Mg/m^3	
Absorption coefficient	4.843 mm^{-1}	
F(000)	3504	
Crystal size	0.15 x 0.12 x 0.10 mm^3	
Theta range for data collection	2.13 to 25.00°.	
Index ranges	-22<=h<=22, -22<=k<=21, -22<=l<=22	
Reflections collected	46214	
Independent reflections	6065 [R(int) = 0.0862]	
Completeness to theta = 25.00°	99.9 %	
Absorption correction	Semi-empirical from equivalents	
Max. and min. transmission	0.620104 and 0.524198	
Refinement method	Full-matrix least-squares on F^2	
Data / restraints / parameters	6065 / 0 / 397	
Goodness-of-fit on F^2	1.026	
Final R indices [I>2sigma(I)]	R1 = 0.0323, wR2 = 0.0582	
R indices (all data)	R1 = 0.0406, wR2 = 0.0605	
Absolute structure parameter	0.026(6)	
Largest diff. peak and hole	0.740 and -0.572 $e.Å^{-3}$	

APPENDIX 19

Crystal data and structure refinement for	**107**•H_2O	
Identification code	oda-097	
Empirical formula	C_{182} H_{161} N_{31} O_{34} U_4	
Formula weight	4278.54	
Temperature	123(2) K	
Wavelength	0.71073 Å	
Crystal system	Triclinic	
Space group	P-1	
Unit cell dimensions	a = 11.33810(10) Å	α = 96.1240(10)°.
	b = 18.5861(2) Å	β = 92.9870(10)°.
	c = 20.4670(2) Å	γ = 101.3150(10)°.
Volume	4193.25(7) $Å^3$	
Z	1	
Density (calculated)	1.694 Mg/m^3	
Absorption coefficient	3.937 mm^{-1}	
F(000)	2110	
Crystal size	0.17 x 0.16 x 0.10 mm^3	
Theta range for data collection	1.84 to 25.00°.	
Index ranges	-13<=h<=10, -21<=k<=22, -24<=l<=23	
Reflections collected	49053	
Independent reflections	14629 [R(int) = 0.0464]	
Completeness to theta = 25.00°	99.0 %	
Absorption correction	Semi-empirical from equivalents	
Max. and min. transmission	0.6710 and 0.5488	
Refinement method	Full-matrix least-squares on F^2	
Data / restraints / parameters	14629 / 30 / 1179	
Goodness-of-fit on F^2	1.069	
Final R indices [I>2sigma(I)]	R1 = 0.0330, wR2 = 0.0634	
R indices (all data)	R1 = 0.0473, wR2 = 0.0681	
Largest diff. peak and hole	0.813 and -0.558 $e.Å^{-3}$	

APPENDIX 20

Crystal data and structure refinement for	**107**•acetone	
Identification code	import	
Empirical formula	$C_{48}H_{42}N_6O_8U$	
Formula weight	1068.91	
Temperature	123(2) K	
Wavelength	0.71073 Å	
Crystal system	Triclinic	
Space group	P-1	
Unit cell dimensions	a = 9.7867(3) Å	α= 89.3360(10)°.
	b = 11.8517(4) Å	β= 89.2420(10)°.
	c = 19.6432(5) Å	γ = 70.7000(10)°.
Volume	2150.10(11) $Å^3$	
Z	2	
Density (calculated)	1.651 Mg/m^3	
Absorption coefficient	3.838 mm^{-1}	
F(000)	1056	
Crystal size	0.20 x 0.15 x 0.15 mm^3	
Theta range for data collection	2.07 to 25.00°.	
Index ranges	0<=h<=11, -12<=k<=14, -23<=l<=23	
Reflections collected	7546	
Independent reflections	7546 [R(int) = 0.0000]	
Completeness to theta = 25.00°	99.8 %	
Max. and min. transmission	0.5968 and 0.5141	
Refinement method	Full-matrix least-squares on F^2	
Data / restraints / parameters	7546 / 0 / 581	
Goodness-of-fit on F^2	1.081	
Final R indices [I>2sigma(I)]	R1 = 0.0319, wR2 = 0.0642	
R indices (all data)	R1 = 0.0387, wR2 = 0.0677	
Largest diff. peak and hole	1.162 and -0.526 $e.Å^{-3}$	

APPENDIX 21

Crystal data and structure refinement		
for	**121** • H_2O	
Identification code	4-oh	
Empirical formula	C_{28} H_{28} N_6 $O_{7.50}$ U	
Formula weight	806.59	
Temperature	123(2) K	
Wavelength	0.71073 Å	
Crystal system	Triclinic	
Space group	P-1	
Unit cell dimensions	a = 10.4273(4) Å	α= 67.380(2)°.
	b = 12.6722(5) Å	β= 69.850(2)°.
	c = 13.2945(5) Å	γ = 85.068(2)°.
Volume	1520.12(10) $Å^3$	
Z	2	
Density (calculated)	1.762 Mg/m^3	
Absorption coefficient	5.394 mm^{-1}	
F(000)	780	
Crystal size	0.20 x 0.05 x 0.04 mm^3	
Theta range for data collection	2.23 to 25.00°.	
Index ranges	-12<=h<=12, -12<=k<=15, -15<=l<=15	
Reflections collected	18957	
Independent reflections	5344 [R(int) = 0.0657]	
Completeness to theta = 25.00°	99.5 %	
Absorption correction	Semi-empirical from equivalents	
Max. and min. transmission	0.8131 and 0.4117	
Refinement method	Full-matrix least-squares on F^2	
Data / restraints / parameters	5344 / 435 / 565	
Goodness-of-fit on F^2	1.133	
Final R indices [I>2sigma(I)]	R1 = 0.0689, wR2 = 0.1572	
R indices (all data)	R1 = 0.0856, wR2 = 0.1661	
Largest diff. peak and hole	5.997 and -1.969 e.$Å^{-3}$	

APPENDIX 22

Crystal data and structure refinement		
for	**127**•acetone	
Identification code	val016	
Empirical formula	C_{25} H_{24} N_2 O_7 U	
Formula weight	702.49	
Temperature	123(2) K	
Wavelength	0.71073 Å	
Crystal system	Monoclinic	
Space group	P21/a	
Unit cell dimensions	a = 8.43500(10) Å	α= 90°.
	b = 13.2878(2) Å	β= 93.4200(10)°.
	c = 21.2529(4) Å	γ = 90°.
Volume	2377.84(6) $Å^3$	
Z	4	
Density (calculated)	1.962 Mg/m^3	
Absorption coefficient	6.875 mm^{-1}	
F(000)	1344	
Crystal size	0.30 x 0.20 x 0.20 mm^3	
Theta range for data collection	2.46 to 25.00°.	
Index ranges	-10<=h<=8, -15<=k<=15, -25<=l<=25	
Reflections collected	18961	
Independent reflections	4173 [R(int) = 0.1120]	
Completeness to theta = 25.00°	99.8 %	
Absorption correction	Semi-empirical from equivalents	
Max. and min. transmission	0.3401 and 0.2322	
Refinement method	Full-matrix least-squares on F^2	
Data / restraints / parameters	4173 / 0 / 320	
Goodness-of-fit on F^2	2.305	
Final R indices [I>2sigma(I)]	R1 = 0.0394, wR2 = 0.1016	
R indices (all data)	R1 = 0.0432, wR2 = 0.1034	
Largest diff. peak and hole	3.042 and -2.456 e.$Å^{-3}$	

APPENDIX 23

Crystal data and structure refinement for	**129**•MeOH	
Identification code	oda-118-tmacl	
Empirical formula	C_{36} H_{46} N_2 O_8 U	
Formula weight	872.78	
Temperature	123(2) K	
Wavelength	0.71073 Å	
Crystal system	Triclinic	
Space group	P-1	
Unit cell dimensions	a = 12.8792(2) Å	α = 90.2870(10)°.
	b = 15.5921(3) Å	β = 90.1480(10)°.
	c = 17.5983(3) Å	γ = 101.6500(10)°.
Volume	3461.11(10) $Å^3$	
Z	4	
Density (calculated)	1.675 Mg/m^3	
Absorption coefficient	4.743 mm^{-1}	
F(000)	1728	
Crystal size	0.40 x 0.08 x 0.05 mm^3	
Theta range for data collection	1.98 to 25.00°.	
Index ranges	-15<=h<=15, -18<=k<=17, -20<=l<=20	
Reflections collected	45373	
Independent reflections	12136 [R(int) = 0.0529]	
Completeness to theta = 25.00°	99.6 %	
Absorption correction	Semi-empirical from equivalents	
Max. and min. transmission	0.7914 and 0.5862	
Refinement method	Full-matrix least-squares on F^2	
Data / restraints / parameters	12136 / 76 / 863	
Goodness-of-fit on F^2	1.024	
Final R indices [I>2sigma(I)]	R1 = 0.0301, wR2 = 0.0534	
R indices (all data)	R1 = 0.0460, wR2 = 0.0574	
Largest diff. peak and hole	0.613 and -0.632 e.$Å^{-3}$	

APPENDIX 24

Crystal data and structure refinement for	**129**•H_2O
Identification code	oda-118-tmaf
Empirical formula	C_{290} H_{363} N_{25} O_{64} U_8
Formula weight	7127.29
Temperature	123(2) K
Wavelength	0.71073 Å
Crystal system	Monoclinic
Space group	P21/c
Unit cell dimensions	a = 26.1430(5) Å α= 90°. b = 14.6744(2) Å β= 90.3000(10)°. c = 18.7730(3) Å γ = 90°.
Volume	7201.8(2) $Å^3$
Z	1
Density (calculated)	1.643 Mg/m^3
Absorption coefficient	4.562 mm^{-1}
F(000)	3526
Crystal size	0.24 x 0.16 x 0.10 mm^3
Theta range for data collection	1.76 to 25.00°.
Index ranges	-31<=h<=31, -17<=k<=17, -22<=l<=22
Reflections collected	83272
Independent reflections	12673 [R(int) = 0.0978]
Completeness to theta = 25.00°	99.9 %
Absorption correction	Semi-empirical from equivalents
Max. and min. transmission	0.6583 and 0.4073
Refinement method	Full-matrix least-squares on F^2
Data / restraints / parameters	12673 / 134 / 887
Goodness-of-fit on F^2	1.040
Final R indices [I>2sigma(I)]	R1 = 0.0537, wR2 = 0.0964
R indices (all data)	R1 = 0.0799, wR2 = 0.1044
Largest diff. peak and hole	2.890 and -1.715 e.$Å^{-3}$

APPENDIX 25

Crystal data and structure refinement for	**129**•DMSO	
Identification code	oda-118	
Empirical formula	$C_{41.30}H_{56}N_2O_9S_{1.70}U$	
Formula weight	1017.01	
Temperature	123(2) K	
Wavelength	0.71073 Å	
Crystal system	Monoclinic	
Space group	P21/n	
Unit cell dimensions	a = 19.2294(3) Å	α = 90°.
	b = 9.86740(10) Å	β = 99.5020(10)°.
	c = 22.4319(3) Å	γ = 90°.
Volume	4197.93(10) $Å^3$	
Z	4	
Density (calculated)	1.609 Mg/m^3	
Absorption coefficient	4.006 mm^{-1}	
F(000)	2036	
Crystal size	0.08 x 0.08 x 0.06 mm^3	
Theta range for data collection	1.84 to 25.00°.	
Index ranges	-22<=h<=22, -11<=k<=11, -26<=l<=26	
Reflections collected	53774	
Independent reflections	7391 [R(int) = 0.1150]	
Completeness to theta = 25.00°	99.9 %	
Absorption correction	Semi-empirical from equivalents	
Max. and min. transmission	0.7950 and 0.7399	
Refinement method	Full-matrix least-squares on F^2	
Data / restraints / parameters	7391 / 16 / 482	
Goodness-of-fit on F^2	1.031	
Final R indices [I>2sigma(I)]	R1 = 0.0431, wR2 = 0.0851	
R indices (all data)	R1 = 0.0640, wR2 = 0.0926	
Largest diff. peak and hole	1.526 and -0.857 $e.Å^{-3}$	

APPENDIX 26

Crystal data and structure refinement for	**(121)$_2$**	
Identification code	oda-043	
Empirical formula	C_{40} H_{32} N_4 O_{18} U_2	
Formula weight	1332.76	
Temperature	123(2) K	
Wavelength	0.71073 Å	
Crystal system	Orthorhombic	
Space group	Pbcn	
Unit cell dimensions	a = 15.5177(4) Å	α = 90°.
	b = 10.2526(3) Å	β = 90°.
	c = 27.5929(8) Å	γ = 90°.
Volume	4389.9(2) Å^3	
Z	4	
Density (calculated)	2.017 Mg/m^3	
Absorption coefficient	7.448 mm^{-1}	
F(000)	2512	
Crystal size	0.28 x 0.19 x 0.10 mm^3	
Theta range for data collection	1.98 to 25.00°.	
Index ranges	-18<=h<=14, -12<=k<=12, -32<=l<=32	
Reflections collected	33197	
Independent reflections	3855 [R(int) = 0.0682]	
Completeness to theta = 25.00°	99.6 %	
Absorption correction	Semi-empirical from equivalents	
Max. and min. transmission	0.5230 and 0.2295	
Refinement method	Full-matrix least-squares on F^2	
Data / restraints / parameters	3855 / 3 / 315	
Goodness-of-fit on F^2	1.222	
Final R indices [I>2sigma(I)]	R1 = 0.0490, wR2 = 0.0899	
R indices (all data)	R1 = 0.0650, wR2 = 0.0941	
Largest diff. peak and hole	1.790 and -3.098 e.Å^{-3}	

APPENDIX 27

Crystal data and structure refinement for	**120**•triethylamine
Identification code	3-OH dimer
Empirical formula	$C_{58}\ H_{70}\ N_6\ O_{14}\ U_2$
Formula weight	1551.26
Temperature	123.0(1) K
Wavelength	0.71073 Å
Crystal system	Orthorhombic
Space group	P c b a
Unit cell dimensions	a = 11.4824(1) Å α= 90°. b = 17.2116(3) Å β= 90°. c = 29.8556(6) Å γ = 90°.
Volume	5900.4(2) $Å^3$
Z	4
Density (calculated)	1.746 Mg/m^3
Absorption coefficient	5.551 mm^{-1}
F(000)	3024
Crystal size	0.30 x 0.20 x 0.15 mm^3
Theta range for data collection	2.73 to 28.50°.
Index ranges	-15<=h<=13, -23<=k<=18, -40<=l<=40
Reflections collected	52057
Independent reflections	7399 [R(int) = 0.1439]
Completeness to theta = 28.50°	98.8 %
Max. and min. transmission	0.4898 and 0.2867
Refinement method	Full-matrix least-squares on F^2
Data / restraints / parameters	7399 / 3 / 346
Goodness-of-fit on F^2	1.027
Final R indices [I>2sigma(I)]	R1 = 0.0732, wR2 = 0.1125
R indices (all data)	R1 = 0.1505, wR2 = 0.1350
Largest diff. peak and hole	1.363 and -1.013 $e.Å^{-3}$

APPENDIX 28

Crystal data and structure refinement	
for	**1**•Cs_2CO_3
Identification code	val010
Empirical formula	C_{43} H_{34} Cs N_4 O_{12} U_2
Formula weight	1407.71
Temperature	123(2) K
Wavelength	0.71073 Å
Crystal system	monoclinic
Space group	P21/n
Unit cell dimensions	a = 12.7269(7) Å α= 90°.
	b = 28.3780(10) Å β= 112.952(3)°.
	c = 13.7985(8) Å γ = 90°.
Volume	4589.0(4) $Å^3$
Z	4
Density (calculated)	2.038 Mg/m^3
Absorption coefficient	7.894 mm^{-1}
F(000)	2620
Crystal size	0.20 x 0.10 x 0.10 mm^3
Theta range for data collection	2.68 to 25.00°.
Index ranges	-15<=h<=14, -33<=k<=33, -16<=l<=16
Reflections collected	24126
Independent reflections	7712 [R(int) = 0.1207]
Completeness to theta = 25.00°	95.3 %
Max. and min. transmission	0.5057 and 0.3012
Refinement method	Full-matrix least-squares on F^2
Data / restraints / parameters	7712 / 0 / 560
Goodness-of-fit on F^2	1.135
Final R indices [I>2sigma(I)]	R1 = 0.0843, wR2 = 0.1573
R indices (all data)	R1 = 0.1338, wR2 = 0.1780
Largest diff. peak and hole	2.101 and -1.723 e.$Å^{-3}$